NASA CR-66725-2

FINAL REPORT

BUOYANT VENUS STATION MISSION FEASIBILITY STUDY FOR 1972 - 1973 LAUNCH OPPORTUNITIES

VOLUME II: TRAJECTORY ANALYSIS FOR 1972 AND 1973 MISSIONS

Donald W. Marquet and Charles E. French

Submitted by: John F. Baxter
John F. Baxter
BVS Study Manager

Approved by: Stanley R. Sadin
Stanley R. Sadin
Program Director,
Venus and Deep Space Programs

Prepared under Contract No. NAS1-7590 by
MARTIN MARIETTA CORPORATION
Denver, Colorado 80201

for

NATIONAL AERONAUTICS AND SPACE ADMINISTRATION

FOREWORD

The use of a bouyant station to explore the atmosphere of Venus has shown great promise in previous studies.* The high temperatures and pressures likely to be encountered and the unknown surface characteristics tend to make the in situ exploration of this planet difficult. The bouyant station concept permits the mission's instruments to be floated in the atmosphere in a moderate environment, localizing the environment problem to relatively compact drop sondes, and avoiding the problems of landing, deployment, and survival on the surface. Relatively simple missions can thus be defined that have the advantages of long duration and mobility over the surface, depending on the existing wind patterns. From such a station, measurements relating both to the atmosphere and the surface can be made. The surface measurements can be obtained either indirectly or by sondes dropped from the parent bouyant station.

This final report on the Bouyant Venus Station Mission Feasibility Study for 1972-1973 Launch Opportunities is submitted by the Martin Marietta Corporation, Denver Division, in accordance with Contract NAS1-7590.

This report is submitted in three volumes as follows:

- Volume I - Mission Summary Definition and Comparison;
- Volume II - Trajectory Analysis for 1972 and 1973 Missions;
- Volume III - Configuration Definition.

*J. F. Baxter: Final Report, Bouyant Venus Station Feasibility Study, Volume I, Summary and Problem Identification.

CONTENTS

	Page
FOREWORD	ii
CONTENTS	iii
LIST OF ILLUSTRATIONS	iv
LIST OF TABLES	vii
SUMMARY	1
INTRODUCTION	1
SYMBOLS	3
PARAMETRIC ANALYSIS SUMMARY	5
Launch Vehicle Performance	5
Direct Mode Targeting	24
Orbit Mode Targeting	47
Orbit Selection Criteria	53
Entry Environment	66
Balloon Deployment and Sonde Trajectory	89
MISSION PROFILE SUMMARIES	94
1972 Flyby Mission	95
1973 Orbiter Mission	109
1973 Venus/Mercury Swingby Mission	126
CONCLUSIONS	136

LIST OF ILLUSTRATIONS

Figure		Page
1	BVS Mission Options	2
2	Venus 1972, Launch Opportunity Parameters	6
3	Venus 1973, Launch Opportunity Parameters	9
4	Venus Entry Velocity vs Hyperbolic Excess Velocity, V_{HE}	13
5	Launch Vehicle Capability after M/C Correction	15
6	SLV3C/C Performance Capability to Venus, Entry from Orbit	17
7	TIIIC Performance Capability to Venus, Entry from Orbit	18
8	TIIIC/C Performance Capability to Venus, Entry from Orbit	19
9	SLV3C/C Performance Capability to Venus, Entry from Approach	20
10	TIIIC Performance Capability to Venus, Entry from Approach	21
11	TIIIC/C Performance Capability to Venus, Entry from Approach	22
12	Weight Sensitivity, Capsule System to Spacecraft	23
13	Planet Approach Geometry Definition	25
14	β / λ Boundaries, Entry from Approach	27
15	β / γ_E Relationship	28
16	ΔV_{EJ} as a Function of γ_E and V_{HE} (h_p = 1000 km)	30
17	ΔV_{EJ} as a Function of γ_E and V_{HE} (h_p = 2000 km)	31
18	ΔV_{EJ} as a Function of γ_E and V_{HE} (h_p = 3000 km)	32
19	α_E as a Function of γ_E and V_{HE} (h_p = 1000 km)	33
20	α_E as a Function of γ_E and V_{HE} (h_p = 2000 km)	34
21	α_E as a Function of γ_E and V_{HE} (h_p = 3000 km)	35
22	Coast Time vs V_{HE}	37
23	Periapsis Angle, τ_o, vs h_p and V_{HE}	38
24	Venus Targeting Map, 1972, Type I, 30° View	39
25	Venus Targeting Map, 1973, Type II, 30° View	41
26	Sensitivity to Navigation Error, γ_E	42

27 One-Sigma γ_E Error vs τ_{EJ} 44
28 τ_{EJ} vs γ_E and V_{HE} 45
29 ΔV_{EJ} vs θ_E 46
30 β / λ Boundaries, Entry from Orbit 48
31 ΔV_D vs λ and β 49
32 α_E vs λ and β 50
33 Targeting Capability, 1973, Entry from Orbit . . . 52
34 Venus Orbit Insertion ΔV Requirements 55
35 Venus Circular Velocities 56
36 $\Delta V_{O.I.}$ Sensitivity, $f(h_p, V_{HE}, e)$ 57
37 Useful Weight in Orbit 58
38 Fifty Year Orbit Lifetime Boundary, Drag 60
39 V_{HE} Vector Geometry, 1973, Type II 61
40 Orbit Periapsis Time History 62
41 Solar Perturbation Orbit Lifetime 65
42 Normalized Drag Coefficient vs Mach Number 67
43 Venus Atmosphere Models, Density vs Altitude . . . 69
44 Venus Atmosphere Models, Ambient Temperature vs Altitude 70
45 Time between Entry and Staging 72
46 Time between 1.0-g Deceleration and Staging . . . 73
47 Peak Entry Drag Deceleration 74
48 Staging Altitude, Lower Atmosphere Model 76
49 Staging Altitude, Upper Atmosphere Model 77
50 Downrange Angle 78
51 Subsonic Probe and Drop Sonde Descent Times . . . 79
52 Stagnation Point Radiation Heating 82
53 Stagnation Point Convection Heating 83
54 Cone Edge Radiation Heating 84
55 Cone Edge Convection Heating 85
56 Aerodynamic Shear Stress at Cone Edge 86
57 Configuration Effects on Aerodynamic Heating . . . 88
58 Time from Chute Deployment to Balloon Inflation . 90
59 Nominal Balloon Inflation Time History 91
60 Drop Sonde Descent Time History 93
61 1972 Flyby Mission, Targeting Summary, First Day 102
62 1972 Flyby Mission, Targeting Summary, Last Day 103
63 $\oplus$-S/C and $\odot$-S/C Time History, 1972 Flyby . . 104
64 Cone-Clock Angle Time History, 1972 Flyby 105
65 Drag Deceleration Time History, 1972 Flyby 106
66 Entry Time History, 1972 Flyby 107

67 Descent Trajectory on Chute, 1972 Flyby 108
68 1973 Orbiter Mission, Targeting Summary, First Day 116
69 1973 Orbiter Mission, Targeting Summary, Last Day 117
70 ⊕-S/C and ⊙-S/C Time History, 1973 Orbiter . 118
71 Cone-Clock Angle Time History, 1973 Orbiter . . . 119
72 Drag Deceleration Time History, Entry from Orbit . 120
73 Entry Time History, Entry from Orbit 121
74 Descent Trajectory on Chute, 1973 Orbiter 122
75 Drag Deceleration Time History, 1973 Orbiter, Entry from Approach 123
76 Entry Time History, 1973 Orbiter, Entry from Approach 124
77 Descent Trajectory on Chute, 1973 Orbiter, Entry from Approach 125
78 1973 Venus/Mercury Swingby Mission, Targeting Summary 132
79 1973 Venus/Mercury Swingby, Drag Deceleration Time History 133
80 1973 Venus/Mercury Swingby, Entry Time History . . 134
81 1973 Venus/Mercury Swingby, Descent Trajectory on Chute 135

LIST OF TABLES

Table		Page
1	Allowable Capsule System Weight	24
2	Orbit Lifetimes	63
3	1972 Flyby Mission Profile, Type I Transfer Trajectory	98
4	1972 Flyby Mission Sequence	100
5	1973 Orbiter Mission Profile, Entry from Orbit . .	111
6	1973 Orbiter Mission Profile, Entry from Approach	113
7	1973 Orbiter Mission Sequence	114
8	1973 Venus/Mercury Swingby Mission Profile	128
9	1973 Venus/Mercury Swingby Mission Sequence . . .	130

FINAL REPORT

BUOYANT VENUS STATION MISSION FEASIBILITY STUDY FOR 1972 - 1973 LAUNCH OPPORTUNITIES

VOLUME II: TRAJECTORY ANALYSIS FOR 1972 AND 1973 MISSIONS

By Donald W. Marquet and Charles E. French

SUMMARY

This report summarizes the results of the trajectory analyses that were performed parametrically in support of the Buoyant Venus Station (BVS) mission study. The range of parameters were related to three reference missions that served as the baselines for the detailed BVS system design studies. The three reference missions are:

1) 1972 flyby;
2) 1973 orbital;
3) 1973 Venus/Mercury swingby.

Parametric data are presented in the following technical areas: (1) launch vehicle performance and launch period selection; (2) direct mode targeting; (3) orbit mode targeting; (4) orbit selection criteria; (5) entry environment; and (6) balloon deployment and drop sonde trajectory.

A detailed mission profile is presented for each of the three reference missions. Use of the parametric data permits construction of mission profiles other than those detailed.

INTRODUCTION

This analysis surveys the various ways of flying a Buoyant Venus Station (BVS) mission and evaluates the options that can be considered. These options are summarized in figure 1. The first option is launch opportunity and launch vehicle capability. Performance capabilities of both the Titan IIIC (TIIIC) and Atlas (SLV3C)/Centaur are presented for both the 1972 and 1973 opportunities. The next series of options deals with the spacecraft operation. Those missions studied include Venus flyby, Venus orbit, and Venus swingby to Mercury. Next, the BVS entry can result from a trajectory deflection from the approach trajectory (direct entry) or from an established Venus orbit (orbital entry). Finally, the communication link from the BVS to Earth can be either direct or via a relay link through the spacecraft.

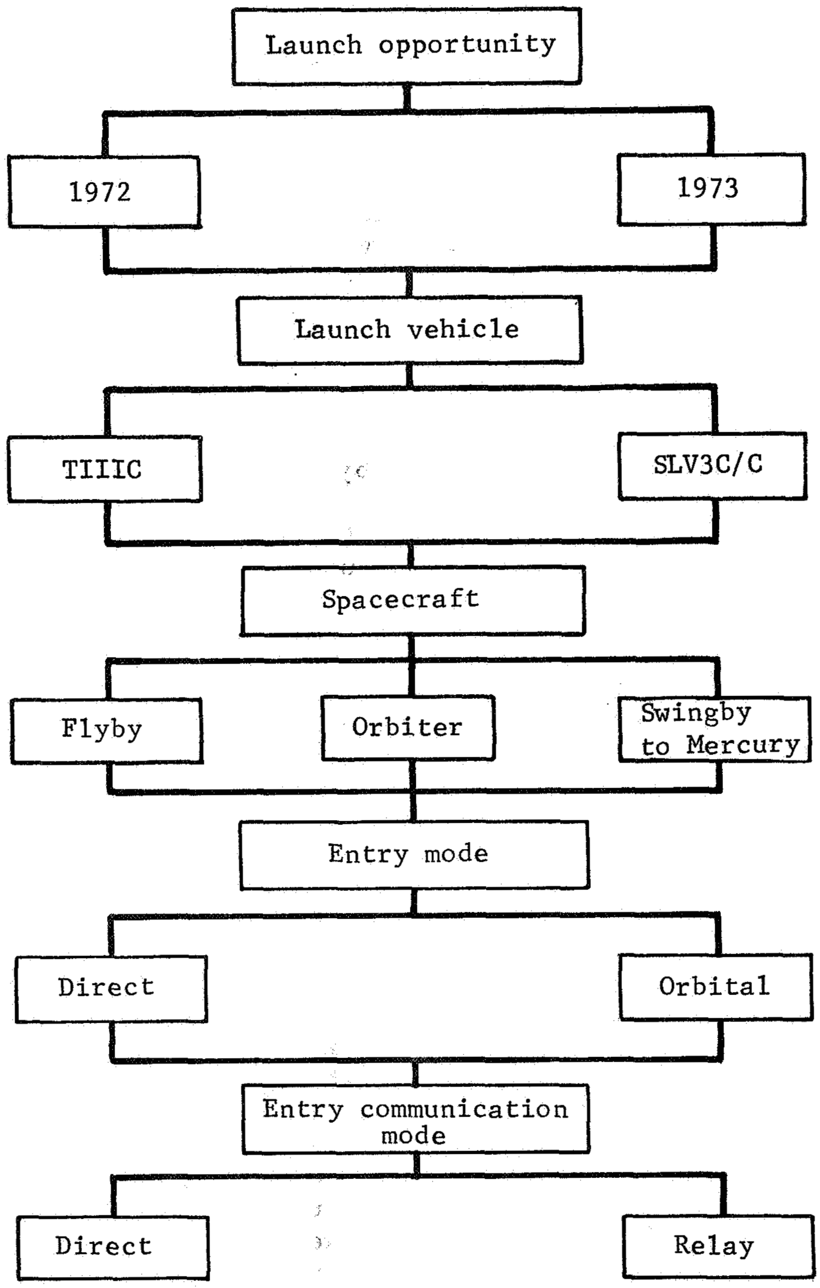

Figure 1.- BVS Mission Options

Each of these options has been studied parametrically. For convenience, typical missions have been formulated to display the effects of the various options on the system design. These missions are:

1) 1972 flyby, direct entry, direct communication link;
2) 1973 orbiter, orbital entry, relay communication link;
3) 1973 swingby to Mercury, direct entry, direct communication link.

This combination of designs displays the major effects of each of the options shown in figure 1. Other mission profiles can be constructed with the parametric data presented below.

The various parametric studies performed are presented in summary form. This is followed by a detailed summary of each of the three basic missions.

The specific parametric studies presented are: (1) launch vehicle performance (1972 and 1973 opportunities); (2) direct mode targeting; (3) orbit mode targeting; (4) orbit selection criteria; (5) entry environment; and (6) balloon deployment and sonde trajectories. Only the factors of major importance are presented in the parametric analysis.

SYMBOLS

B_E	entry ballistic coefficient, $slug/ft^2$
B_P	subsonic probe and drop sonde ballistic coefficient, $slug/ft^2$
C_D	drag coefficient
C_3	Earth departure energy, km^2/sec^2
DLA	declination of departure asymptote, deg
g	drag deceleration, Earth gravitation units
h_p	altitude of periapsis above mean planet radius, km
R_{EJ}	radius from planet center at ejection, km

t_c	coast time, min
t_E	time from entry to probe impact, min
V_E	entry velocity at entry altitude, fps
V_{HE}	hyperbolic excess velocity, km/sec
V_{SP}	circular orbital speed at periapsis altitude, m/sec
ΔV_D	velocity increment of deorbit maneuver, m/sec
ΔV_{EJ}	velocity increment of ejection maneuver, m/sec
$\Delta V_{O.I.}$	velocity increment of orbit insertion maneuver, m/sec
Δw	shift in Venus orbit approach trajectory periapsis, deg
α_E	entry vehicle angle of attack at entry, deg
α_P	antenna aspect angle, deg
β	targeting angle, central angle measured from entry point to spacecraft periapsis, deg
γ_E	entry flight path angle, negative down, deg
θ_E	angle between flyby trajectory plane and the BVS entry vehicle trajectory plane, deg
λ	lead angle, central angle between the spacecraft and the entry vehicle at entry, deg
ρ_C	communication distance, AU
τ_{EJ}	angle between the spacecraft velocity vector and ejection velocity vector, deg
τ_O	angle between spacecraft periapsis and V_{HE}, deg
φ_L	angle between V_{HE} and entry point, deg
$\odot$	Sun

$\oplus$ Earth

♀ Venus

☿ Mercury

PARAMETRIC ANALYSIS SUMMARY

Launch Vehicle Performance

The launch vehicle performance data are presented for the Titan IIIC (TIIIC) and Atlas (SLV3C)/Centaur (SLV3C/C) for both the 1972 and 1973 Venus launch opportunities. The data are presented first by defining the energy requirements for the missions. The launch vehicle capability is then presented for the applicable energy range for both flyby and orbiting spacecraft. The detailed performance for each of the three reference missions is presented as part of the mission profile summaries section.

Launch opportunity energy contours.- The launch opportunity parameters for the 1972 and 1973 missions are presented in figures 2 and 3, respectively. The data shown in figures 2(a) and 3(a) are presented in terms of constant C_3 countours versus launch date and encounter date. The parameter C_3 is the vis viva energy (per unit mass) and is related to the required injection velocity by:

$$V_{inj_{\oplus}} = \sqrt{C_3 + \frac{2\mu_{\oplus}}{r_{inj}}}$$

where:

$\mu_{\oplus}$ = Earth gravitational constant (398 603.2 km^3/sec^2)

$r_{inj} = R_{\oplus} + h_{inj} = 6378.2 + h_{inj}$, km,

h_{inj} = injection altitude, km.

Data are shown for both Type I (lower contours) and Type II (upper contours) heliocentric transfers. These data show that the Type II transfers have lower energy requirements for both opportunities, but require approximately two months longer cruise times to Venus.

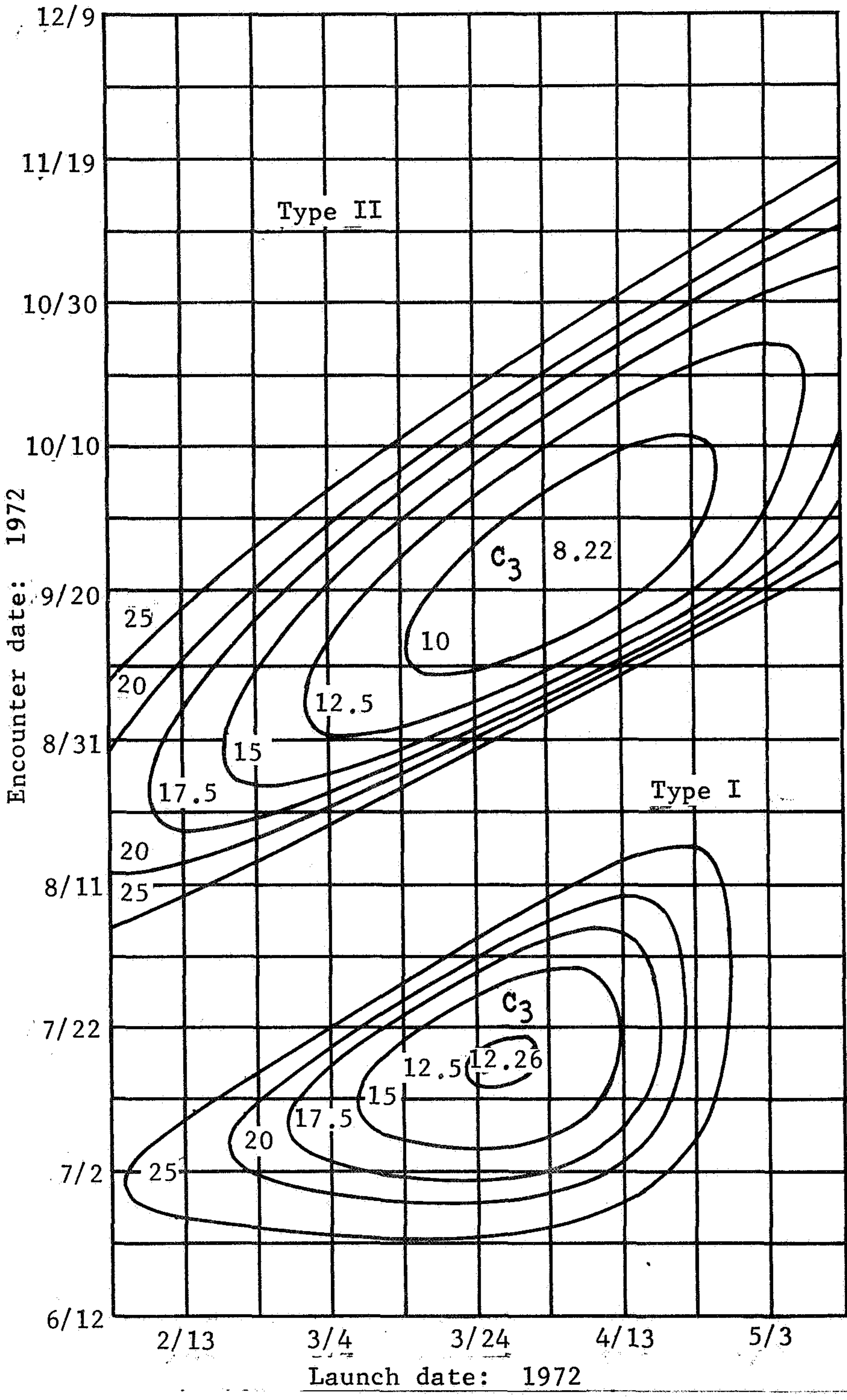

(a) Earth Departure Energy C_3, km^2/sec^2

Figure 2.- Venus 1972, Launch Opportunity Parameters

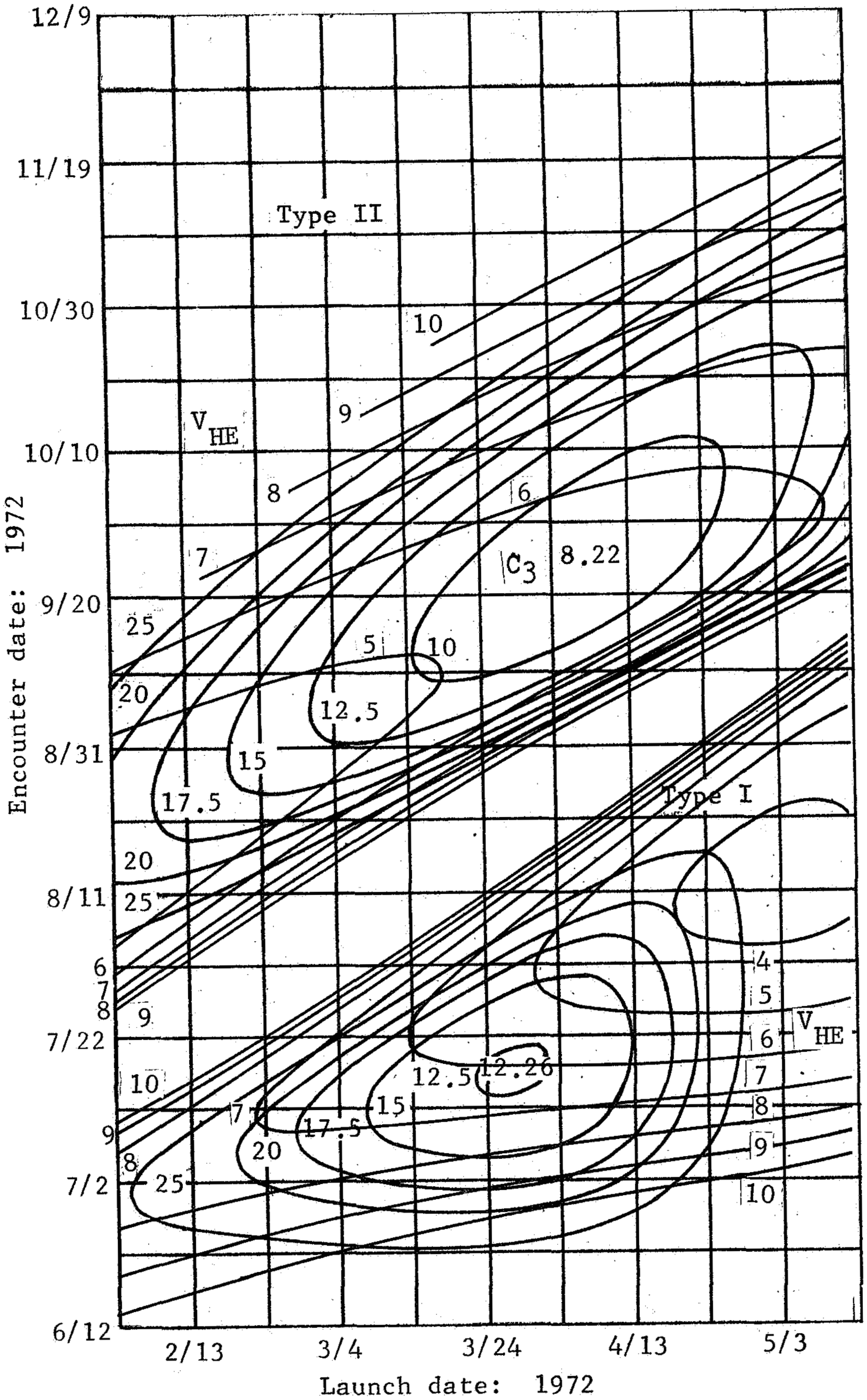

(b) Earth Departure Energy C_3, km^2/sec^2 and Venus Approach Velocity V_{HE}, km/sec

Figure 2.- Continued

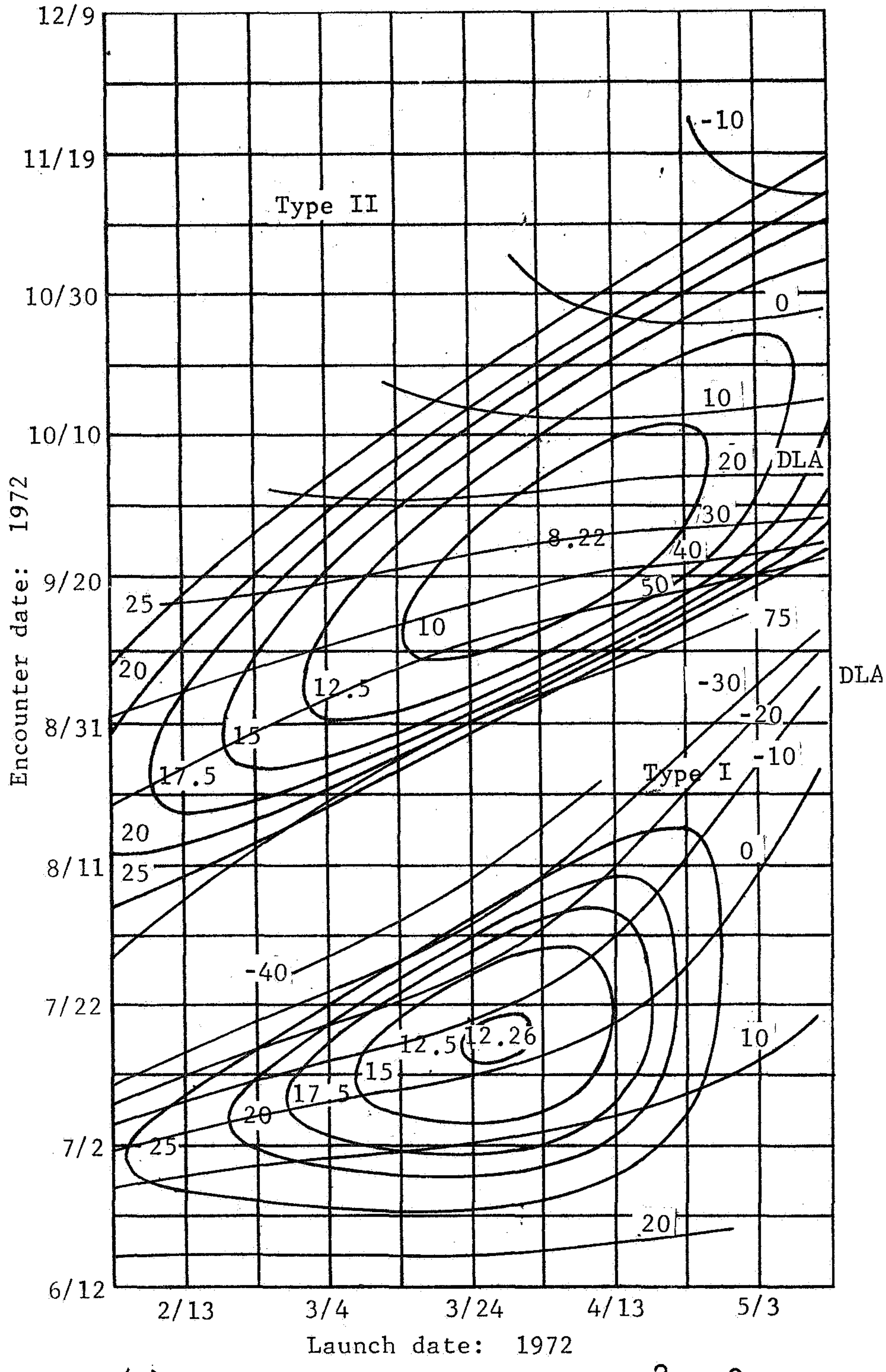

(c) Earth Departure Energy C_3, km^2/sec^2, and Declination Angle, DLA, Degrees

Figure 2.- Concluded

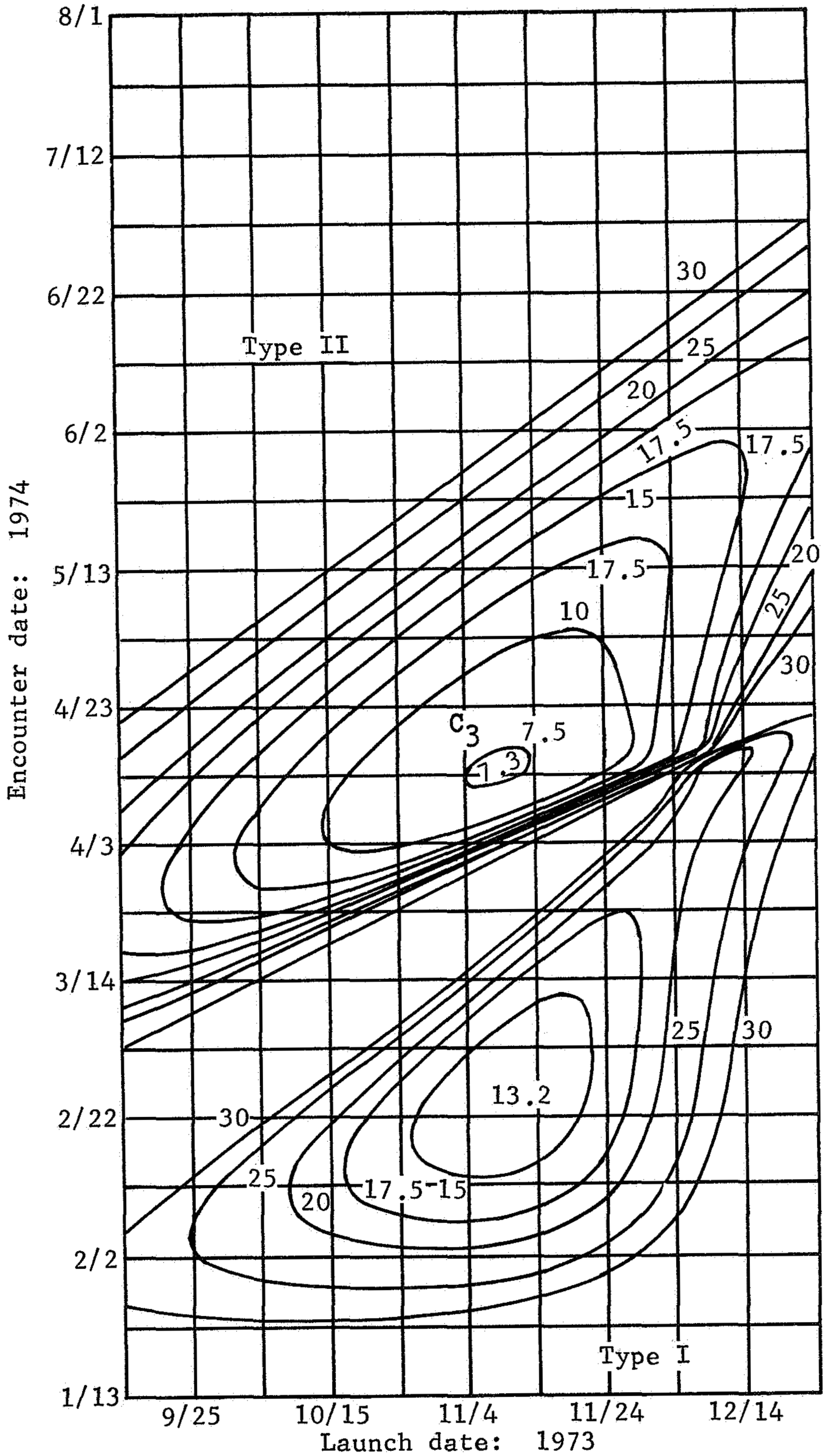

(a) Earth Departure Energy, C_3, km^2/sec^2

Figure 3.- Venus 1973, Launch Opportunity Parameters

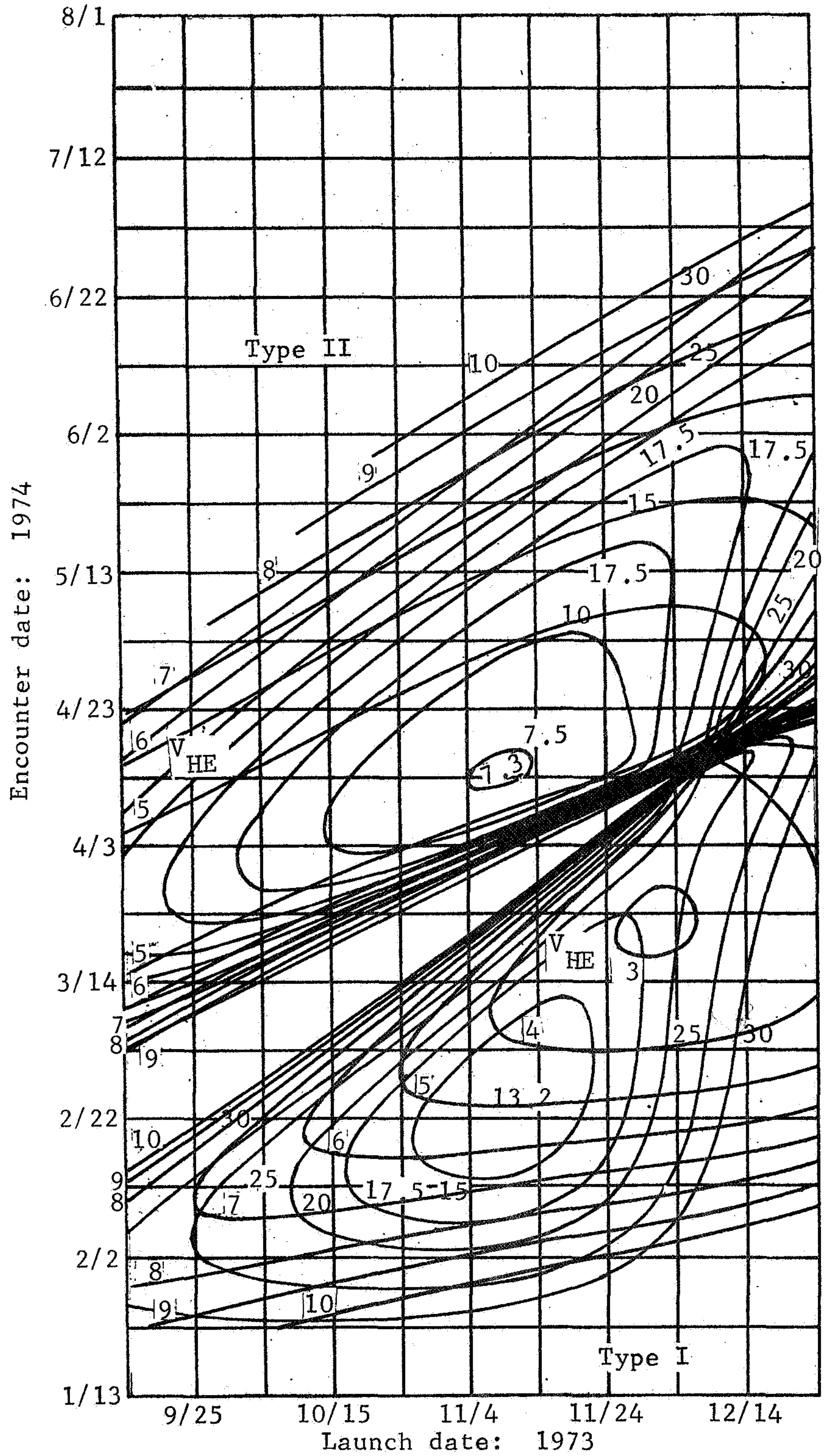

(b) Earth Departure Energy, C_3, km^2/sec^2, and Venus Approach Velocity, V_{HE}, km/sec

Figure 3.- Continued

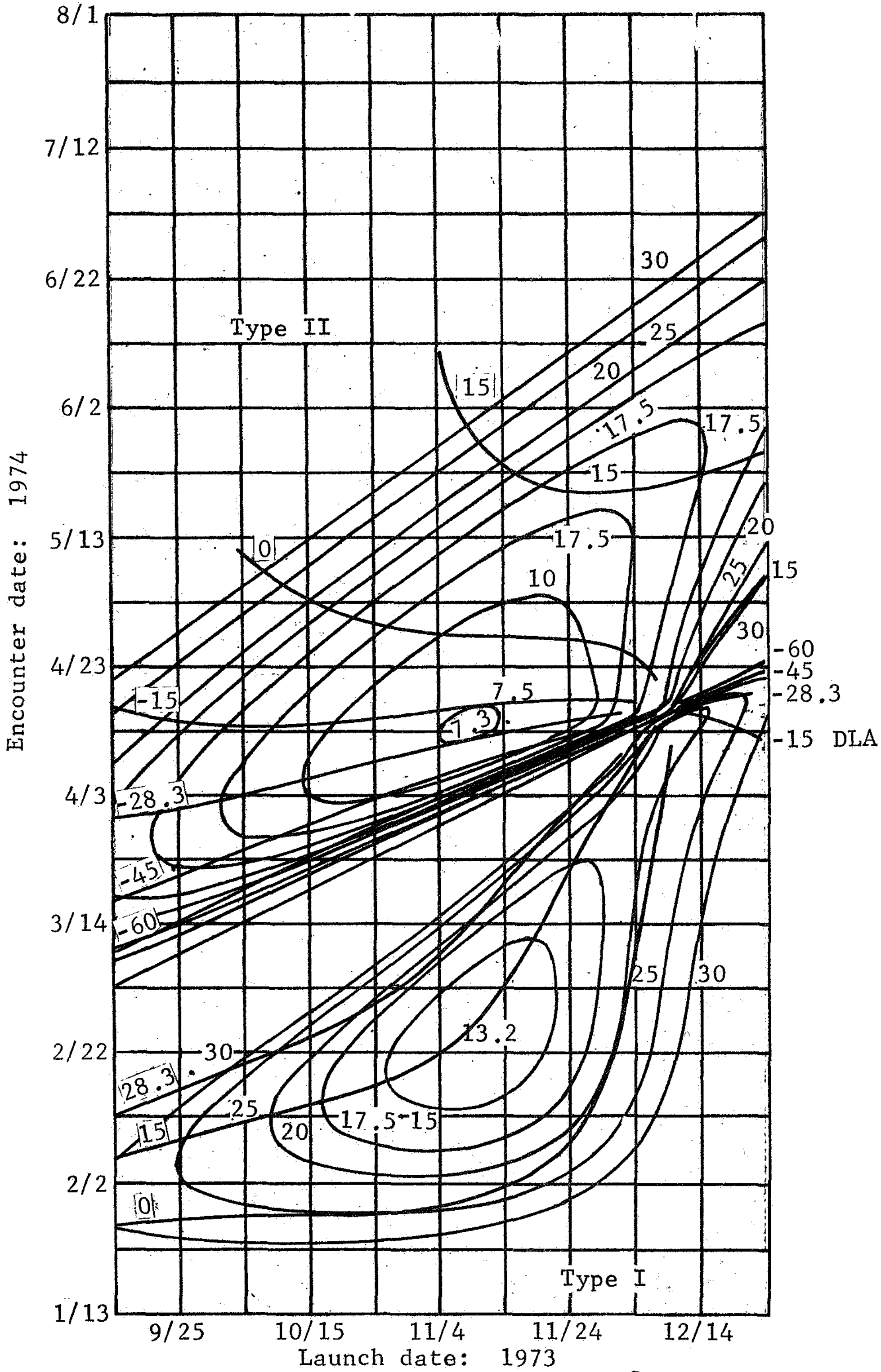

(c) Earth Departure Energy, C_3, km^2/sec^3 and Declination Angle, DLA, Degrees

Figure 3.- Concluded

Figures 2(b) and 3(b) show the Venus approach velocity, V_{HE}. This parameter is akin to the C_3 parameter and is related to Venus approach velocity by:

$$V_{♀} = \sqrt{V_{HE}^2 + \frac{2\mu_{♀}}{r_{♀}}}$$

where:

$\mu_{♀}$ = Venus gravitational constant, 324 860 km^3/sec^2,

$r_{♀}$ = radius from center of Venus, km.

Thus V_{HE} is most important when considering the orbit mode (i.e., orbit insertion ΔV). However, it is also directly related to the BVS entry velocity for the direct entry mode, as is illustrated in figure 4. Typically, an entry velocity of 38 000 fps corresponds to a V_{HE} of approximately 5.5 km/sec. A low V_{HE} is generally desirable on all counts. A V_{HE} less than 6 km/sec is possible for both Type I and II trajectories for both opportunities. The only exception is the Venus swingby to Mercury mission described later in this report.

Figures 2(c) and 3(c) show the declination of the departure asymptote (DLA). This parameter is directly related to launch aximuth requirements.
The following characteristics apply:

1) For $-28.5^\circ \leq$ DLA $\leq 28.5^\circ$, the launch azimuth can be 90° (due east) with a total daily launch window of 6 hr using a maximum launch azimuth of 115°;

2) For $-36^\circ \leq$ DLA $\leq 36^\circ$, the launch azimuth will be 90° to 115° with a minimum 2 hr per day launch window;

3) For $-50^\circ \leq$ DLA $\leq 50^\circ$, the launch azimuth will be 90° to 45° with a minimum 2 hr per day launch window.

DLA within $\pm 36^\circ$ are required for satisfying normal Air Force Eastern Test Range (AFETR) safety limits, with exceptions up to 50° a possibility.

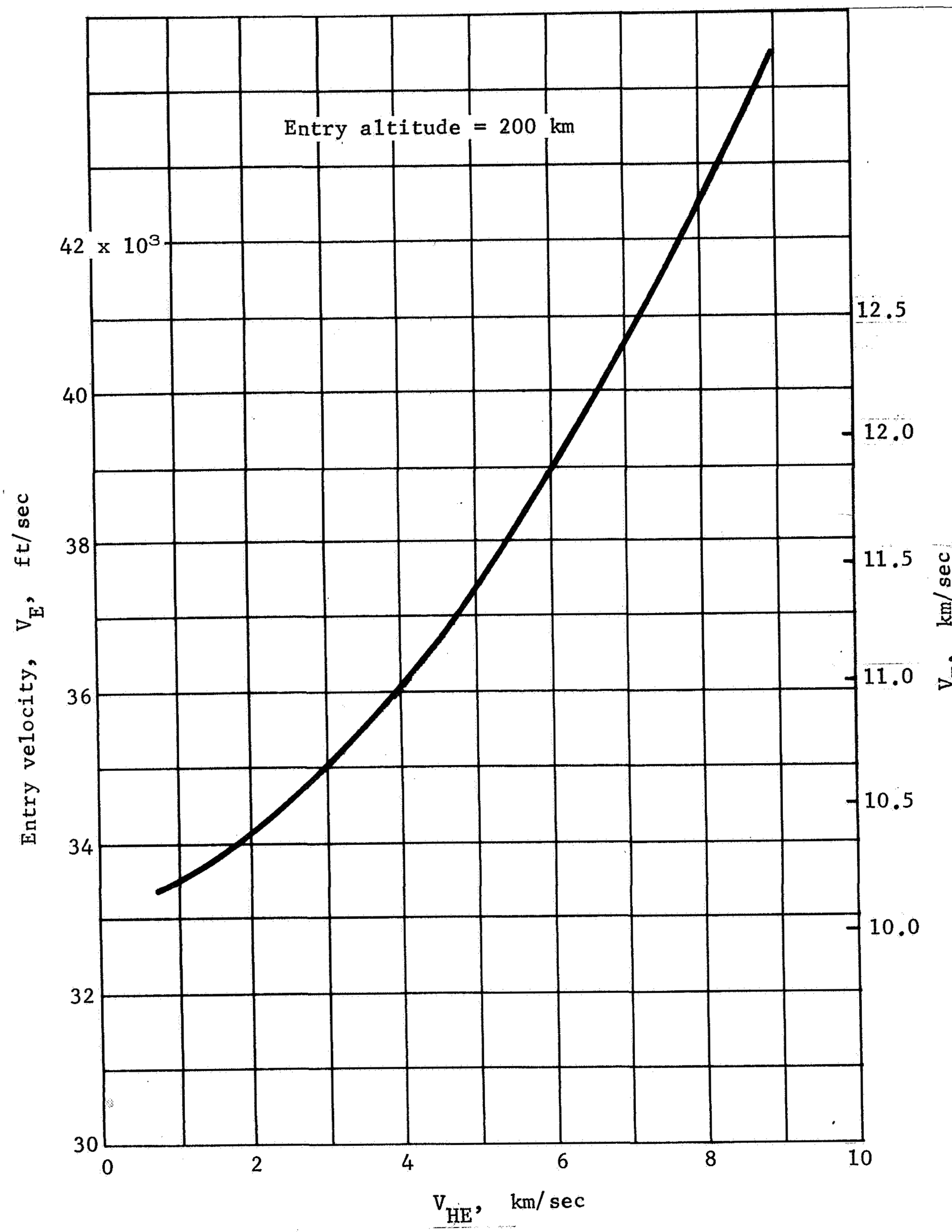

Figure 4.- Venus Entry Velocity vs Hyperbolic Excess Velocity, V_{HE}

Launch vehicle capability.- The preceding data have defined the energy requirements for the 1972 and 1973 Venus opportunities. This will now be related to the launch vehicle capability. The primary data, shown in figure 5, show the total cruise weight after midcourse corrections for three launch vehicles as a function of C_3. Both the TIIIC and SLV3C/C are shown with the Titan IIIC/Centaur, for reference. These data have been corrected for the factors shown in the following tabulation.

	SLV3C/C	TIIIC	TIIIC/C
Earth parking orbit, n. mi.	90	90	100
Launch azimuth, deg	[a]115	115	115
$\Delta V_{L.Az}$, fps	170	170	170
Gravity/maneuver losses, fps	[a]50	50	50
Fixed fairing/adapter weight, lb	[a]133	220	220
Jettisoned fairing weight, lb	Surveyor[a]	1480	1480
Midcourse $\Delta V_{M/C}$, mps	75	75	75
Midcourse $\Delta V_{M/C}$, fps	(246)	(246)	(246)

[a]Assumed included in basic data taken from:

Centaur Monthly Configuration Performances and Weight Status Report. GDC 63-0495-36, May 21, 1966.

Atlas SLV3C/Centaur Information for Mercury-Venus Study. JPL 291 MP-66-1168, June 23, 1966.

The data in figure 5 show the importance of maintaining low values of C_3. The weight shown can be distributed between the spacecraft and BVS capsule system.

The launch vehicle performance capability for the case where the spacecraft goes into Venus orbit is presented in terms of allowable BVS capsule system weight where capsule system weight includes the entry system, deflection propulsion module, capsule to spacecraft adapter, and sterilization canister. The reference orbit used here has a periapsis altitude of 2000 km and an eccentricity of 0.8 (i.e., 2000 x 66 440 km; periapsis by apoapsis altitude).

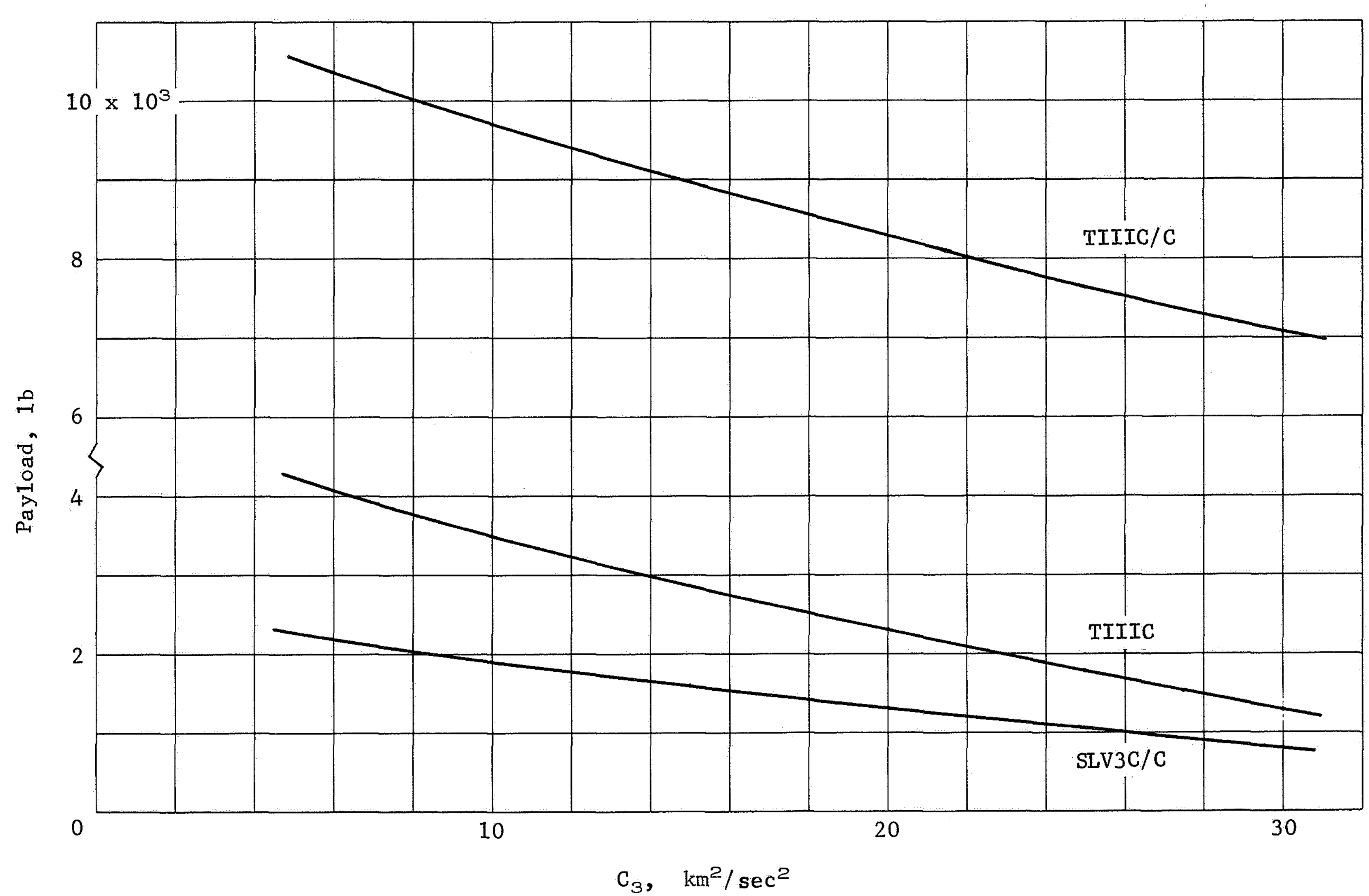

Figure 5.- Launch Vehicle Capability After M/C Correction

Two cases are presented. The first assumes that the total cruise vehicle goes into orbit and the BVS enters from orbit. The performance capabilities of the SLV3C/C, TIIIC, and TIIIC/C for this mode are shown in figures 6,7, and 8, respectively, as a function of C_3 and V_{HE}. The orbit insertion maneuver is calculated using the following assumptions:

1) Specific impulse, I_{sp} = 302 sec;

2) Propellant mass fraction = 0.82;

3) Maneuver losses, ΔV = 5 mps (16.4 fps).

These data assume an orbiter useful weight (excluding the orbit insertion propulsion module) of 661 lb.* In this case, greater orbiter weights result in lower capsule system weights on one-for-one pound basis.

The second set of data assumes that the capsule system is deflected from the approach trajectory before the spacecraft orbit insertion maneuver. The allowable capsule system weight for each of the launch vehicles is shown in figures 9, 10, and 11 for the SLV3C/C, TIIIC, and TIIIC/C, respectively. The assumed useful orbiter weight for these data is 1010 lb. The data can be corrected to other orbiter weights with the use of the sensitivity data shown in figure 12.

The above data are summarized in table 1 for a typical design $C_3 = 10\ km^2/sec^2$ and $V_{HE} = 5$ km/sec. These data show that the SLV3C/C is not particularly suitable for the orbiting spacecraft mission. In addition, the performance gains achievable by using the entry from approach mode make this an obvious choice on a strictly performance basis. Other factors, discussed below, must be considered before a decision can be made. These factors include communication link geometry and entry environment considerations.

---

*Study of Applicability of Lunar Orbiter Subsystems to Planetary Orbiters. NASA CR-66302. The Boeing Company, March 15, 1967.

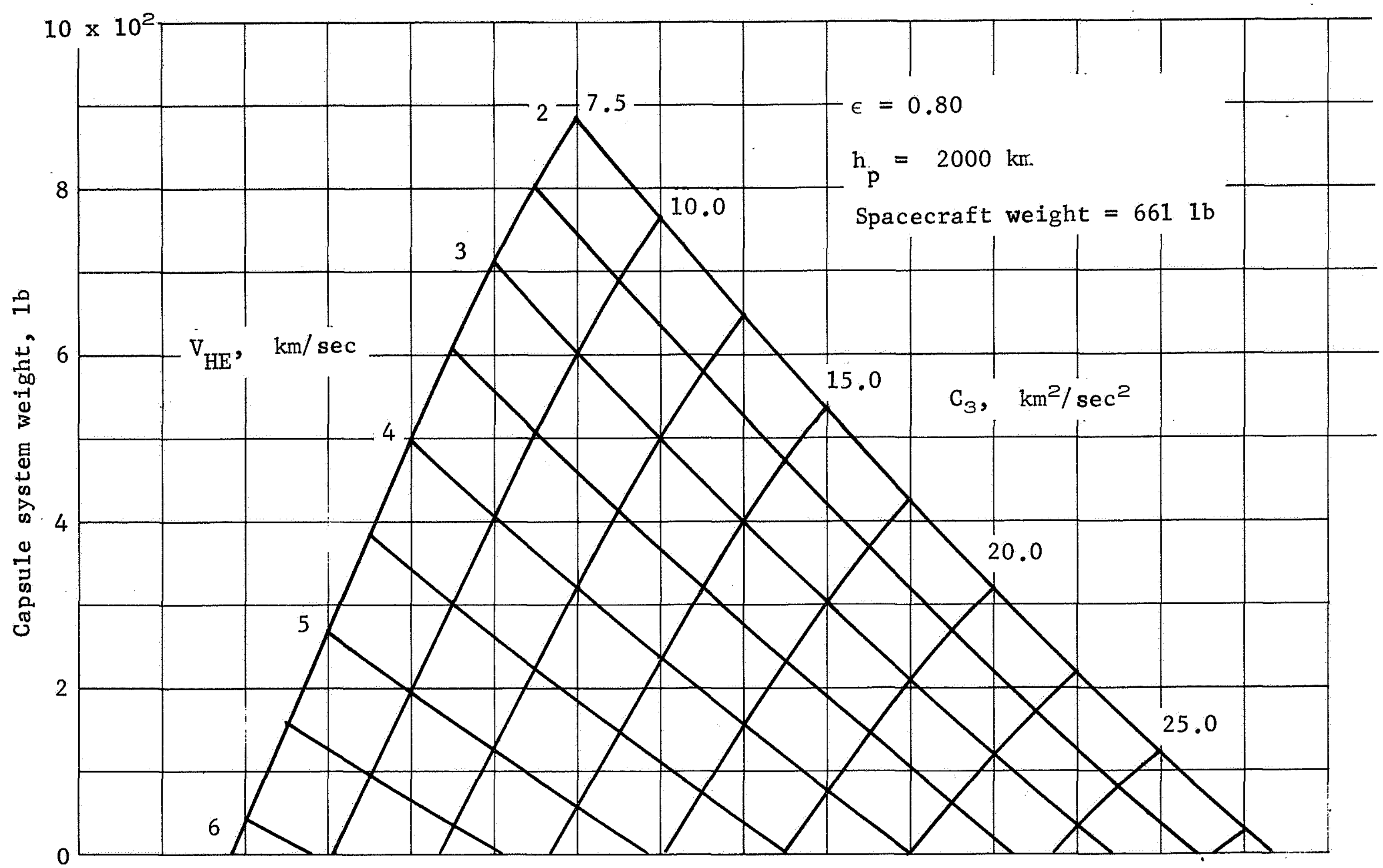

Figure 6.- SLV3C/C Performance Capability to Venus, Entry from Orbit

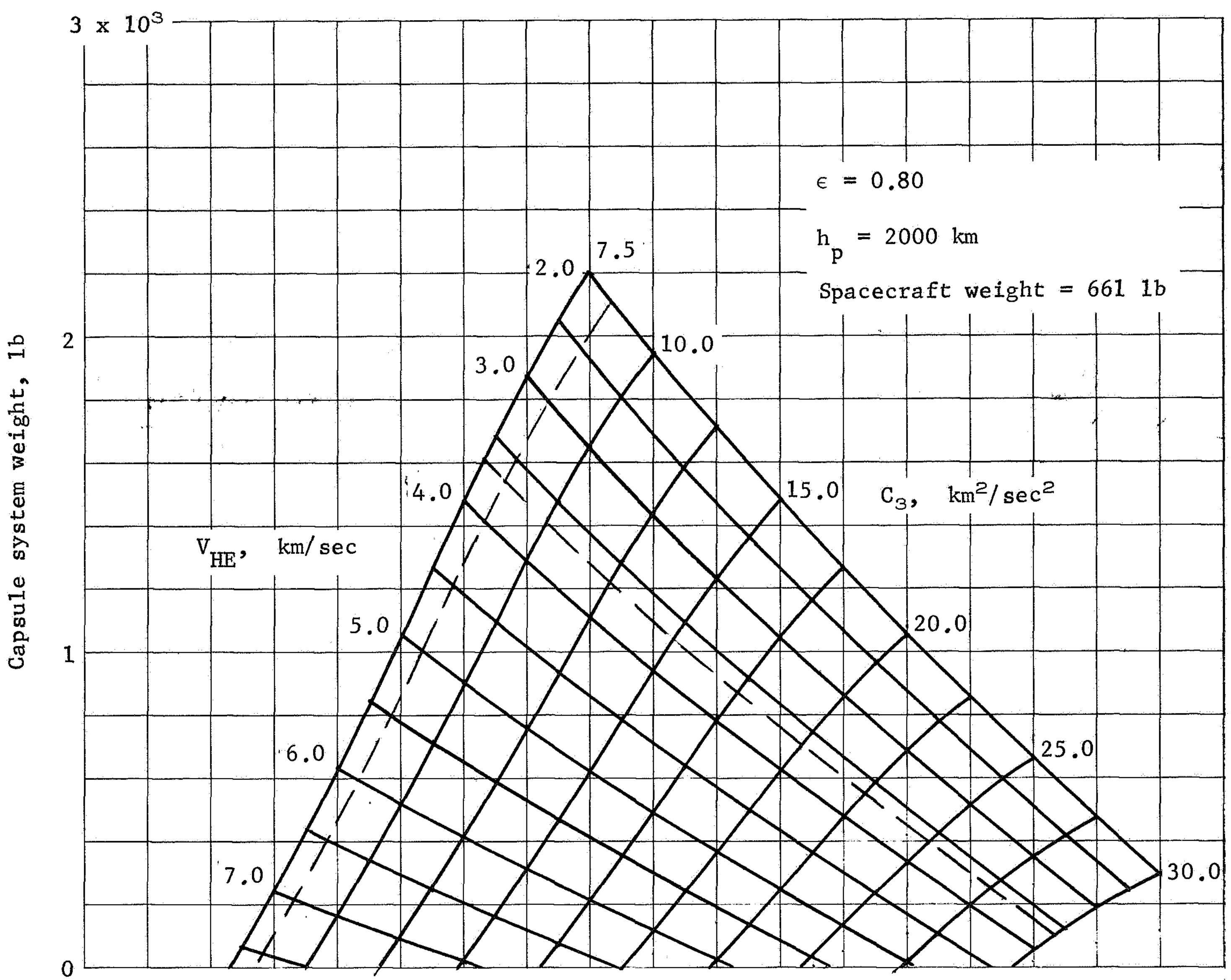

Figure 7.- TIIIC Performance Capability to Venus, Entry from Orbit

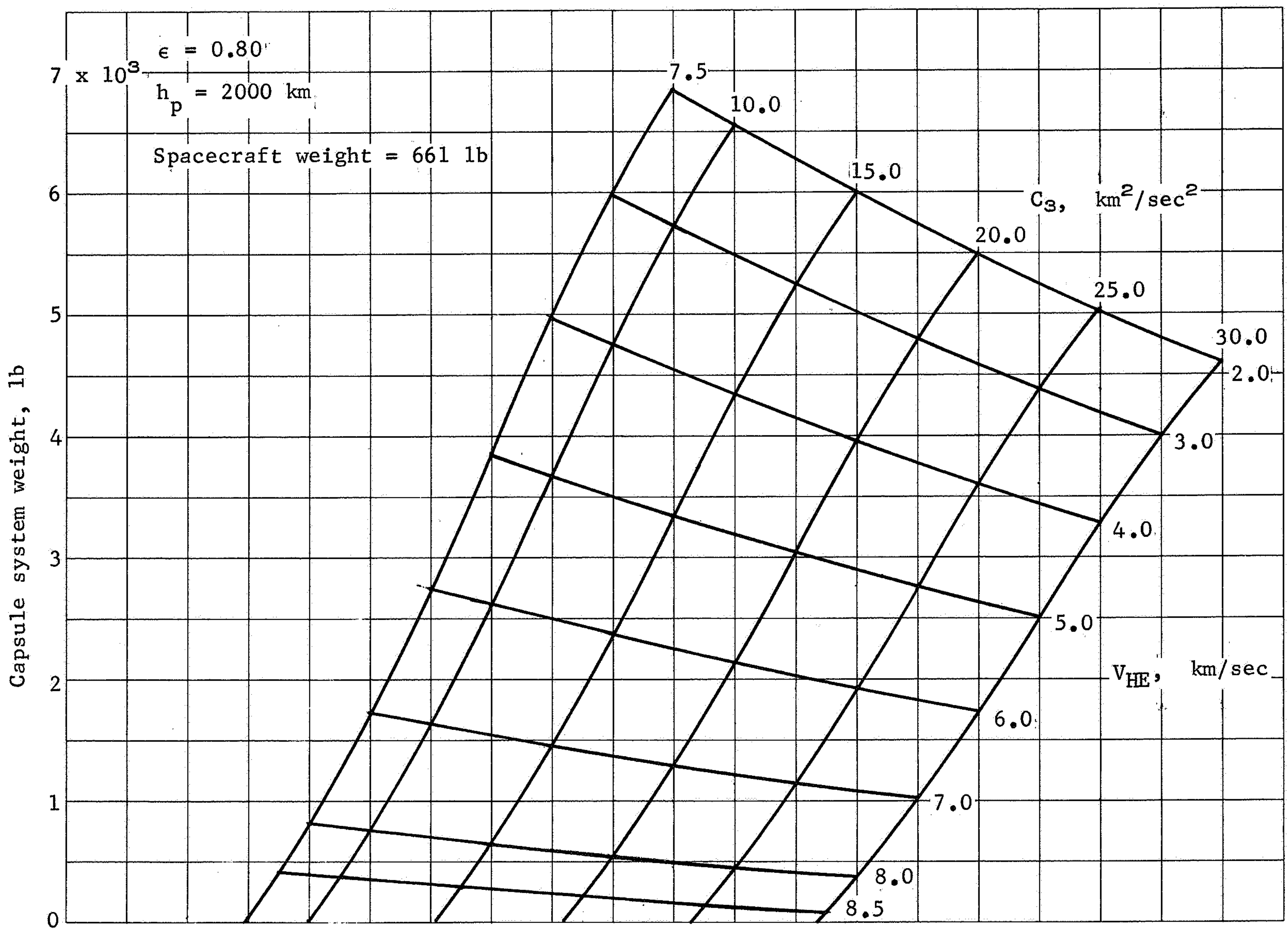

Figure 8.- TIIIC/C Performance Capability to Venus, Entry from Orbit

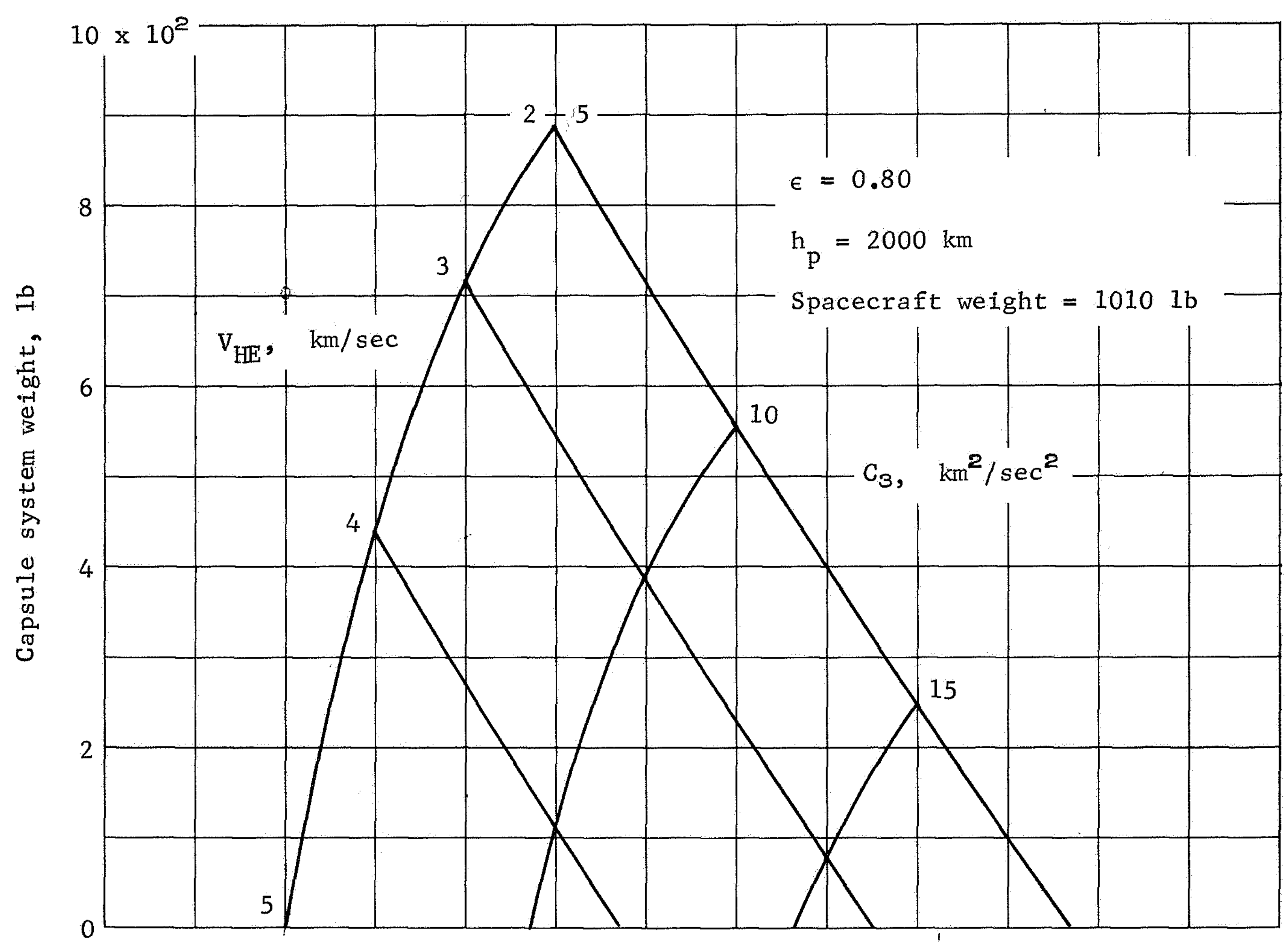

Figure 9.- SLV3C/C Performance Capability to Venus, Entry from Approach

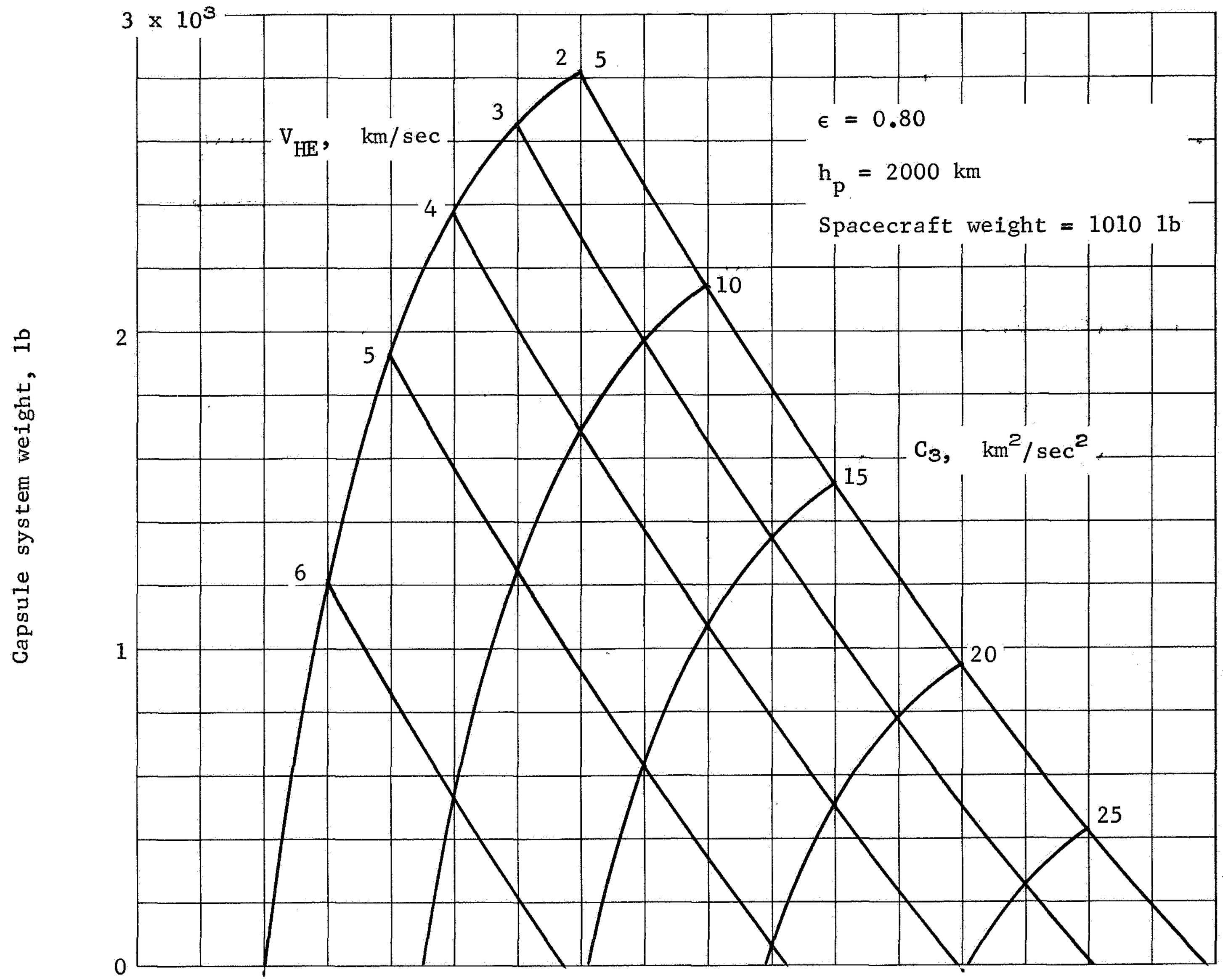

Figure 10.- TIIIC Performance Capability to Venus, Entry from Approach

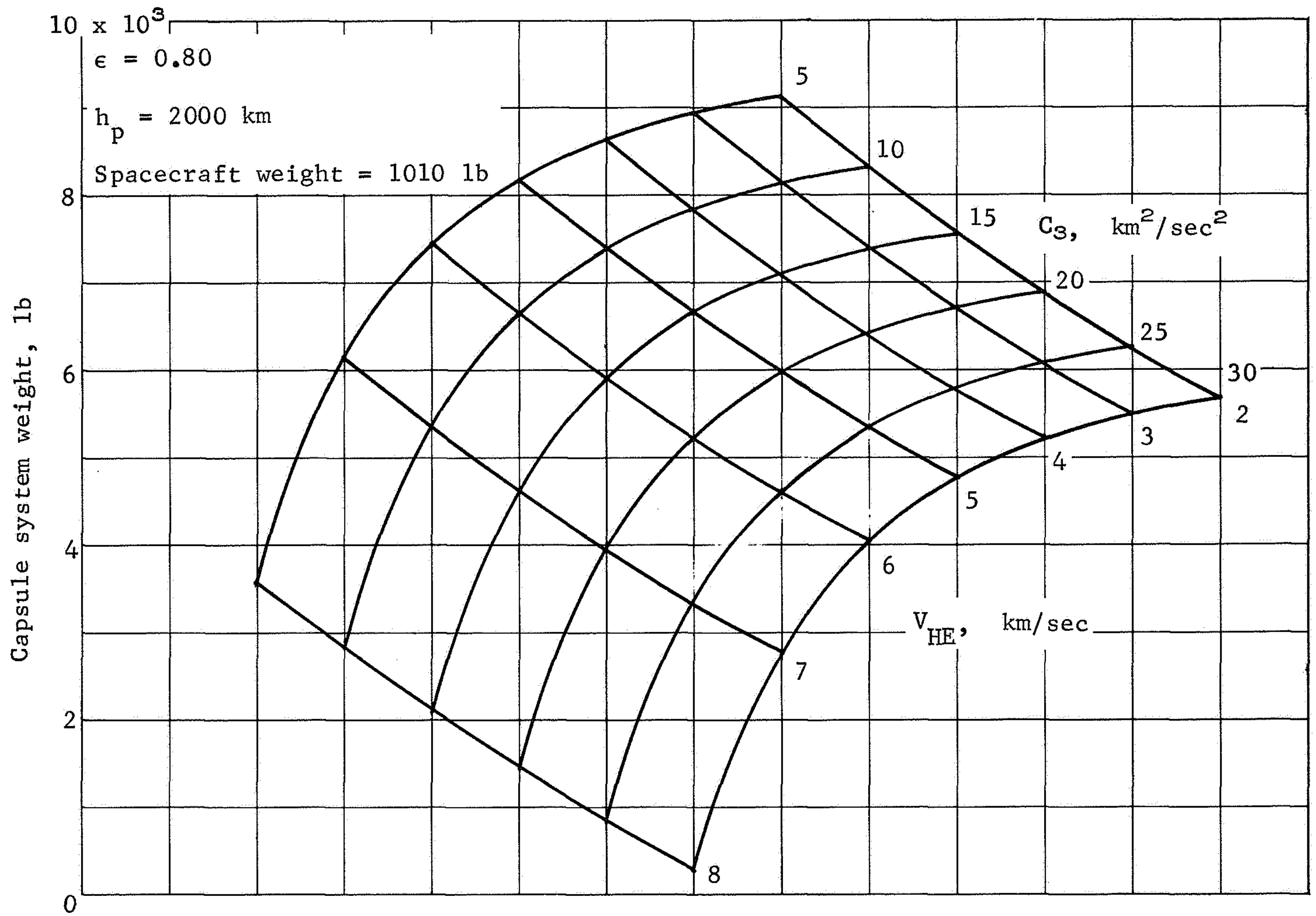

Figure 11.- TIIIC/C Performance Capability to Venus, Entry from Approach

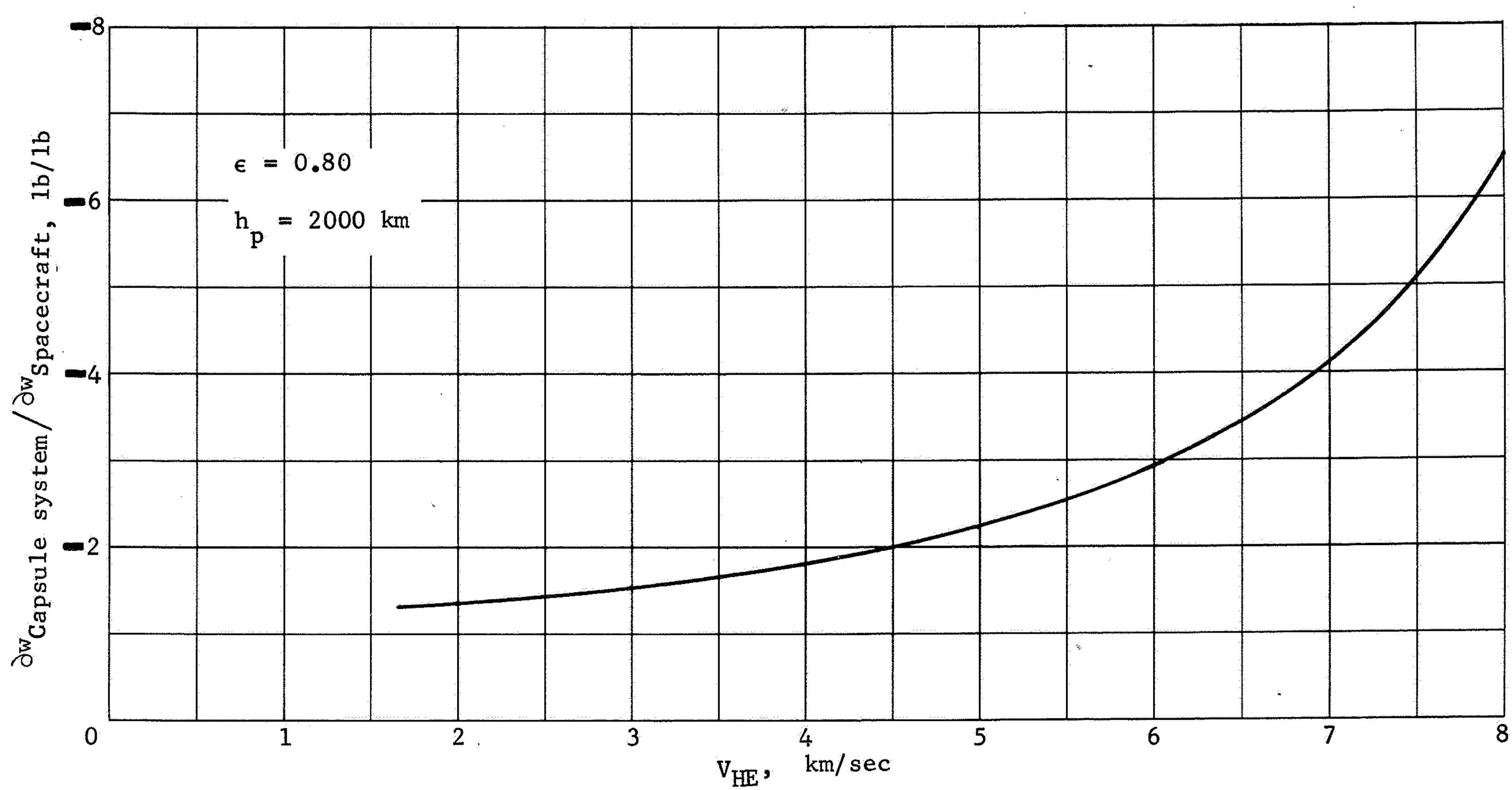

Figure 12.- Weight Sensitivity, Capsule System to Spacecraft

TABLE 1.- ALLOWABLE CAPSULE SYSTEM WEIGHT

Vehicle	Entry from orbit weight, lb		Entry from approach weight, lb	
	Orbiter	Capsule System	Orbiter	Capsule System
SLV3C/C	661	194	[a]661	510
TIIIC	661	905	1010	1240
TIIIC/C	661	3670	1010	7380
Orbit: h_P = 2000 km, ϵ = 0.8 C_3 = 10 km^2/sec^2 V_{HE} = 5 km/sec				
[a]Cannot achieve mission at 1010 lb.				

Direct Mode Targeting

In-plane.- The targeting analysis determines the required ejection ΔV to deflect the BVS/entry vehicle onto an entry trajectory with a required entry flight path angle, γ_E. Only near-side ejections in the plane of the approach trajectory are considered in this section. The relative geometry between the support spacecraft and BVS/entry vehicle during entry must be such that a relay link is possible up to subsonic probe impact. A spin-stabilized attitude control system is used for the BVS/entry vehicle after ejection. The ejection maneuver must be made such that the capsule angle of attack at entry, α_E, is less than about 20°. The targeting analysis also determines the influence of launch date/arrival date combination and γ_E on the possible declination and right ascension on Venus at which the BVS may be deployed. Finally, the targeting analysis considers the dispersion in γ_E due to navigation uncertainty at the time of ejection and due to execution errors in the ejection maneuvers.

The relative geometry between the spacecraft and BVS/entry vehicle at entry is shown in figure 13. The entry altitude is taken to be 200 km above the surface of Venus.

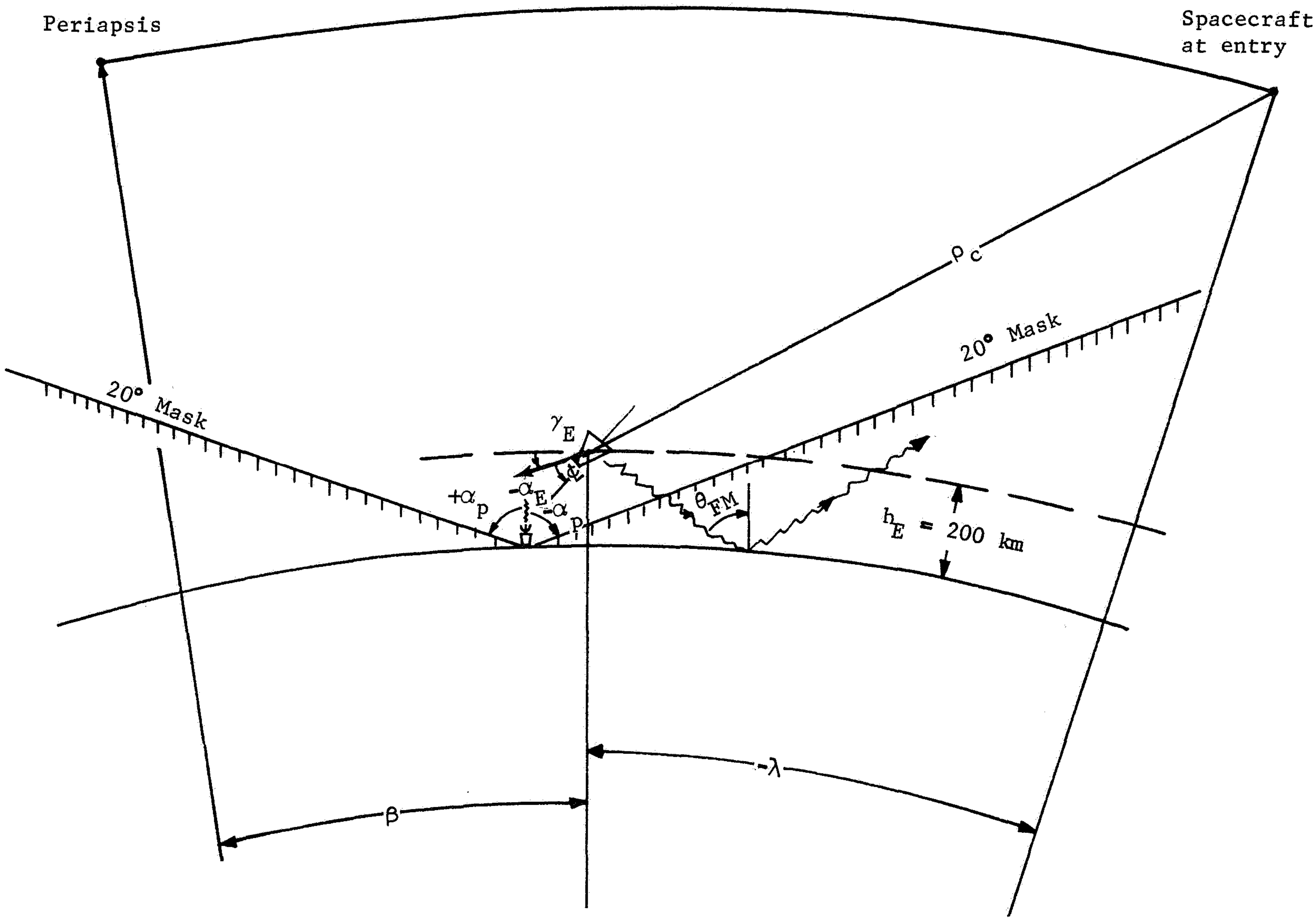

Figure 13.- Planet Approach Geometry Definition

The BVS/entry vehicle at entry is located with respect to the spacecraft periapsis by the angle β. The central angle between the BVS/entry vehicle and spacecraft at entry is termed the spacecraft lead angle, λ. The λ is negative if the spacecraft lags the BVS/entry vehicle at the time of entry. Also shown at entry are the communication distance, ρ_C, and the fading margin parameter, θ_{FM}. Significant multipath losses occur when θ_{FM} is greater than 60°. The spacecraft lead angle must be selected so that the spacecraft is above a 20° elevation mask at the time of probe impact. This is equivalent to requiring a probe antenna aspect angle, α_p, less than 70°. The ballistic coefficient of the probe is selected to result in a time from entry to probe impact of 30 minutes.

For a given entry location, β, the spacecraft lead angles corresponding to the parameters above can be determined. An example for a hyperbolic excess velocity of 5.0 km/sec and a spacecraft periapsis altitude of 2000 km is given in figure 14. Communication distances at entry of 10 000 and 15 000 km are shown. The difference between an elevation mask at touchdown of 20 and 34° is illustrated. The entry location is directly a function of the design entry flight path angle, γ_E. The β corresponding to γ_E between -20 and -40° are shown. For a given γ_E then the λ must be such that α_p is between ±70°. For example, a γ_E of -30° requires λ between -39.5 and -63.5° to have the probe impact in view of the spacecraft. To have short communication distances at entry, to reduce losses due to multipath, and to keep the ΔV_{EJ} as low as possible, the λ selected for the ejection maneuver strategy corresponds to the α_p equal to a 70° line. The fading margin boundary restricts γ_E shallower than -25°. Similar boundaries have been constructed for h_p of 1000 and 3000 km and V_{HE} of 3 and 7 km/sec. An increase in periapsis altitude of 1000 km decreases the λ required for an α_p of 70° by about 8°. An increase in V_{HE} of 2.0 km/sec decreases the λ required for an α_p of 70° by about 2°.

The entry location is a function of V_{HE} as well as γ_E as shown in figure 15. The curves shown are for an h_p of 2000 km. A decrease in h_p of 1000 km increases β by 2°.

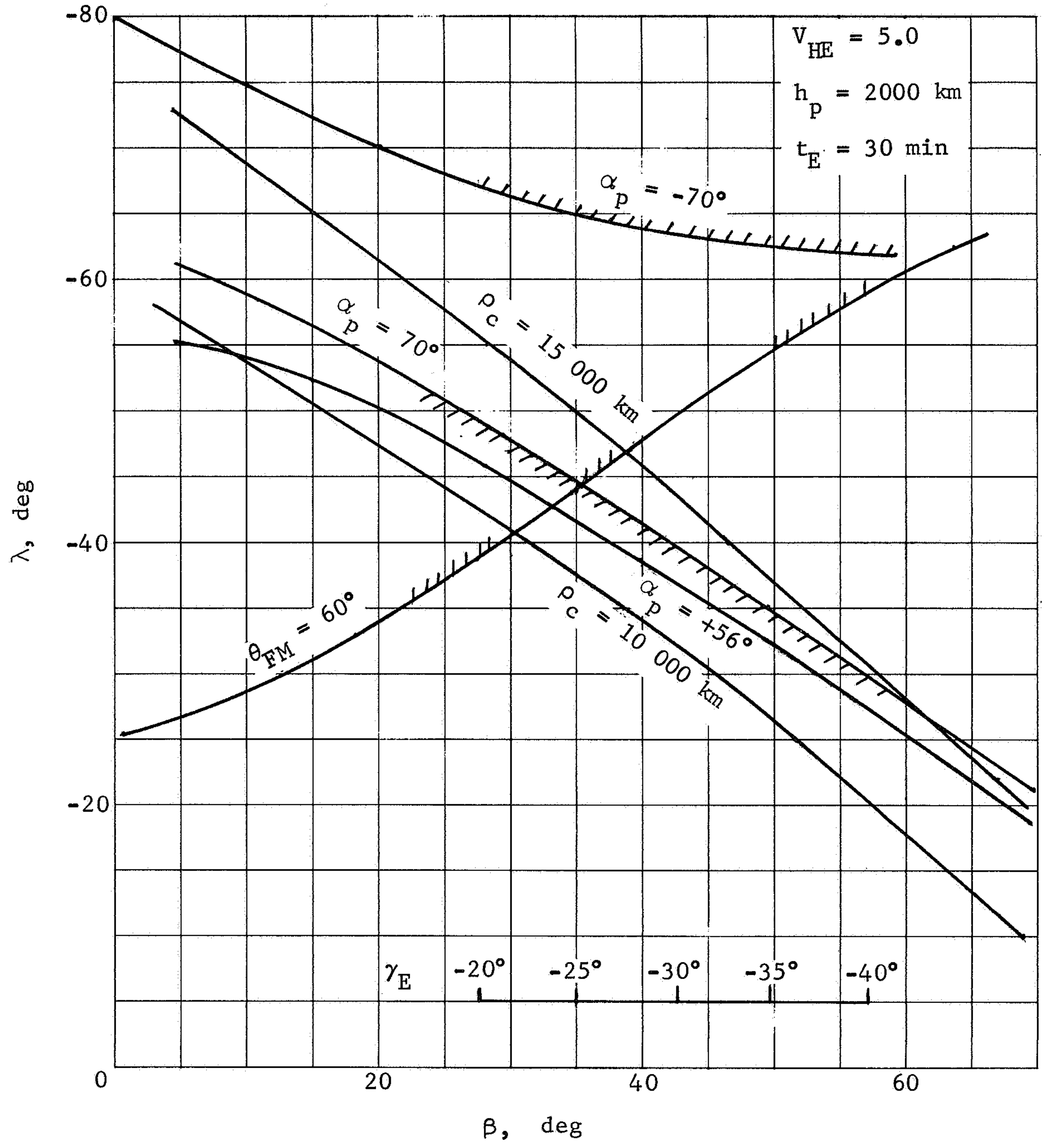

Figure 14.- β / λ Boundaries, Entry from Approach

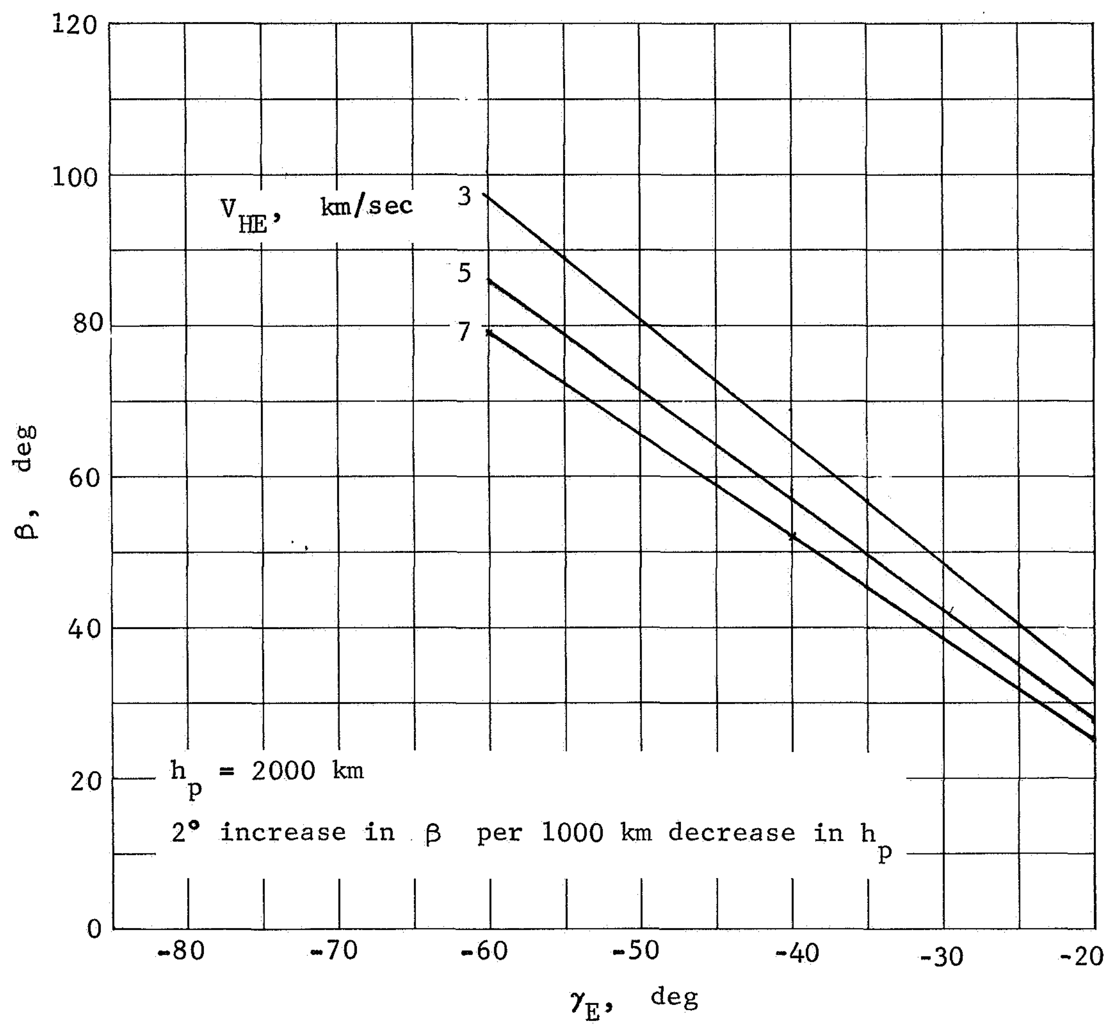

Figure 15.- β / γ_E Relationship

The ΔV_{EJ} required to give an α_P of 70° is shown in figure 16 as a function of V_{HE} and γ_E. The spacecraft periapsis altitude is 1000 km and the distance from Venus at which ejection occurs is 1×10^6 km.

Only data for R_{EJ} of 1.0×10^6 km need be shown since the ΔV_{EJ} is inversely proportional to R_{EJ} for R_{EJ} greater than about 100 000 km. Therefore, if ΔV_o is the ejection ΔV for an R_{EJ} of 1.0×10^6 km, and if R_{EJ} is any ejection distance, in millions of km, the ΔV at this R_{EJ} is ΔV_o R_{EJ}.

The ΔV_{EJ} in figure 16 is seen to increase with both increasing V_{HE} and γ_E. The effect of higher h_p is seen in figures 17 and 18. For a V_{HE} of 3.0 km/sec, increasing h_p increases ΔV_{EJ} slightly. For example, with a γ_E of -30° increasing h_p from 1000 to 3000 km increases the ΔV_{EJ} from 18 to 24 m/sec. For a V_{HE} above about 5.0 km/sec increasing h_p decreases ΔV_{EJ}. For example, with a γ_E of -30° and a V_{HE} of 7.0 km/sec the ΔV_{EJ} decreases from 73 to 44 m/sec as h_p increases from 1000 to 3000 km. For a V_{HE} of 5.0 km/sec the corresponding decrease is from 40 to 33 m/sec. The change in ΔV_{EJ} with h_p is seen to be nonlinear. A change in h_p from 1000 to 2000 km results in a larger variation in ΔV_{EJ} than a change from 2000 to 3000 km.

The angle of attack at entry assuming a BVS/entry vehicle spin stabilized in the ΔV_{EJ} direction is shown as a function of V_{HE} and γ_E in figure 19 for an h_p of 1000 km.

The effect of higher h_p, as shown in figures 20 and 21, is to increase the α_E negatively. For a V_{HE} of 5.0 km/sec and a γ_E of -30° the α_E increases negatively from +2.0 to -34° as h_p increases from 1000 to 3000 km. The α_E is directly a function of the ejection angle, τ_{EJ}. This is the angle between the velocity vector of the spacecraft at the time of ejection and the ΔV_{EJ}, and is defined negatively.

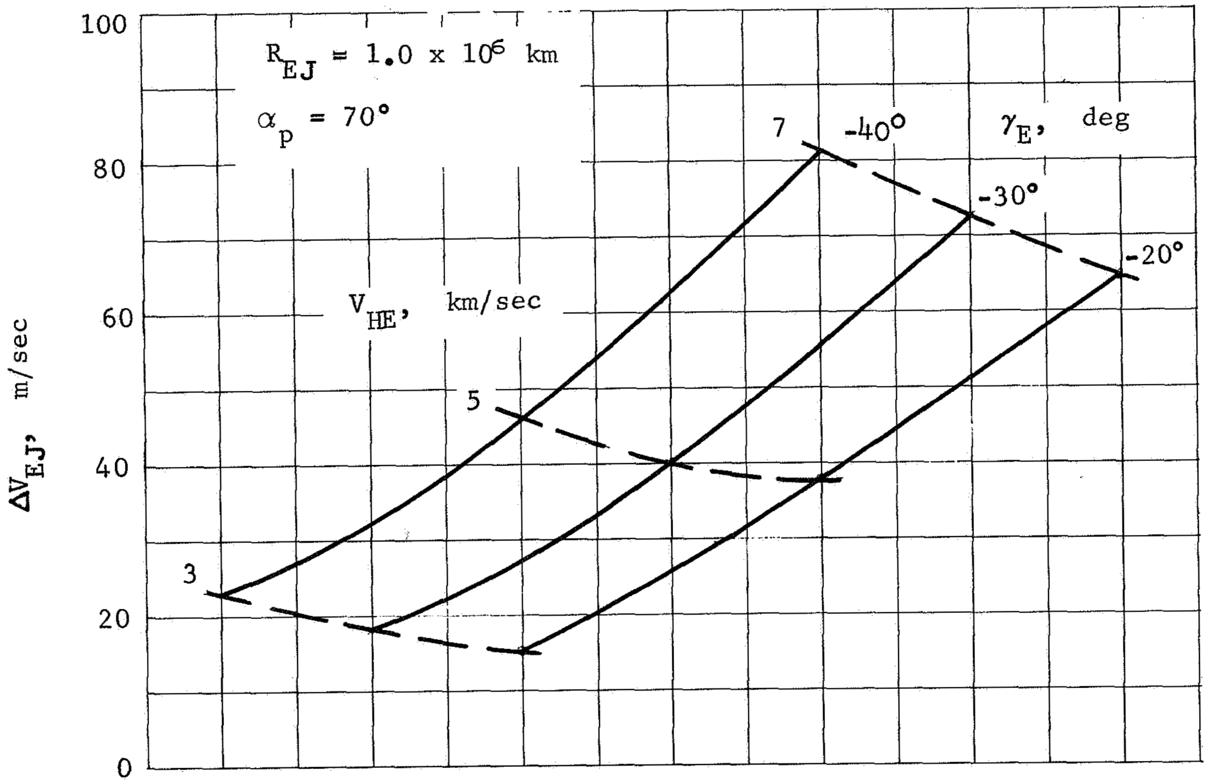

Figure 16.- ΔV_{EJ} as a Function of γ_E and V_{HE} (h_p = 1000 km)

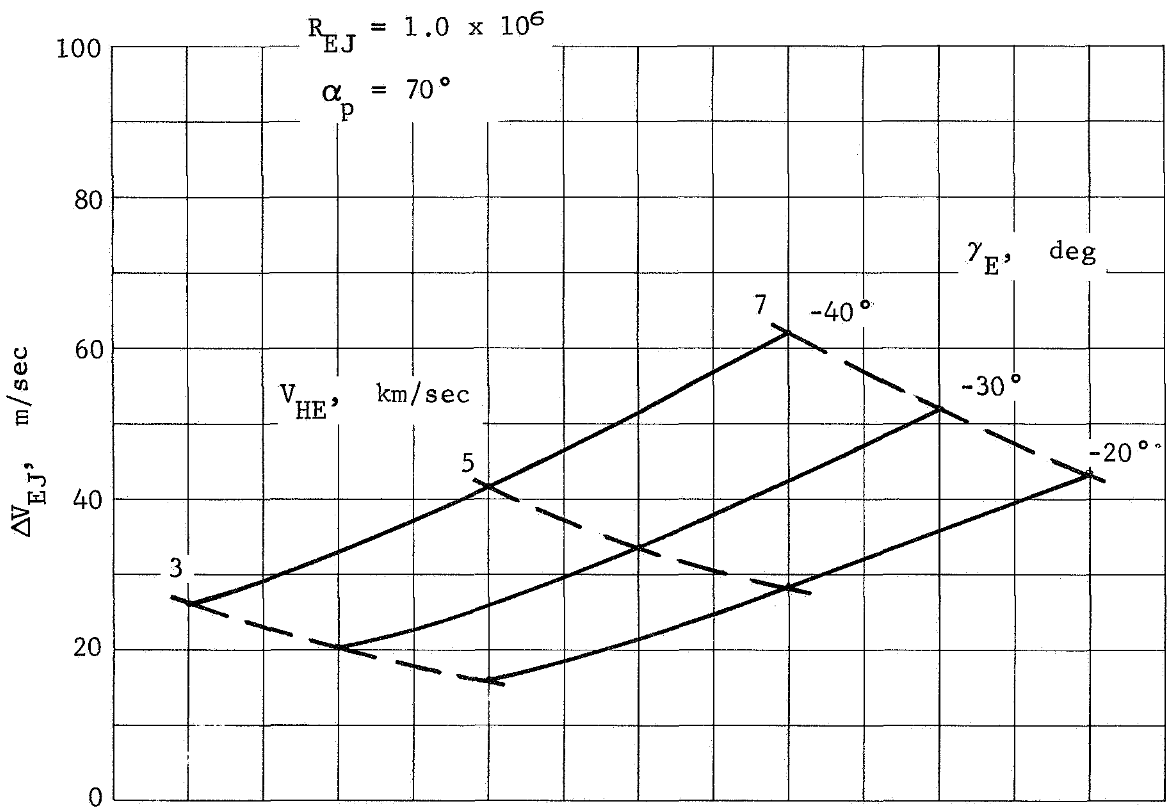

Figure 17.- ΔV_{EJ} as a Function of γ_E and V_{HE} (h_p = 2000 km)

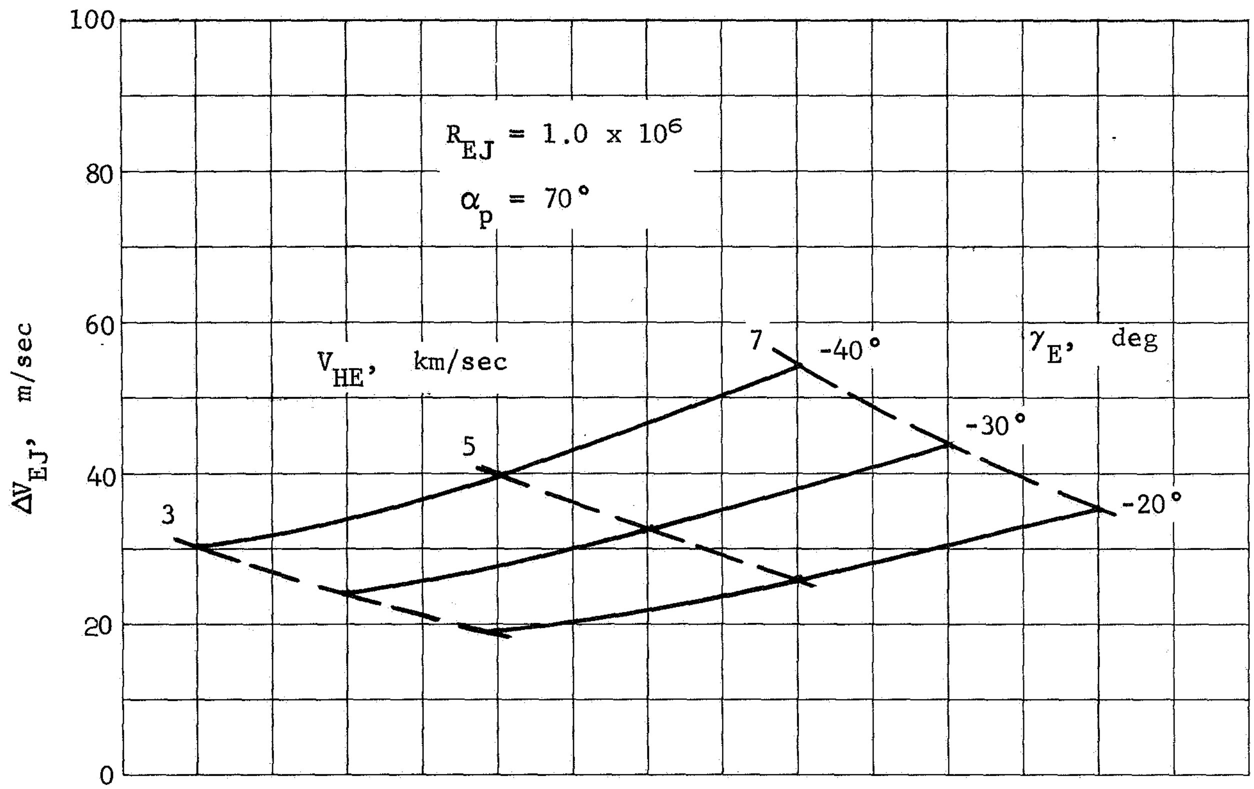

Figure 18.- ΔV_{EJ} as a Function of γ_E and V_{HE} (h_p = 3000 km)

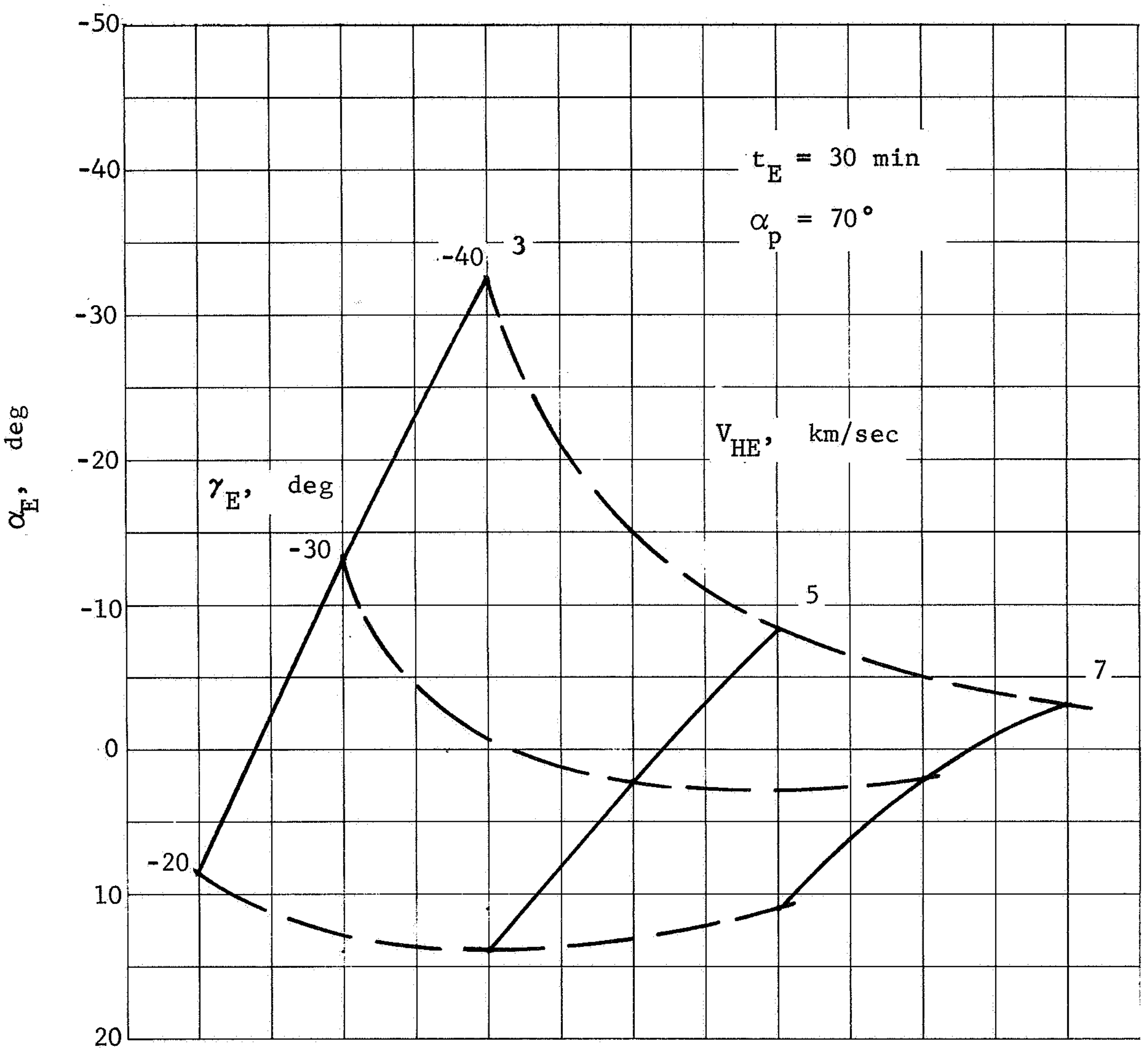

Figure 19.- α_E as a Function of γ_E and V_{HE} (h_p = 1000 km)

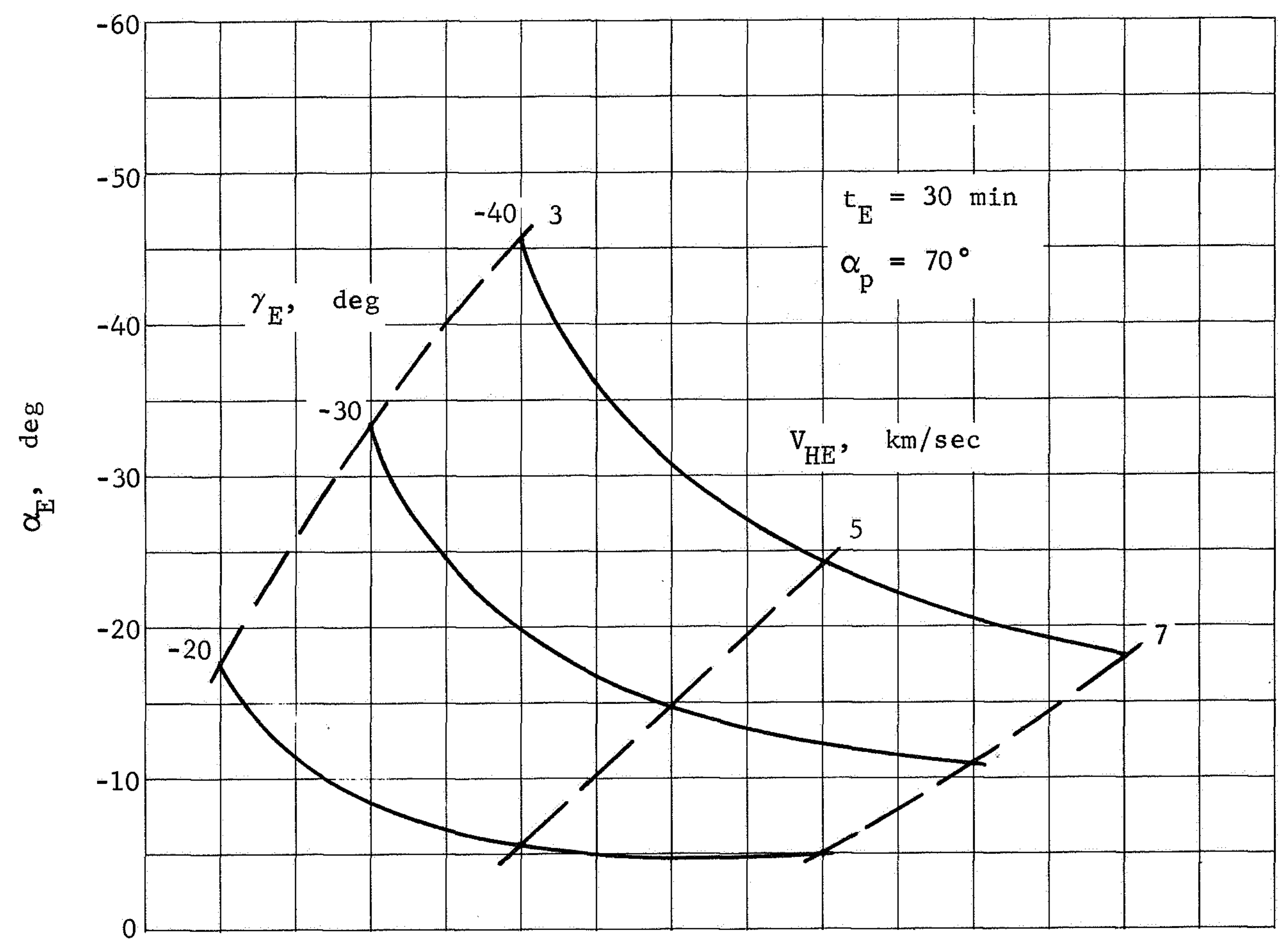

Figure 20.- α_E as a Function of γ_E and V_{HE} (h_p = 2000 km)

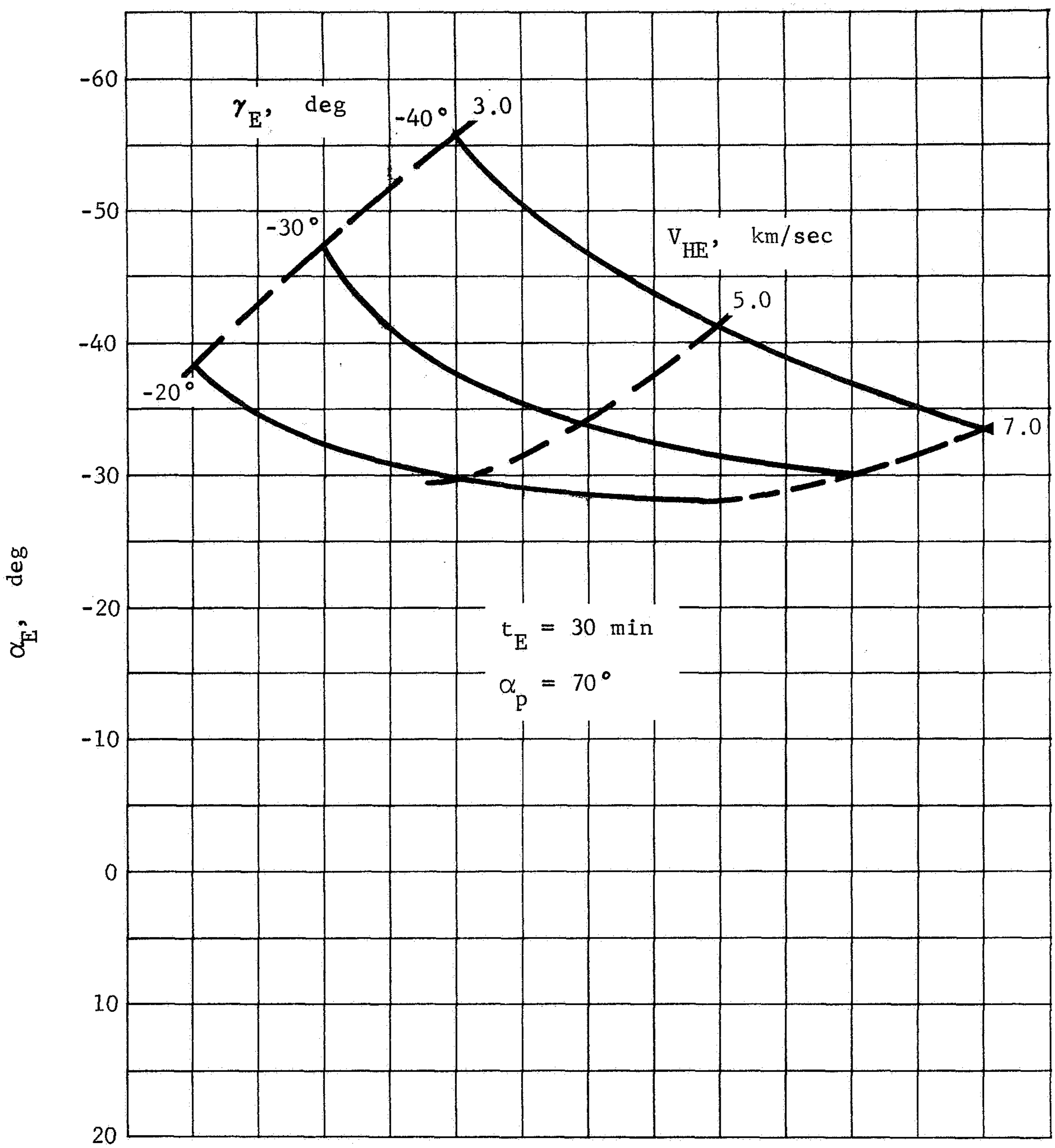

Figure 21.- α_E as a Function of γ_E and V_{HE} (h_p = 3000 km)

A τ_{EJ} of about -90° corresponds to minimum ΔV_{EJ}, but the resulting λ is less than the α_P of 70°. The higher the h_p the more negative the τ_{EJ}, and in turn, the more negative the α_E. The data shown in figures 19 thru 21 are independent of R_{EJ}, again for R_{EJ} greater than 100 000 km. With a V_{HE} of 5.0 km/sec the h_p should not be above 2300 km to keep the α_E less than -20°.

The BVS/entry vehicle coast time, time from ejection to entry, is directly proportional to R_{EJ}. It is shown as a function of V_{HE} in figure 22 for an R_{EJ} of 1.0×10^6 km. The coast time is independent of γ_E or h_p to within a few tenths of an hour.

The downrange angle traversed through the atmosphere during entry is only a few degrees so that the location of BVS deployment with respect to the spacecraft periapsis is approximately equal to β. The β variation with γ_E, V_{HE}, and h_p is shown in figure 15. The location of spacecraft periapsis with respect to the hyperbolic excess velocity is given by the angle τ_o as shown in figure 23. The entry location with respect to V_{HE}, φ_L, is the sum of β and τ_o. The change in τ_o with h_p is equal and opposite the change in β with h_p. Thus, the BVS deployment location with respect to the hyperbolic excess velocity vector is only dependent on γ_E and V_{HE}. For example, with a γ_E of -30° and a V_{HE} of 5.0 km/sec the BVS deployment occurs 94.5° from the hyperbolic excess velocity vector.

The next step in identifying possible locations of the BVS above the Venusian surface is to determine the V_{HE} position as a function of launch date/arrival date combinations. The V_{HE} positions are shown for the 1972-I opportunity in figure 24. Arrival dates between July 17 and August 6, 1972, and launch dates between March 24 and April 23, 1972, are shown.

The right ascension is measured in the Venusian orbital plane from the ascending node of the Venusian orbital plane on the ecliptic plane. Recent observations have shown that the Venusian equator is inclined less than a degree to the Venusian orbital plane.

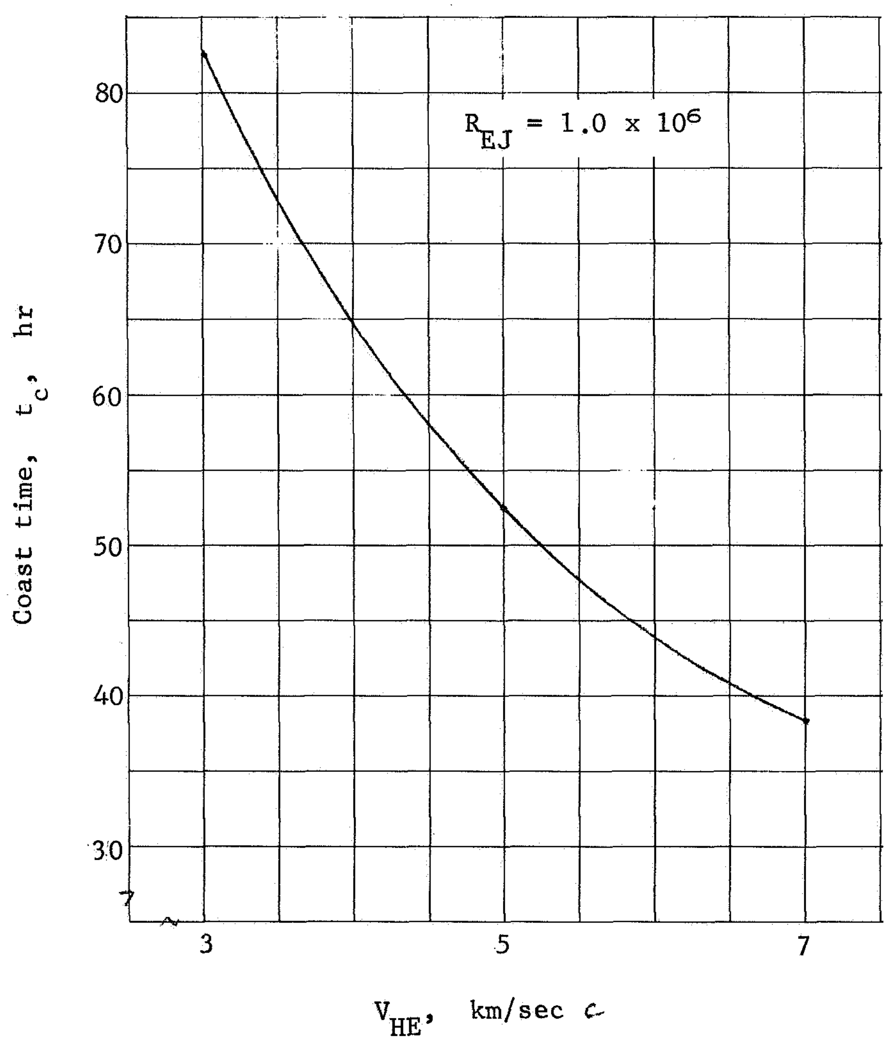

Figure 22.- Coast Time vs V_{HE}

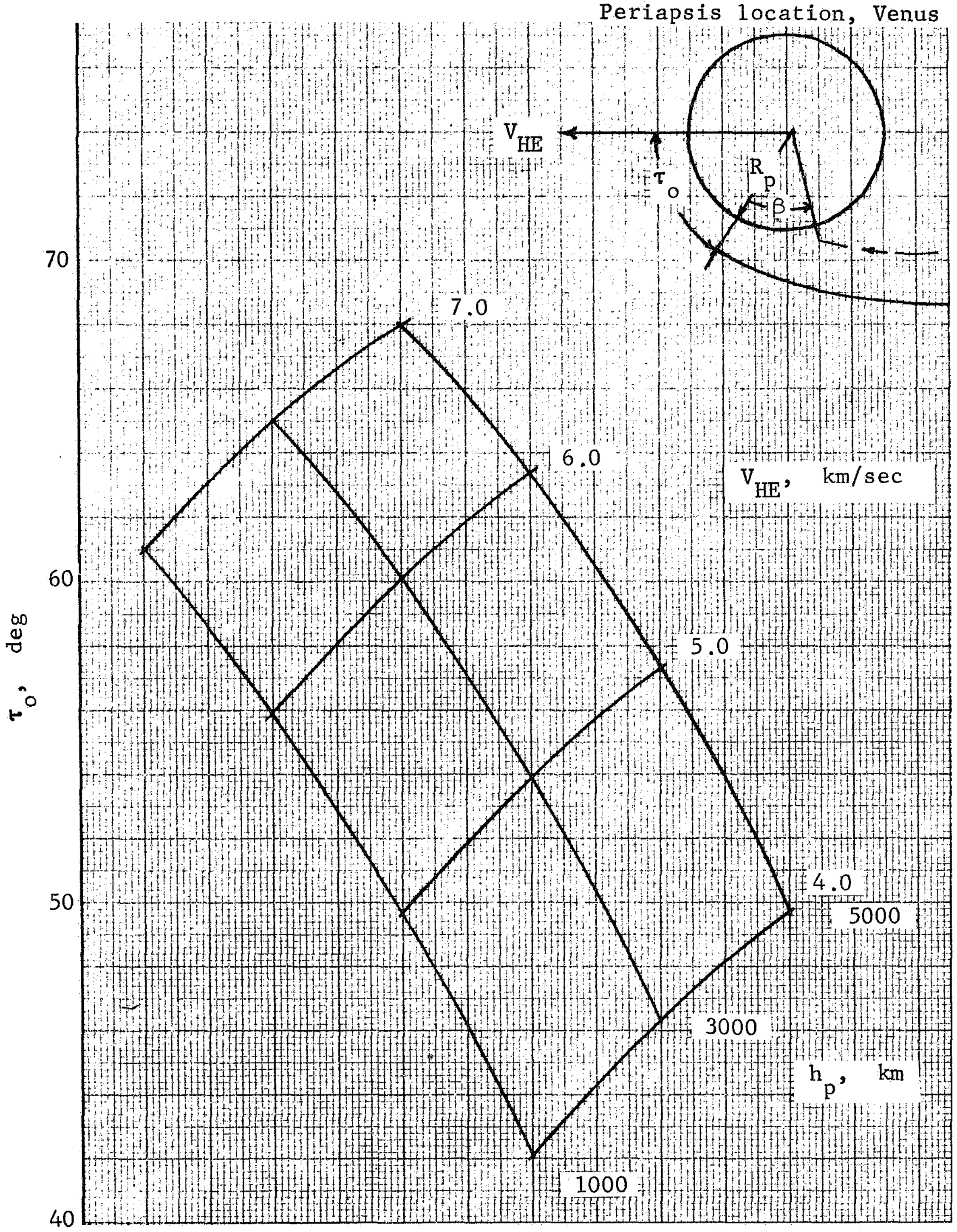

Figure 23.- Periapsis Angle, τ_o, vs h_p and V_{HE}

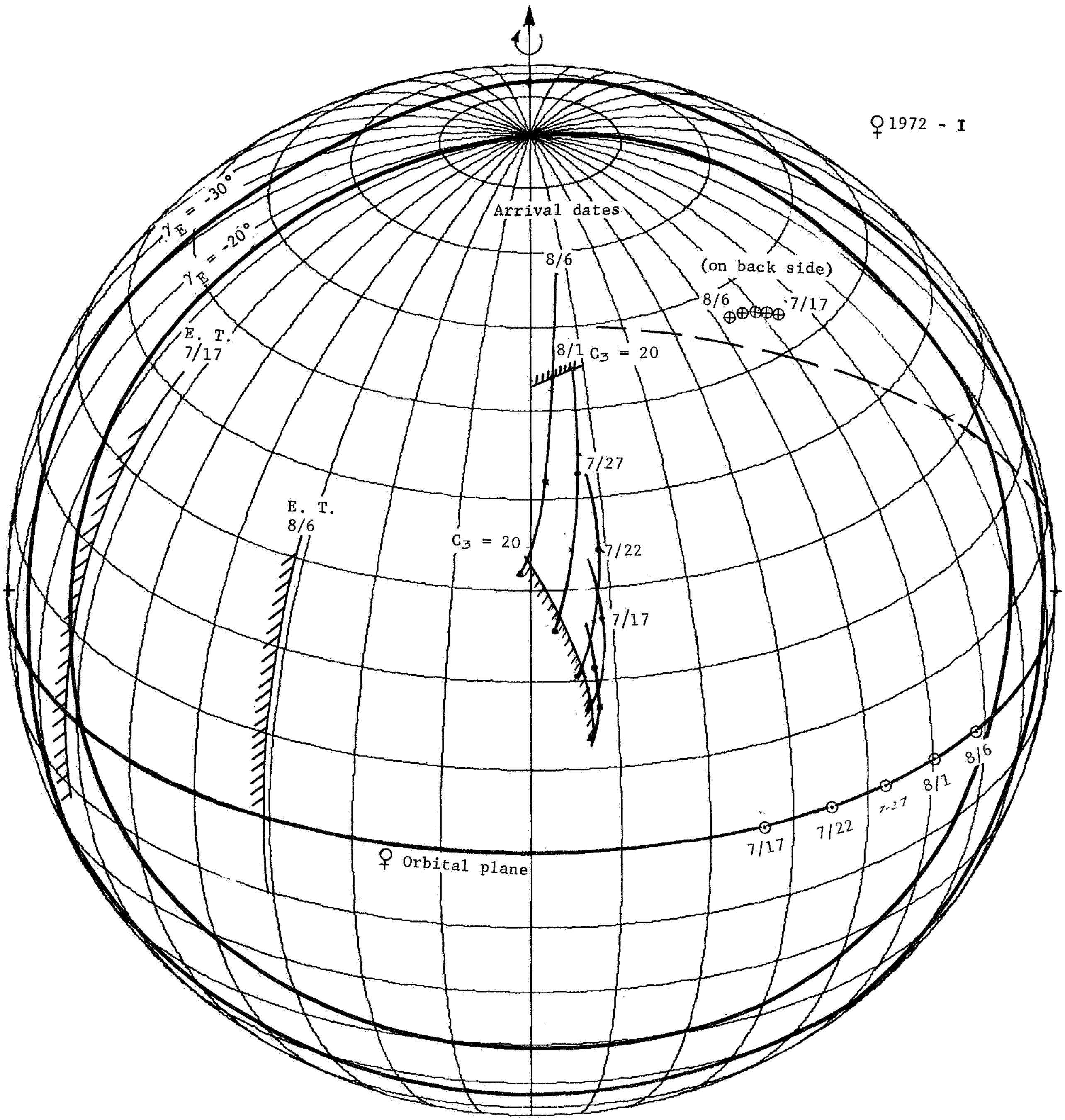

Figure 24.- Venus Targeting Map, 1972, Type I, 30° View

The declination is also measured with respect to the Venusian orbital plane. The V_{HE} locations lie within a 10° right ascension band and have declinations between 13 and 68°. Boundaries corresponding to launch energy requirements, C_3, of 20 km^2/sec^2 are shown. The locations of the subsolar and subearth points are functions only of arrival date and are shown. Note that the subearth points are on the backside of Venus in this figure and have declinations near 5°. The evening terminator is shown for the earliest and latest arrival dates.

The angle between the V_{HE} and entry point, φ_L, is a function of γ_E and V_{HE} magnitude as described above. The locus of entry points for γ_E of -20 and -30° is shown. Since a γ_E of -20° is about the shallowest that can be aimed for, because of the skipout boundary and entry dispersions in γ_E, the unobtainable region of Venus lies inside this locus.

The V_{HE} locations for the 1973-II opportunity are shown in figure 25 for arrival dates between April 3 and May 13, 1974, with launch dates between September 25 and December 14, 1974. The locations of the subsolar point are shown on the backside of the planet. The subearth point is on the backside for the April 3 arrival date and swings around to the front for the May 13 arrival date. No attempt has been made to show what region on the planet is unobtainable due to the peculiar shape of the V_{HE} region that covers a right ascension band of 40° and declinations from -27 to 65°.

Dispersions in entry flight path angle, γ_E, are due to two error sources: navigation uncertainty at the time of ejection by Earth-based tracking, and maneuver execution uncertainty composed of a pointing uncertainty and an impulse uncertainty. The navigation uncertainty at the time of capsule ejection is expressed in terms of uncertainty in the impact parameter, b. This is the distance from Venus to the asymptote of the spacecraft trajectory. The sensitivity of γ_E to b is shown as a function of V_{HE} and nominal γ_E in figure 26. A typical 1σ error in b based on the present DSN capability is 100 km. Thus for a V_{HE} of 5.0 km/sec and a γ_E of -30° the resulting 1σ dispersion in γ_E is 0.7°. The sensitivity of the entry location, β, to b is about 1.3 times as great as the γ_E sensitivity.

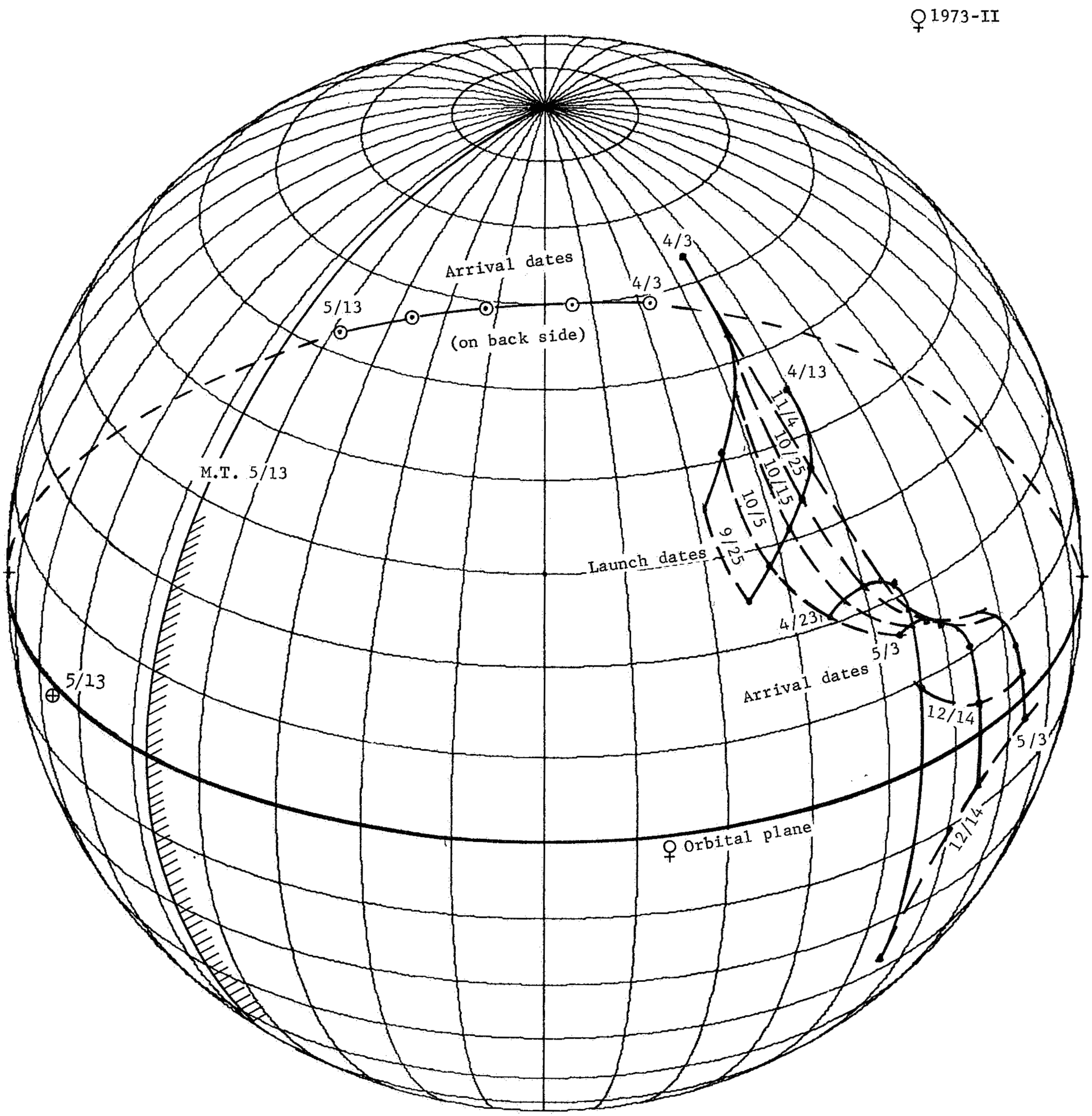

Figure 25.- Venus Targeting Map, 1973, Type II, 30° View

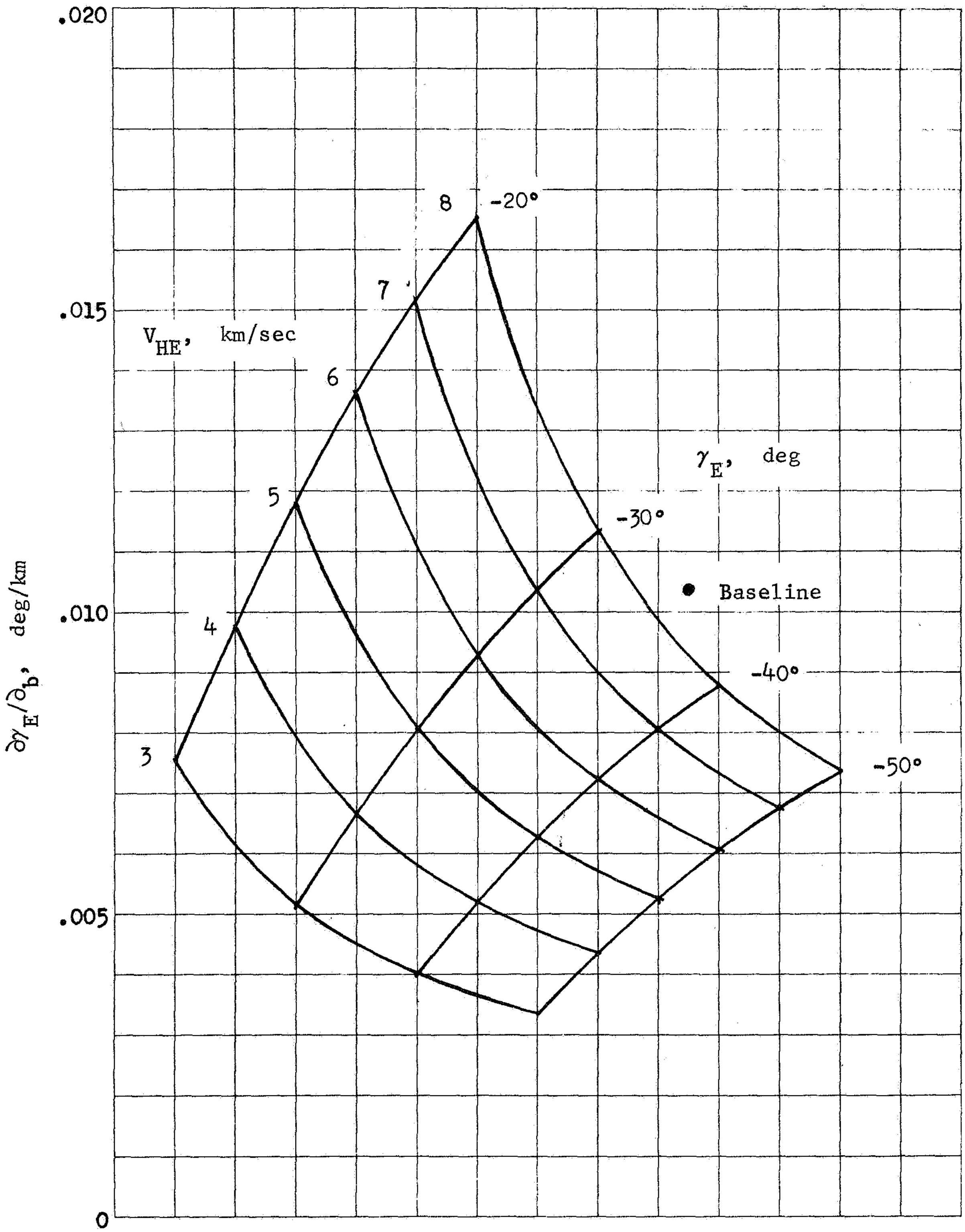

Figure 26.- Sensitivity to Navigation Error, γ_E

The sensitivity of γ_E to a pointing error at ejection is strongly a function of the ejection angle, τ_{EJ}, as shown in figure 27. The sensitivity to R_{EJ}, γ_E, or V_{HE} is slight. The 1σ pointing error is taken to be 0.5°. The variation of τ_{EJ} with V_{HE} and γ_E required for an α_P of 70° is shown in figure 28 for an h_p of 2000 km. For example, a γ_E of -30° and a V_{HE} of 5.0 km/sec requires a τ_{EJ} of -41°. This then results in a 1σ dispersion in γ_E of about 0.4°. As discussed previously, lower h_p requires smaller τ_{EJ} and in turn larger dispersions in γ_E. From figure 28 it is seen that low τ_{EJ} result from high V_{HE} and shallow γ_E. A V_{HE} of 7.0 km/sec and a γ_E of -20° result in a 0.6 dispersion in γ_E.

The dispersion in γ_E due to an impulse error is independent of τ_{EJ}, but increases with increasing h_p, V_{HE}, and γ_E. The dispersion in γ_E, because of a 1σ impulse error that is 19.33% of the nominal value, is always less than 0.2°. The total dispersion in γ_E is then the rss of the three error sources described. For a γ_E of -30°, V_{HE} of 5.0 km/sec, and h_p of 2000 km, the total 1σ dispersion in γ_E is 0.83°.

Out of plane.- The Venus/Mercury swingby mission requires a specific flyby trajectory near Venus with a specific inclination to the Venus orbital plane. To obtain a BVS/entry vehicle entry location that is 40° from the subearth point (direct link for BVS) with a reasonably shallow γ_E the ejection maneuver must be out of the plane of the flyby trajectory. An example of the propulsive requirement for out of plane ejection maneuvers is given in figure 29, where θ_E is the angle between the flyby trajectory plane and the BVS/entry vehicle trajectory plane. For a nearside entry in the flyby trajectory plane, $\theta_E = 0°$, the ΔV_{EJ} required is 30 m/sec. For an entry 90° from the flyby trajectory plane the ΔV_{EJ} required is 70 m/sec. For a far side entry in the flyby trajectory plane, $\theta_E = 180°$, the ΔV_{EJ} required is 99 m/sec.

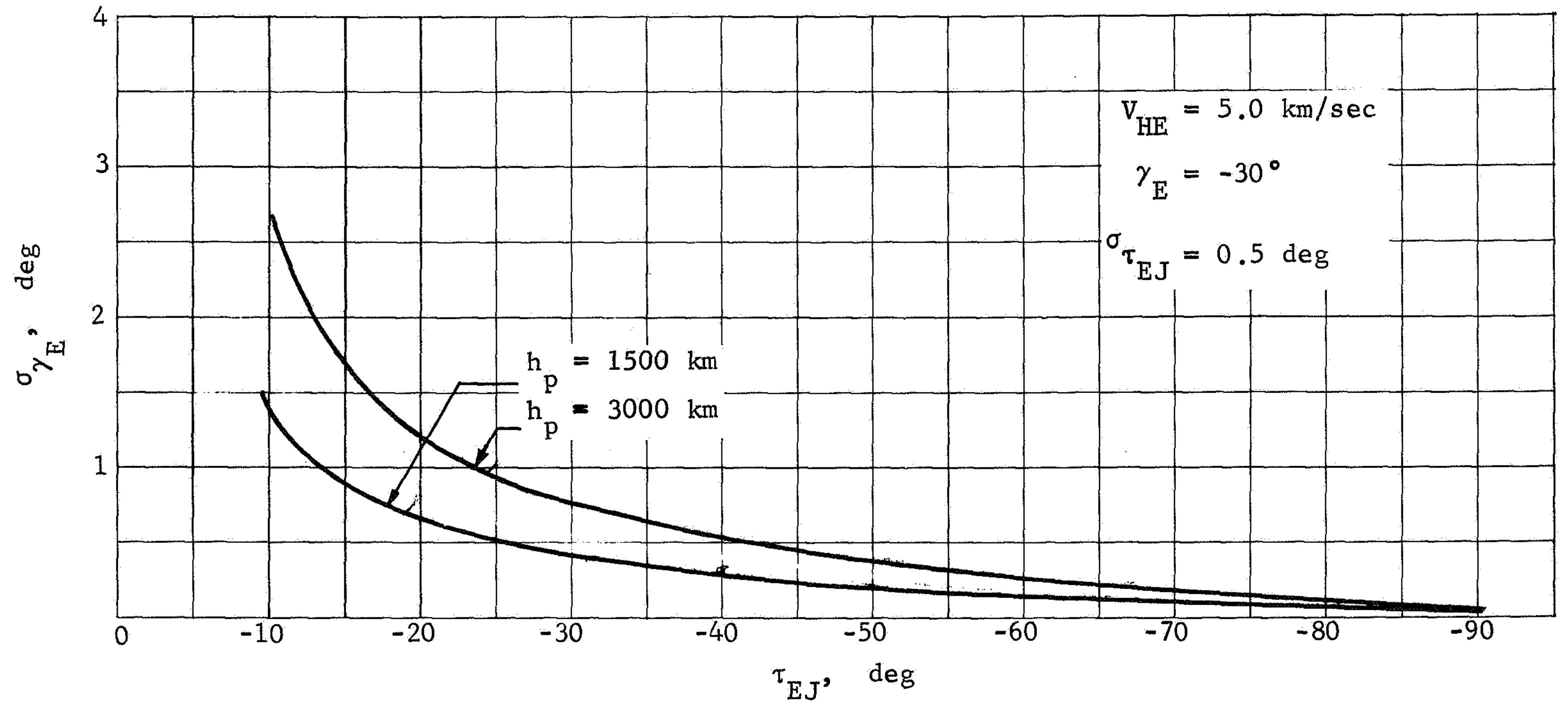

Figure 27.- One Sigma γ_E Error vs τ_{EJ}

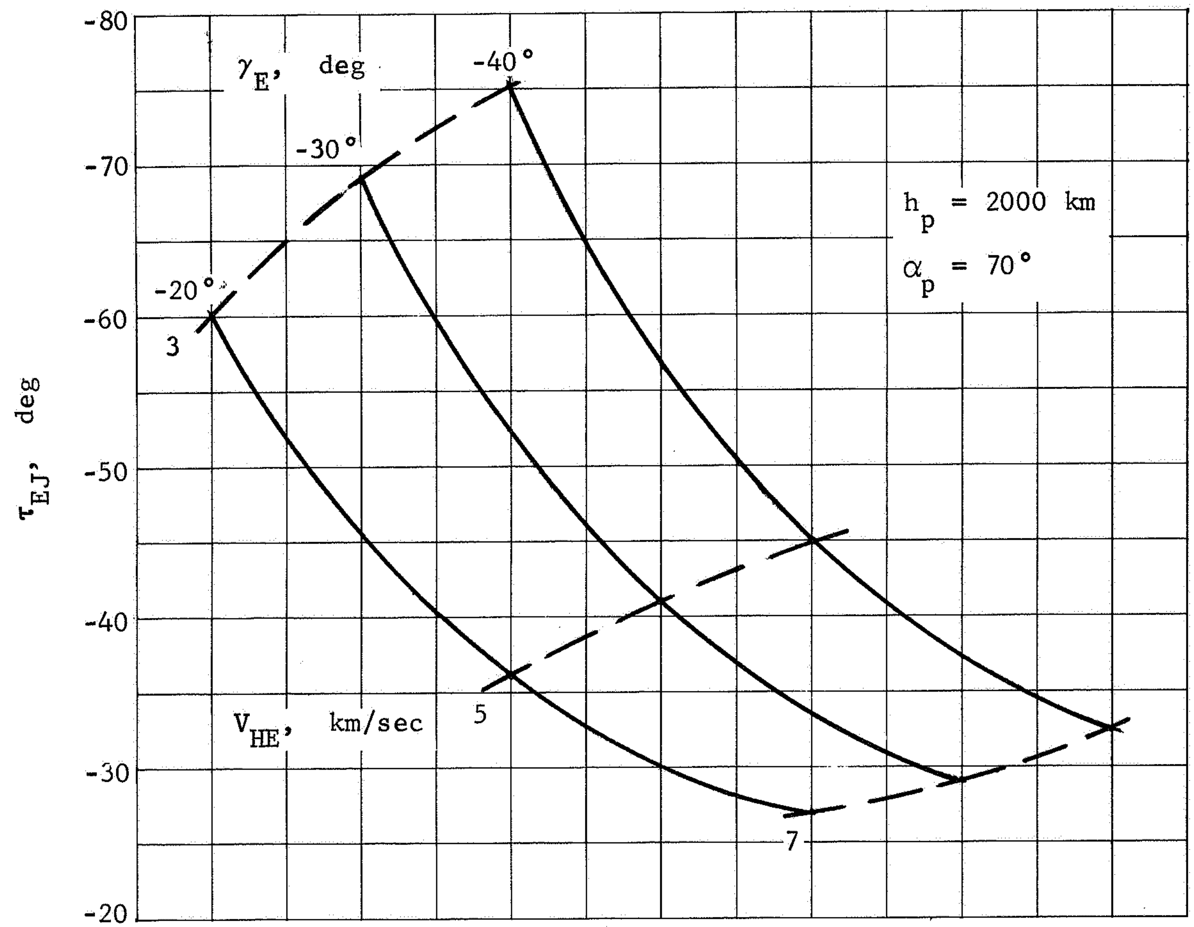

Figure 28.- τ_{EJ} vs γ_E and V_{HE}

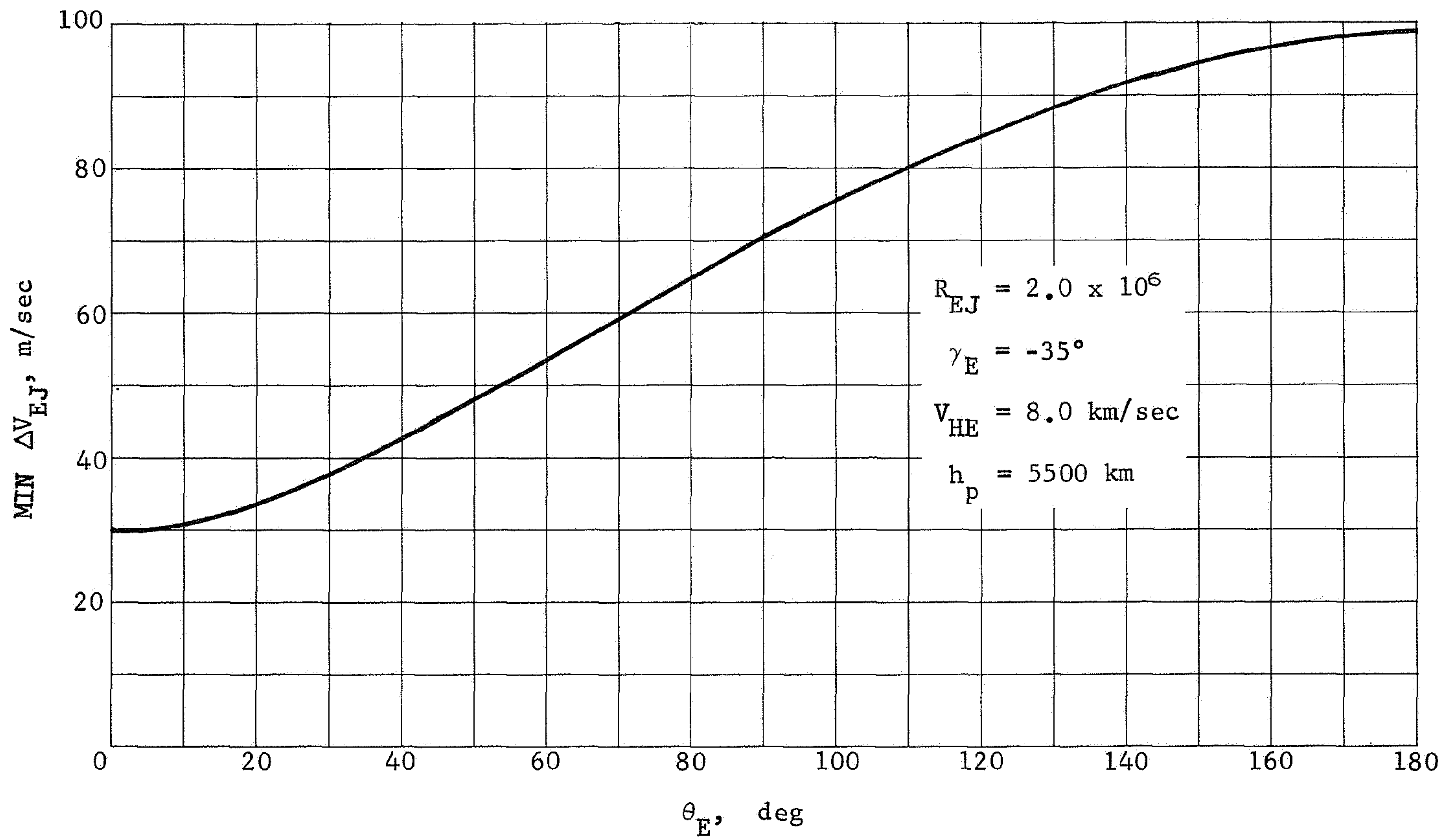

Figure 29.- MIN ΔV_{EJ} vs θ_E

The total dispersion in γ_E due to both navigation and maneuver execution uncertainty is 1.33°.

Orbit Mode Targeting

The preferred mission mode for the 1973-II mission is deflection of the BVS/entry vehicle from an orbit about Venus. The orbit discussed in this section has a periapsis altitude of 2000 km and an eccentricity of 0.8. The targeting analysis determines the required deorbit impulse, ΔV_D, consistent with the telecommunication requirements for a relay link from deorbit to probe impact. The ground rules used for this link are similar to those discussed in the previous section for the direct mode. The targeting analysis also determines the entry location, β, as a function of γ_E and ΔV_D. The navigation uncertainty at the time of deorbit can be expressed in terms of a covariance matrix in position and velocity after several orbits of tracking from Earth. This covariance matrix can be propagated to the entry altitude to determine entry dispersions. The entry dispersions due to execution errors are handled similarly to the direct mode. Details of the orbit mode error analysis are not given, but the resulting 1σ dispersion in γ_E is less than a degree.

The geometry shown in figure 13 is equally applicable for the orbit mode. Parameters relating to the relay communication constraints are shown in figure 30 as a function of β and orbiter lead angle, λ. As with the direct mode, the λ must be selected as a function of β to lie between the α_P of ±70°. A boundary corresponding to a 20° mask above the local horizontal at entry is shown instead of the fading margin angle of 60°. This boundary allows somewhat larger negative λ than the fading margin boundary.

The variation of ΔV_D with λ is shown as a function of β for a γ_E of -30° in figure 31. The absolute minimum ΔV_D occurs for a β of 66°, and is 215 m/sec. The ΔV_D is greater than 250 m/sec for β less than 59.6° and β greater than 69.5°. The deorbit location true anomaly increases in the direction of the arrows, and the coast time, time from deorbit to entry, is decreasing. The coast time is constrained to be less than 10 hr because of thermal control and attitude control considerations. The angle of attack at entry is shown in figure 32.

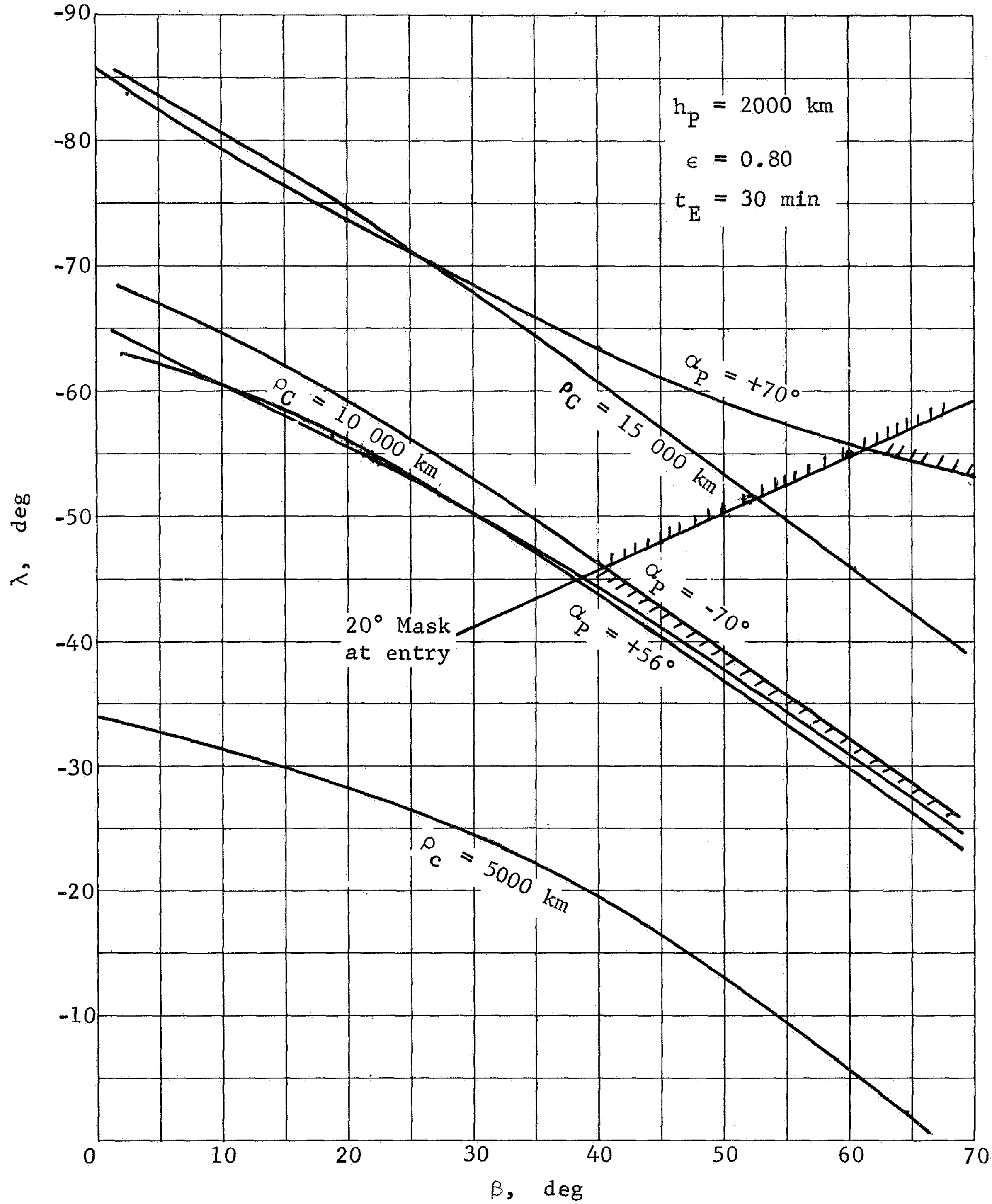

Figure 30.- β/ λ Boundaries, Entry from Orbit

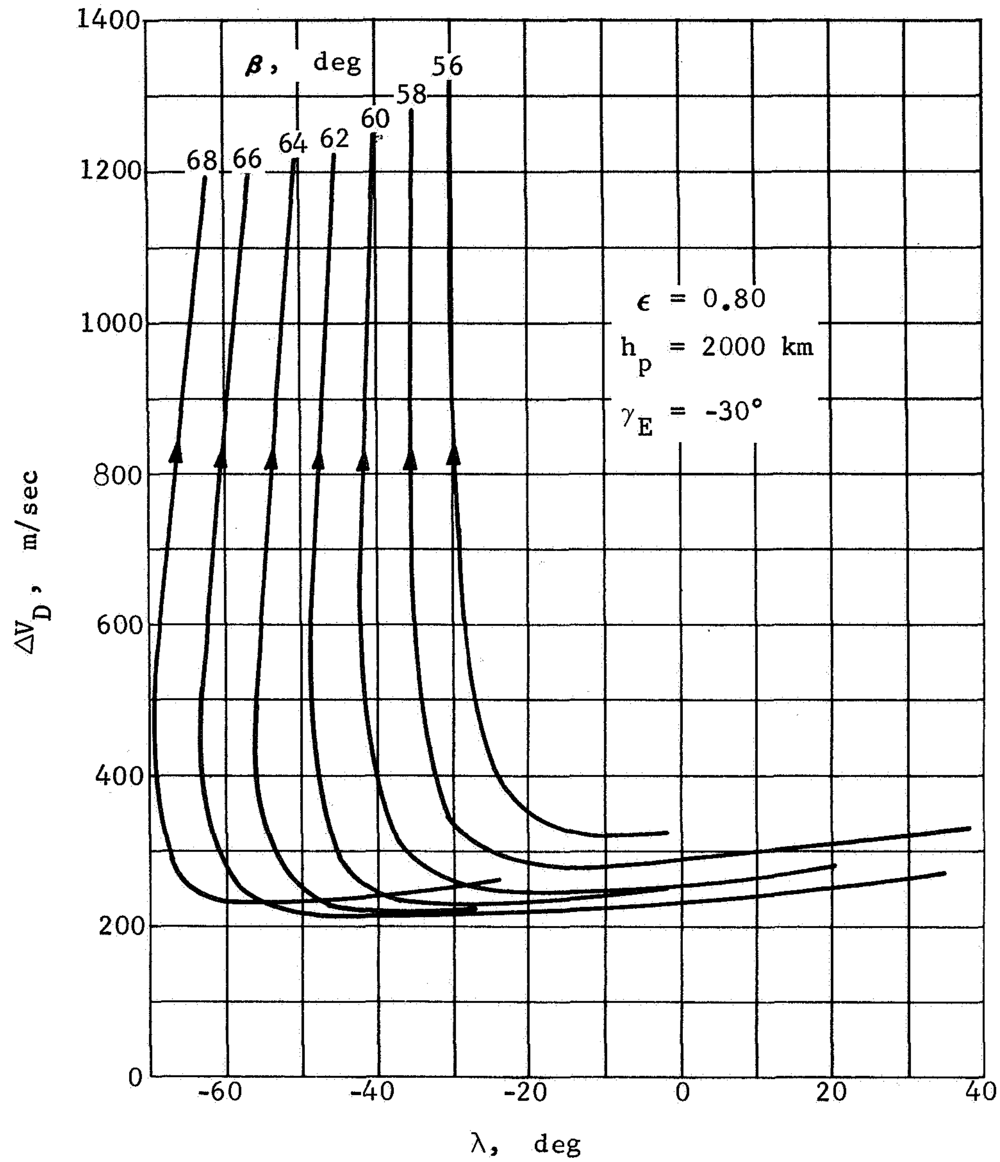

Figure 31.- ΔV_D vs λ and β

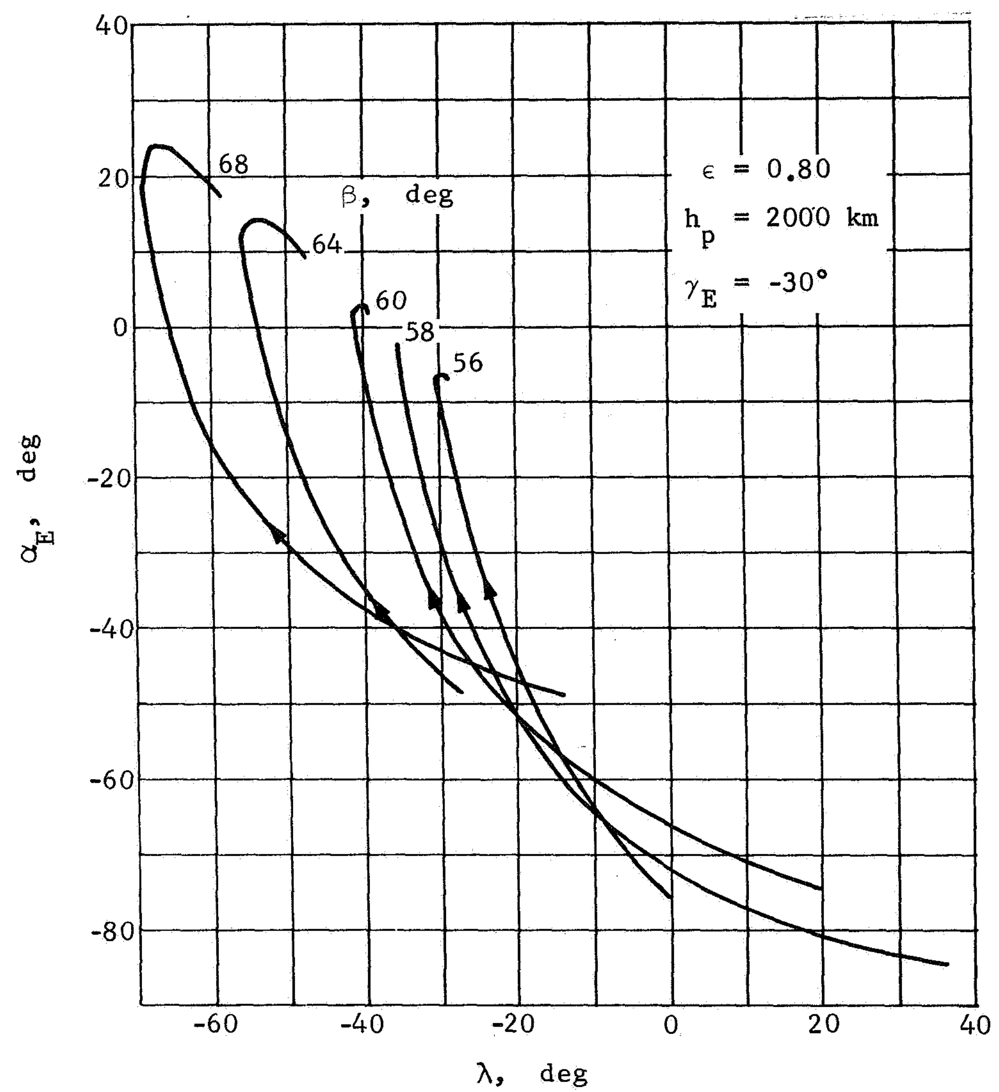

Figure 32.- α_E vs λ and β

The relationship between β, λ, and γ_E is shown in figure 33 for ΔV_D of 250 m/sec. Any β/λ combination inside of the closed contours is obtainable with a ΔV_D of 250 m/sec or less. Also shown are boundaries corresponding to:

1) α_E equal to -20°;
2) Coast time less than 10 hr;
3) Elevation mask of 20° above the local horizontal at entry;
4) α_P equal to 70°.

For a given γ_E and ΔV_D sizing there exists a range of β satisfying all the above constraints. For example, with a γ_E of -27° and a ΔV_D of 250 m/sec or less, β between 54.6 and 58.3 are obtainable. By varying γ_E between -27 and -33°, β between 54.6 and 70.2° are obtainable, a $\Delta\beta$ of 15.6°. To obtain a greater targeting capability (larger $\Delta\beta$) the γ_E range must be extended. Steeper γ_E than -33° require ΔV_D above 250 m/sec to satisfy all constraints. Shallower γ_E than -27° are not feasible because of the narrowing region formed by boundaries 3) and 4) above. Thus a $\Delta\beta$ of 15.6° is the largest obtainable with a ΔV_D sizing of 250 m/sec.

The central angle between the V_{HE} and entry point, φ_L, is equal to β plus τ_o as for the direct mode if orbit insertion occurs at periapsis of the approach spacecraft trajectory. Insertion at this location results in the minimum propulsive requirement. The periapsis of the orbit can be shifted by insertion at other than periapsis of the approach trajectory with a higher orbit insertion ΔV. If a positive shift is defined by the angle Δw, then the φ_L is β plus τ_o minus Δw. If large enough periapsis shifts are used, the entry point can be anywhere over Venus.

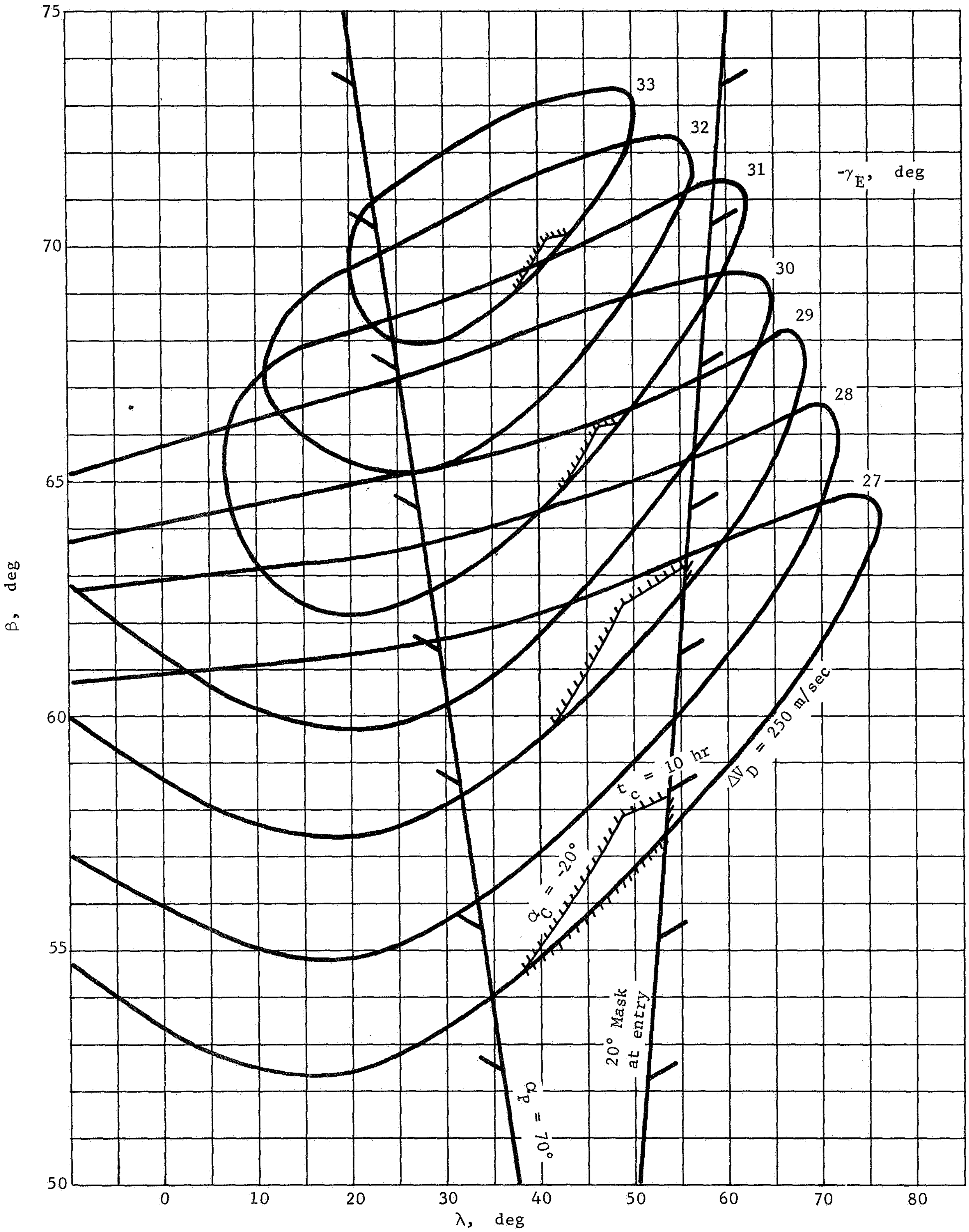

Figure 33.- Targeting Capability, 1973, Entry from Orbit

Orbit Selection Criteria

The orbit selection criteria are based on the scientific objectives of the mission, system performance from a payload point of view, and orbit lifetime. The selected orbit, 2000 x 66 400 km (ϵ = 0.8), inclined approximately 50° to the Venus orbital plane, is a compromise solution. The factors leading to this selection for each of the three criteria, above, are summarized in the following sections.

Science objectives.- The scientific objectives for the orbiting spacecraft mission include both orbiting spacecraft and BVS requirements or needs. For this mission, the entry point that best satisfies the BVS mission desires is near the subsolar point, slightly northern latitude, and slightly east of the subsolar meridian. This entry results in an expected wind drift pattern that will eventually carry the BVS into the north polar region. This desire can only be partially satisfied, primarily on the basis of orbit lifetime requirements. The actual landing area ends up at a northern latitude near the subsolar point, but slightly to the west of the subsolar meridian. The wind drift pattern will result in BVS crossing the western terminator at middle latitudes. The BVS entry point constraints are primarly approach trajectory geometry limits rather than orbit size and shape.

The orbiting science package (as discussed in Volume III) includes:

1) Ultraviolet spectrometer;
2) Infrared spectrometer;
3) Photo imaging;
4) Magnetometer and plasma probe;
5) S-band occultation;
6) Celestial mechanics

The first two experiments ideally require relatively low eccentricity orbits, i.e., apoapsis altitudes less than approximately 30 000 km for resolution and ground traces that include both the subsolar and polar region. The selected orbit only partially satisfies these requirements, but still results in a scientifically significant mission. The photo imaging experiment requires a relatively low altitude, near-circular orbit. This is not possible, but the selected orbit does satisfy this experiment requirement over a large part of the planet. The magnetometer and plasma probe experiment requires a relatively high eccentricity orbit that passes within 500 km of the surface near the subsolar point. Orbit lifetime eliminates the 500-km capability, but the selected orbit should still result in good fields and particles mapping. Earth occultation is required on the S-band occultation experiment. This is satisfied, but no attempt has been made to optimize either orbit geometry or size for this experiment. The celestial mechanics experiment would require a middle inclination orbit, perhaps with somewhat less eccentricity than the selected orbit. However, estimates of planet oblateness can be made with the selected orbit.

The selected orbit does not fully satisfy all of the scientific objectives (nor can any single orbit). It does reasonably satisfy most of the scientific objectives of the mission. The primary information that cannot be obtained is the thermal mapping at the poles.

Performance considerations.- The launch period and launch vehicle analyses presented above have resulted in the selection of launch periods that optimize the launch vehicle capability over 20-day launch periods. This analysis defines the range of C_3, earth departure energy, and V_{HE}, Venus approach energy, which the launch vehicle and orbit insertion motors must provide. From strictly a performance viewpoint, highly elliptical orbits are desirable. Nondimensionalized orbit insertion ΔV is shown in figure 34 as a function of V_{HE} and orbit eccentricity, ϵ. The supplementary data required to get the actual ΔV is presented in figure 35. Figure 34 shows that both low V_{HE}, a function of launch period, and high eccentricity lead to low ΔV. The sensitivity to periapsis altitude is not obvious from figures 34 and 35. The data in figure 36 are boundaries where $\partial \Delta V / \partial h_p = 0$ as a function of periapsis altitude, V_{HE}, and eccentricity. Conditions to the right of the boundaries result in increased $\Delta V_{O.I.}$ required for increased h_p. For the high eccentricities considered, increased h_p requires increased $\Delta V_{O.I.}$ for the normal V_{HE}. The significance of $\Delta V_{O.I.}$ on useful weight in orbit is shown in figure 37. Here useful weight is defined as weight at orbit insertion motor ignition minus total loaded propulsion module weight. The low $\Delta V_{O.I}$ resulting from highly eccentric orbits is important. The selected launch period and orbit require a maximum $\Delta V_{O.I}$ of approximately 1.95 km/sec resulting in a usefull weight in orbit to total spacecraft weight ratio 0.43 in the worst case.

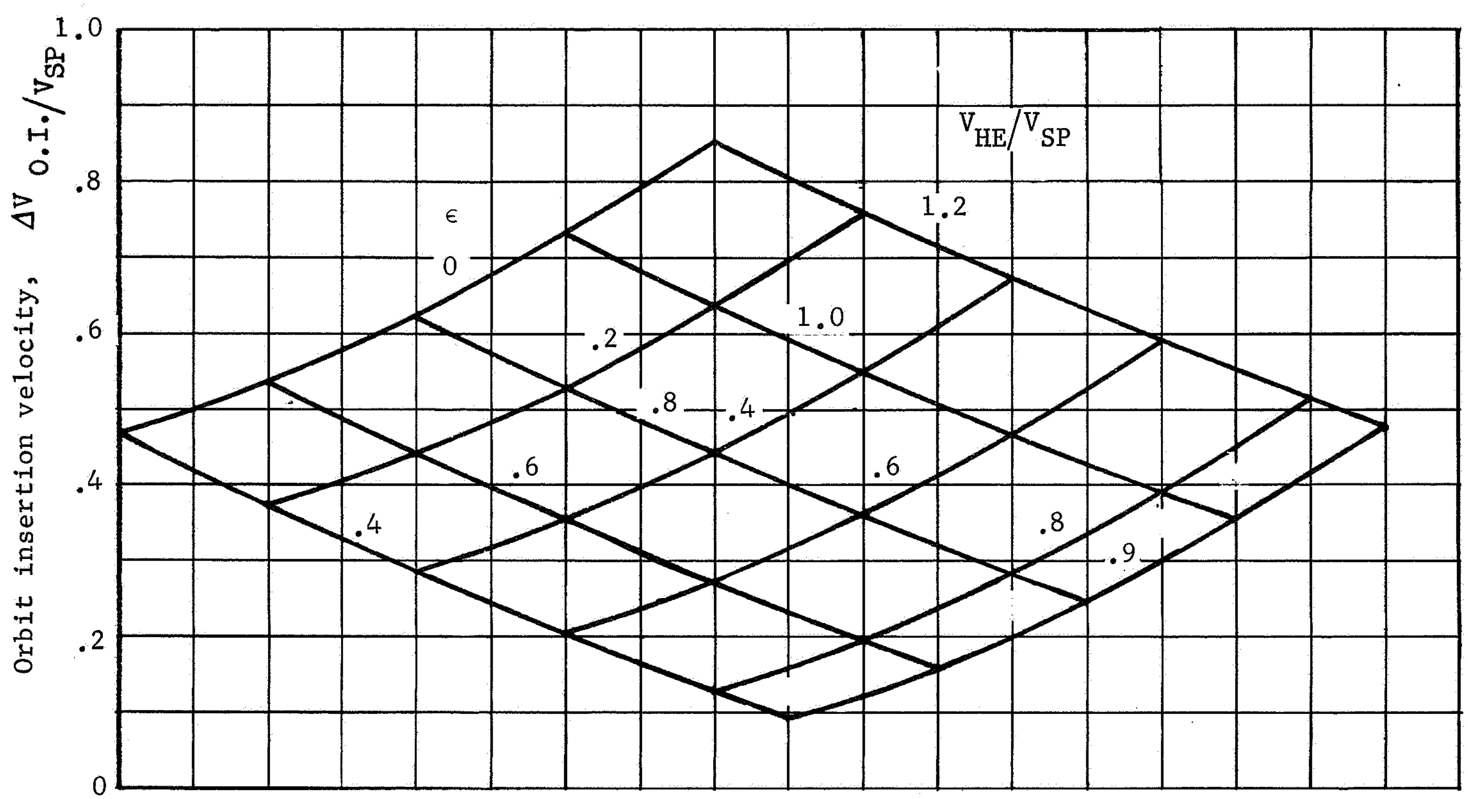

Figure 34.- Venus Orbit Insertion ΔV Requirements

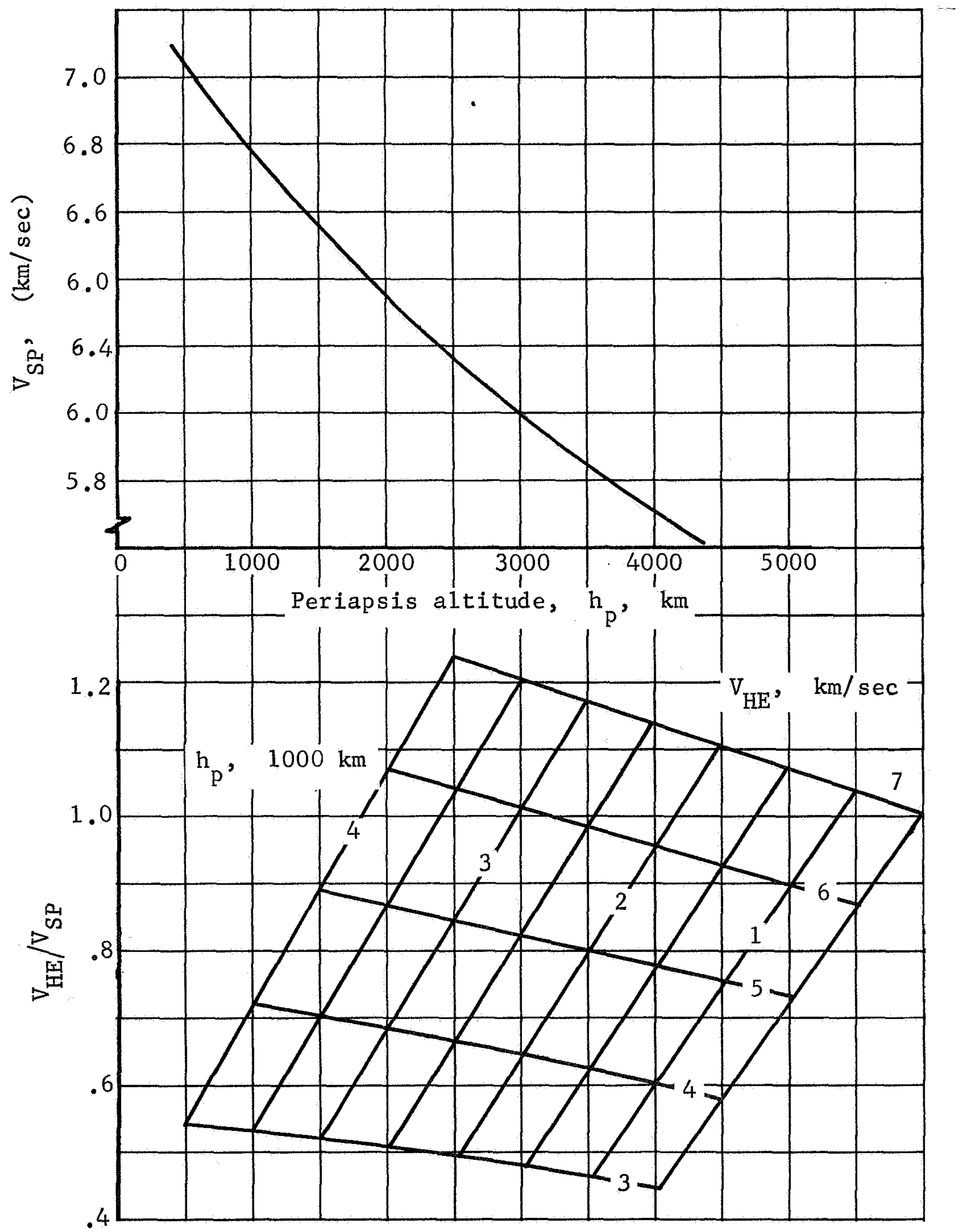

Figure 35.- Venus Circular Velocities

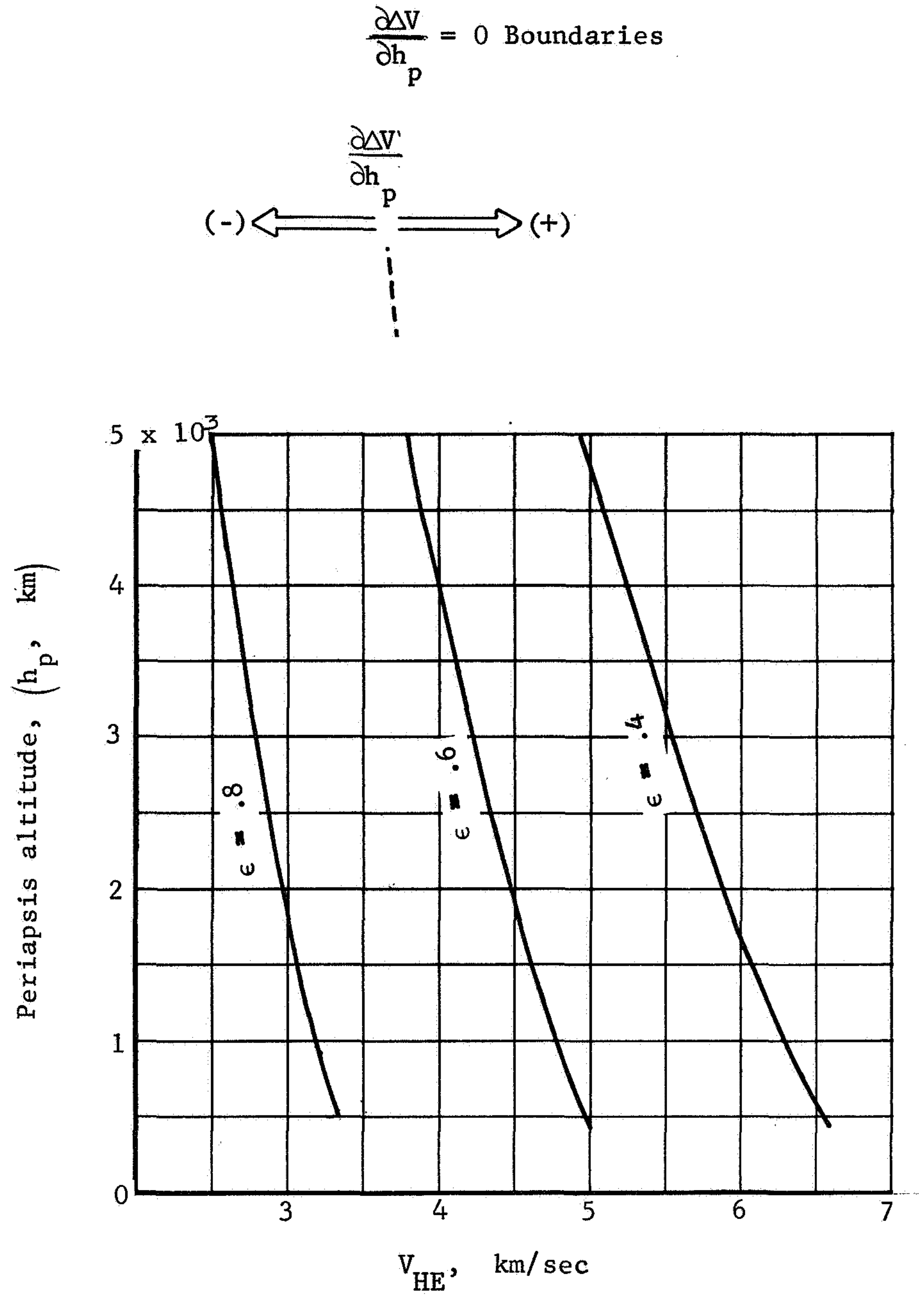

Figure 36.- $\Delta V_{O.I.}$ Sensitivity $f\left(h_p,\ V_{HE},\ \epsilon\right)$

$$W_{Use}/W_O = \frac{1}{\lambda}\left\{\exp\left(\frac{\Delta V}{C_j} - (1 - \lambda)\right)\right\}$$

W_{Use} = Useful weight (initial weight minus loaded propulsion system)

W_O = Weight at start of orbit insertion maneuver

λ = Propellant mass fraction (0.85)

$C_j = gI_{sp}$ = (32.174)(302)

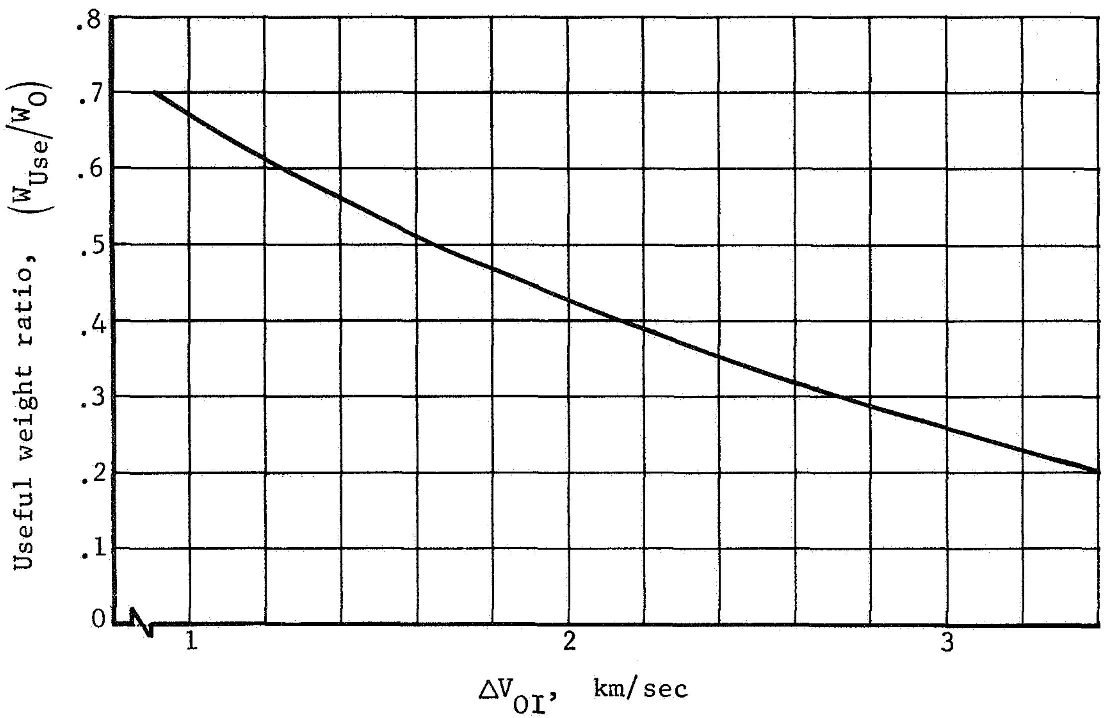

Figure 37.- Useful Weight in Orbit

Orbit lifetime.- This analysis assumes a required orbit lifetime of 50 years to comply with planetary quarantine requirements for the unsterilized orbiting spacecraft. The lifetime analysis includes two primary effects, drag and solar gravitation perturbations.

The drag lifetime boundary for a conservative atmosphere and a spacecraft ballistic coefficient of 0.25 slug/ft^2 is shown in figure 38. This boundary suggest a minimum periapsis altitude of 300 to 400 km. The encounter uncertainties at the time of the last midcourse correction must be added to this minimum to define the minimum allowable aim periapsis altitude. This raises the minimum allowable periapsis altitude to approximately 1000 km. The reference orbit has a nominal periapsis altitude of 2000 km, primarily to improve the relay communication link geometry.

The orbit stability as affected by solar gravitational perturbations and the interplay of potential oblateness effects is a more critical factor.

The declination of the V_{HE} vector on a typical day in the launch period is 35.6°. The loci of possible approach trajectory and, typically, the orbit periapsis locations are shown in figure 39. The variable around the locus is orbit inclination or right ascension of the ascending node.

Twenty typical orbit orientations over the range of inclinations have been investigated and the results summarized in table 2. Representative periapsis altitude variations over 50 years are shown in figure 40 for reference orbits 6, 7, and 8 of table 2. Solar gravitational effects, as can be seen, can cause periapsis altitude perturbations of over 10 000 km over this period, up or down.

The solar gravitational perturbation can be visualized with the aid of the following approximate solution:

$$h_p = K_o \left[K_1 \sin \left(2 \Gamma_{\odot} + K_2\right) + K_3 t \; K_4\right]$$

where

$\Gamma_{\odot}$ = sun motion relative to planet,

K_o = function of orbit size (i.e., h_p, ϵ),

$K_1 - K_4$ = function of orbit geometry (i.e., inclination, i, and argument of periapsis, ω).

$B = 0.25$ slug/ft^2

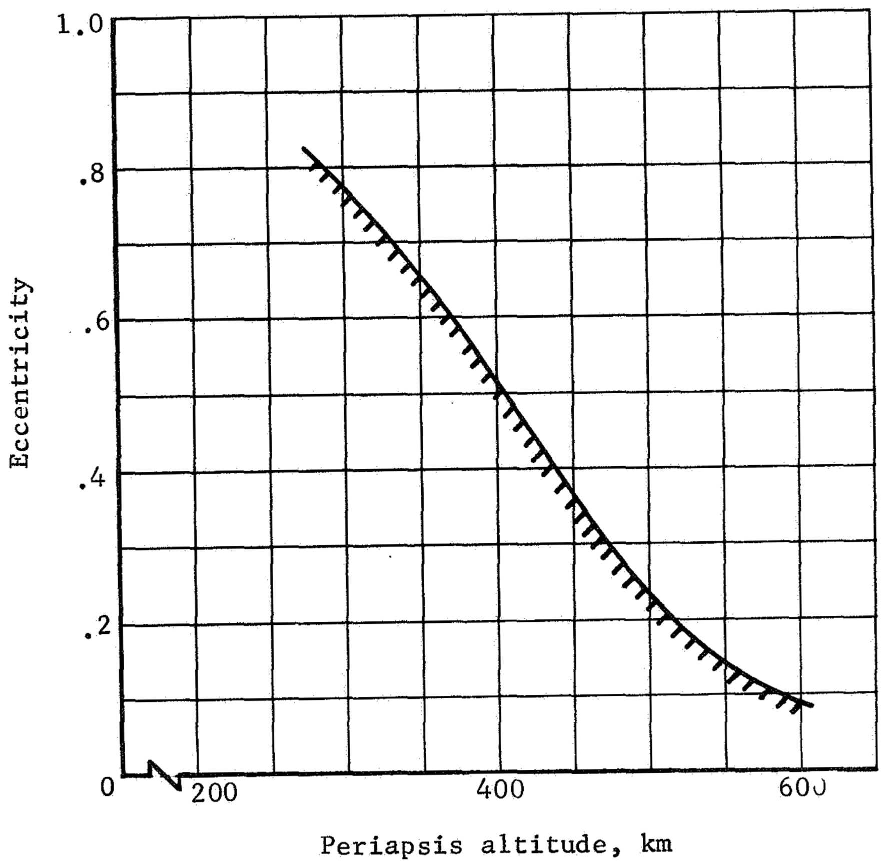

Figure 38.- Fifty Year Orbit Lifetime Boundary, Drag

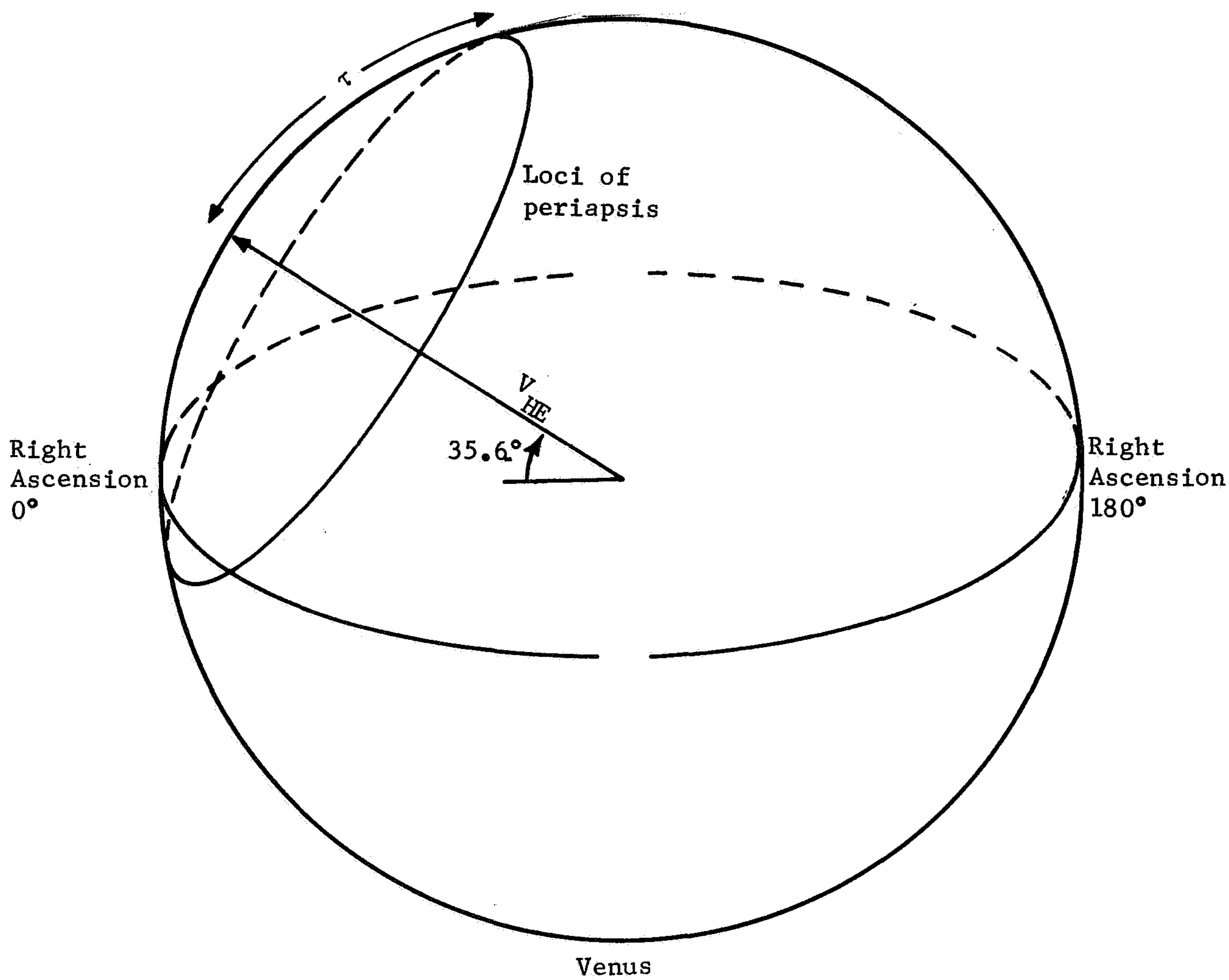

Figure 39.- V_{HE} Vector Geometry, 1973, Type II

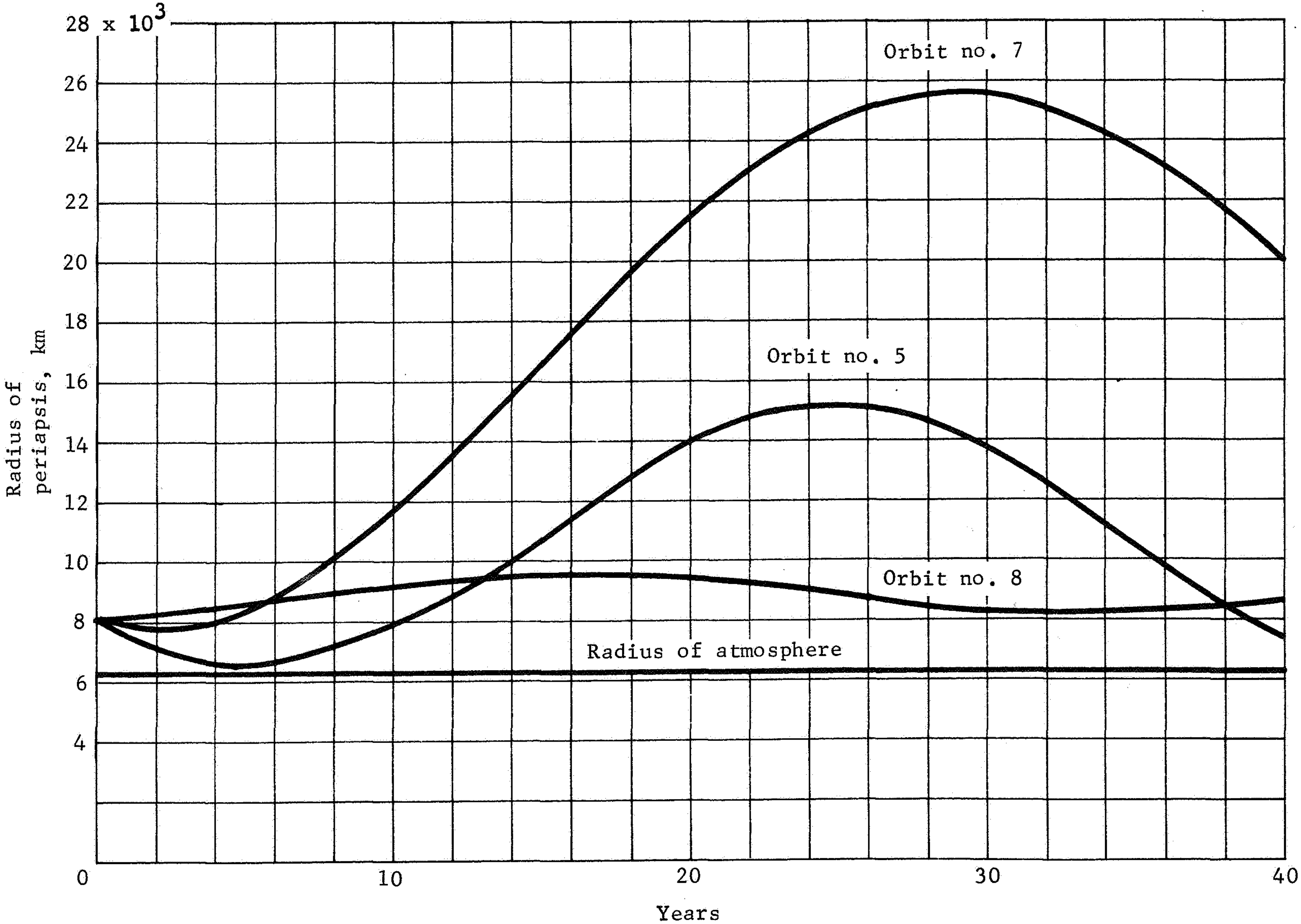

Figure 40.- Orbit Periapsis Time History

TABLE 2.- ORBIT LIFETIMES

Orbit reference no.	Inclination, deg	Right ascension, deg	Argument of periapsis, deg	Approximate lifetime, yr
1	90	0.	-11.4	12
2	95	3.583	-11.25	11.5
3	105	11.067	-9.333	11
4	120	24.417	-4.6	8.2
5	135	45.717	8.4	5.1
6	144.4	90.	43.	50+
7	135	134.283	78.6	50+
8	120	155.583	90.8	50+
9	105	168.933	95.933	7.9
10	95	176.417	97.25	6.8
11	90	180.	97.4	6.8
12	85	183.583	97.25	6.8
13	75	191.067	95.933	7.9
14	60	204.417	90.8	50+
15	45	225.717	78.6	50+
16	35.6	270.	43.	50+
17	45	314.283	8.4	5.1
18	60	335.583	-4.6	8.2
19	75	348.933	-9.933	11
20	85	356.417	-11.25	11.5

This approximate solution suggests a periodic variation with a period of one-half Venus year plus a secular variation that is proportional to the product, $\sin 2\omega \sin^2 i$. The long-term variations in inclination and, principally, argument of periapsis, ω, change the character of the secular term into a long period oscillation. This variation is shown in figure 40. Thus, argument of periapsis is an important forcing function. The geometry that helps guarantee a long lifetime is that which has a near-zero secular term in the above equation with an ω variation such that the secular term becomes positive, i.e., start at the bottom of the long period oscillation.

The data presented in table 2 are shown graphically in figure 41. It is apparent that there are two orbit inclination regions that have satisfactory lifetimes; approximately 37 to 65° on the right and 115 to 144° on the left. The region on the left is the one corresponding to the selected orbit, inclination of 50°, or 130° by the definitions used in this analysis. The other "safe" region does not satisfy the BVS entry point requirements of entry near the subsolar point.

The importance of ω in establishing the solar perturbation effects leads to concern when considering the ω drift due to oblateness. To a first order, oblateness varies ω by

$$\Delta\omega = \frac{3\pi J_2 R^2 (2 - 5/2 \sin^2 i)}{p^2}$$

It is possible for oblateness to accelerate the argument of periapsis into a quadrant that gives a negative secular variation in the above equation and keep it there long enough to fail the orbit. Since the oblateness constant, J_2, for Venus is not known, it was varied parametrically to determine its effect. Values of J_2 up to approximately 0.00063 (Earth is 0.00108, Mars is 0.0026) did not materially affect the reference orbit. Values above 0.00065) drove the argument of periapsis faster than the solar perturbations, effectively superimposing another shorter period oscillation on the data shown in figure 40. Values of J_2 between 0.00063 and 0.00065 were most severe in terms of driving ω into the (negative K_3) first quadrant. However, the periapsis altitude increase that preceded these ω was generally sufficiently great to preclude failure of the orbit.

Orbit selection summary.- The selected orbit is a 2000 x 66 440 km, $\epsilon = 0.8$, orbit inclined approximately 50° to the Venus orbital plane. The orbit does satisfy both the BVS and orbiter scientific objectives with some compromises. It also satisfies the orbit lifetime criteria although the potential effects of planet oblateness should be studied in more detail.

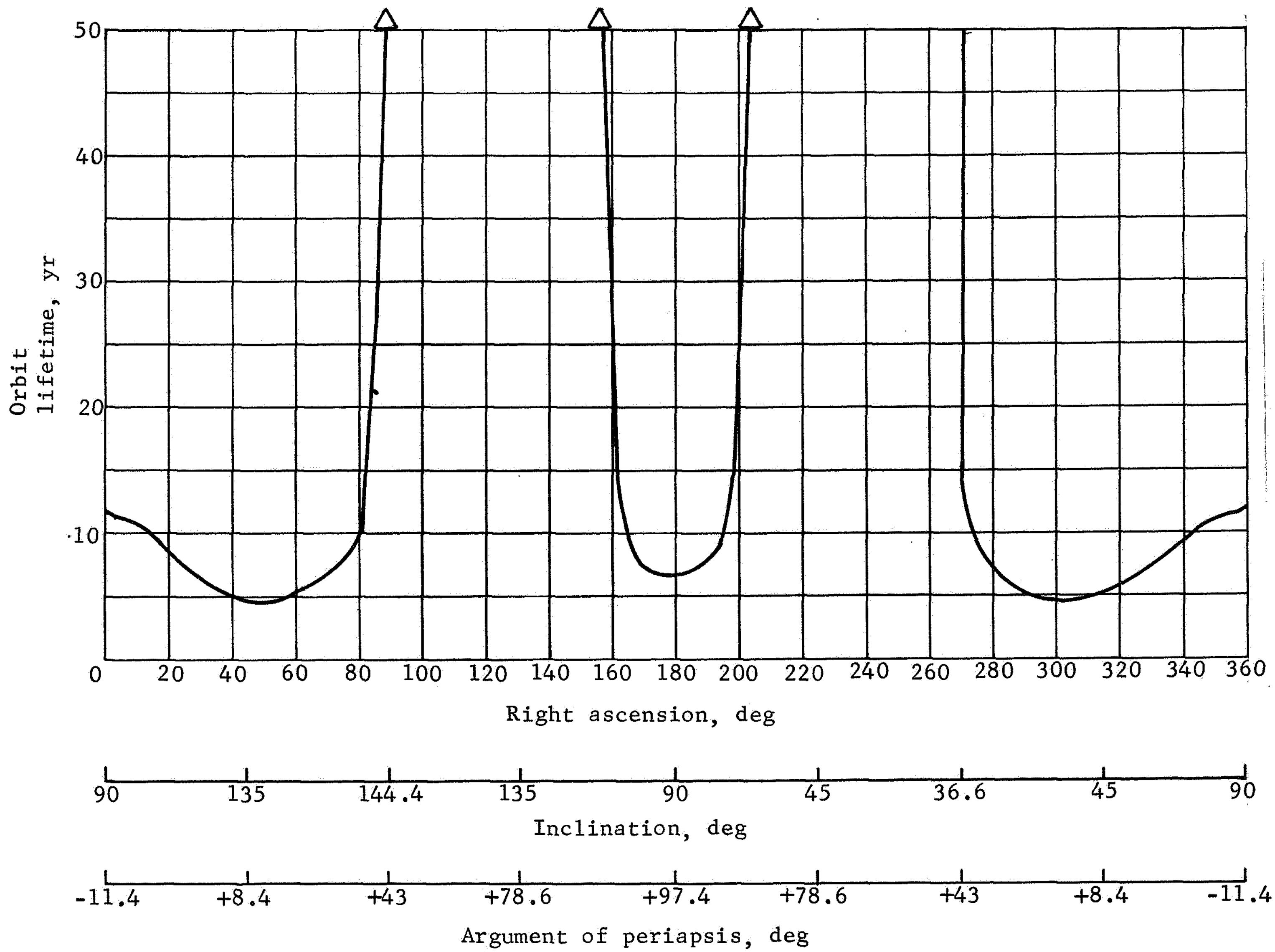

Figure 41.- Solar Perturbation Orbit Lifetime

Entry Environment

The entry trajectory is that portion of the mission profile from entry altitude (specified as 200 km above the mean planet surface) down to the altitude at which the aeroshell is staged from the BVS (defined as Mach 0.5). The entry trajectory analysis is based on a blunted 55° half-angle cone aeroshell configuration. Entry condition variables studied are entry velocity, entry flight path angle, ballistic coefficient, and atmosphere model. Entry trajectory environment parameters that are of primary interest to the BVS system are drag deceleration, time history to staging condition, and downrange angle traveled during entry. Descent time during free fall for the subsonic probe and drop sondes, which are dropped after staging, is presented in addition to the entry trajectory.

Parametric entry trajectory data are presented in the form of carpet plots with the dependent variable a function of entry velocity, entry flight path angle, and atmosphere model. For the parameters presented (time sequence functions, peak drag decelerations, altitude for staging, and downrange angle) ballistic coefficient is not a significant forcing parameter over the range studied (0.20 to 0.60 slug/ft^2). The range of entry velocities includes entry from a Venus orbit (32 000 fps) to direct entry from a Venus/Mercury swingby mission (44 000 fps).

The parametric summary plots presented here are derived from a matrix of entry trajectory calculations performed on a CDC 6400 computer. The simulation is a point mass program, and therefore does not include the effects of vehicle dynamics. For the small angles of attack (< 20°) associated with the missions studied here, a point mass simulation provides satisfactory entry environment data.

Entry vehicle drag coefficient used in the trajectory calculation is a function of Mach number. The normalized drag coefficient as a function of Mach number is shown in figure 42. Ballistic coefficients referenced in this report are based on the hypersonic drag coefficient for the entry trajectories and on the Mach = 0.0 level for the drop probe and sondes.

The following symbols are used in the text and curves of this section:

V_E entry velocity at entry altitude (200 km)

γ_e entry flight path angle at entry altitude (negative downward)

B_E entry vehicle ballistic coefficient, M/C_DA, slug/ft^2

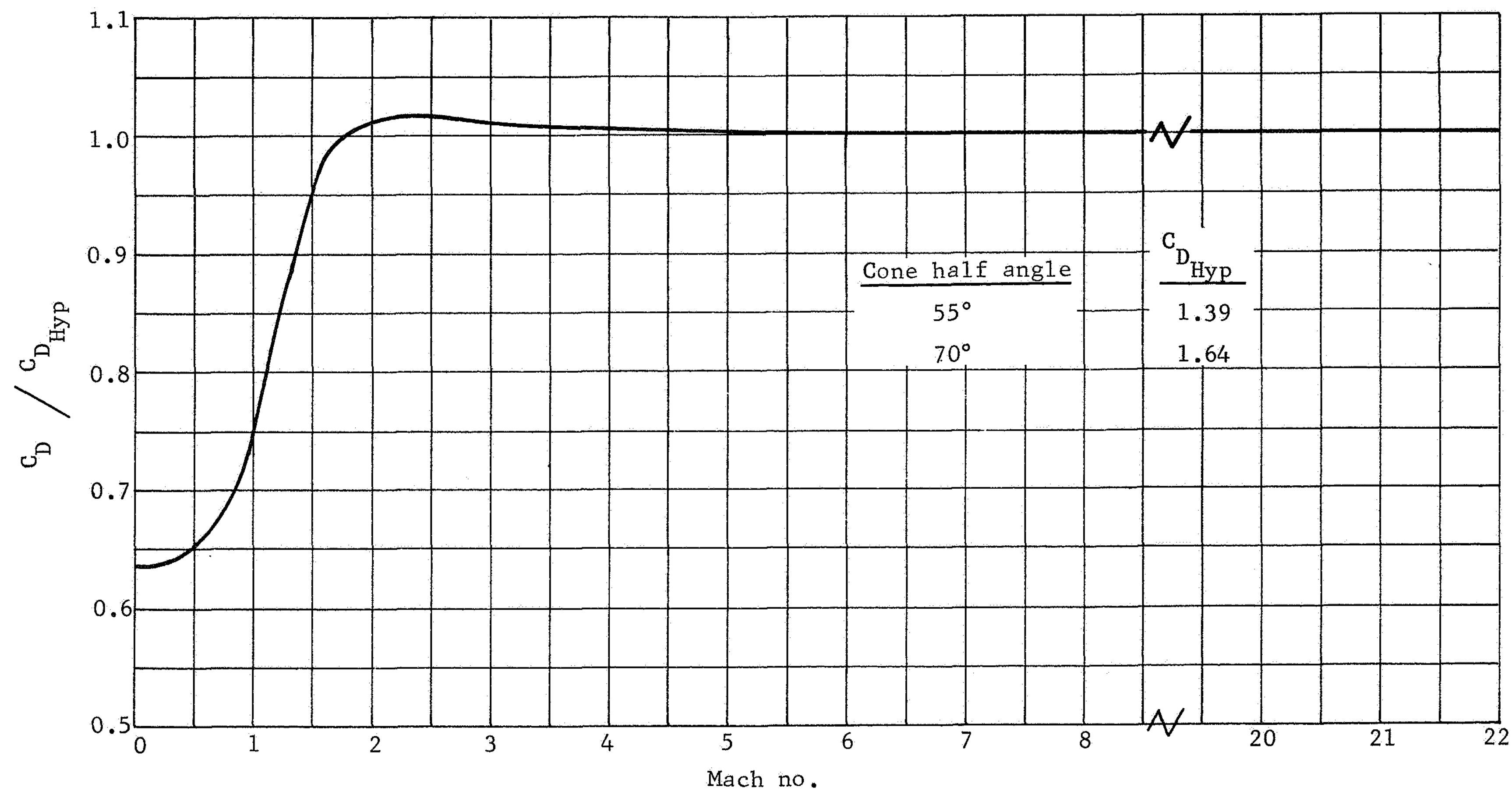

Figure 42.- Normalized Drag Coefficient vs Mach Number

B_P subsonic probe and drop sonde ballistic coefficient

C_D drag coefficient, hypersonic level for B_E, Mach 0.0 for B_P

A reference area, maximum body cross sectional area.

The rotation rate of Venus is so low as to be insignificant in its effect on trajectory characteristics. Rotation rate is therefore taken as zero in the trajectory calculation.

The following planetary characteristics are used in the trajectory calculations:

Planet radius, 6050 km (19 850 050 ft);

Gravitational constant, μ, 324 859.61 km^3/sec^2 (1.1472092×10^{16} ft^3/sec^2);

Rotation rate, 0.0 rad/sec;

Atmosphere models, Lower and Upper (defined in Vol III, Appendix A).

The atmosphere models have the characteristics listed in the following tabulation.

Model	Lower	Upper
Surface pressure, psi	1481.	1580.
Surface density, $slug/ft^3$	0.13009	0.14084
Surface temperature, °R	1372	1404
Stratosphere temperature, °R	396	446
Composition, % by volume		
CO_2	85	95
N_2	15	5
Molecular weight	41.61	43.21
Specific heat ratio	1.34	1.33

Density versus altitude and temperature versus altitude for the upper and lower model atmospheres are shown in figure 43 and 44. The relatively small difference in density between the two models is reflected in the relative insensitivity of the entry environment characteristics to atmosphere model.

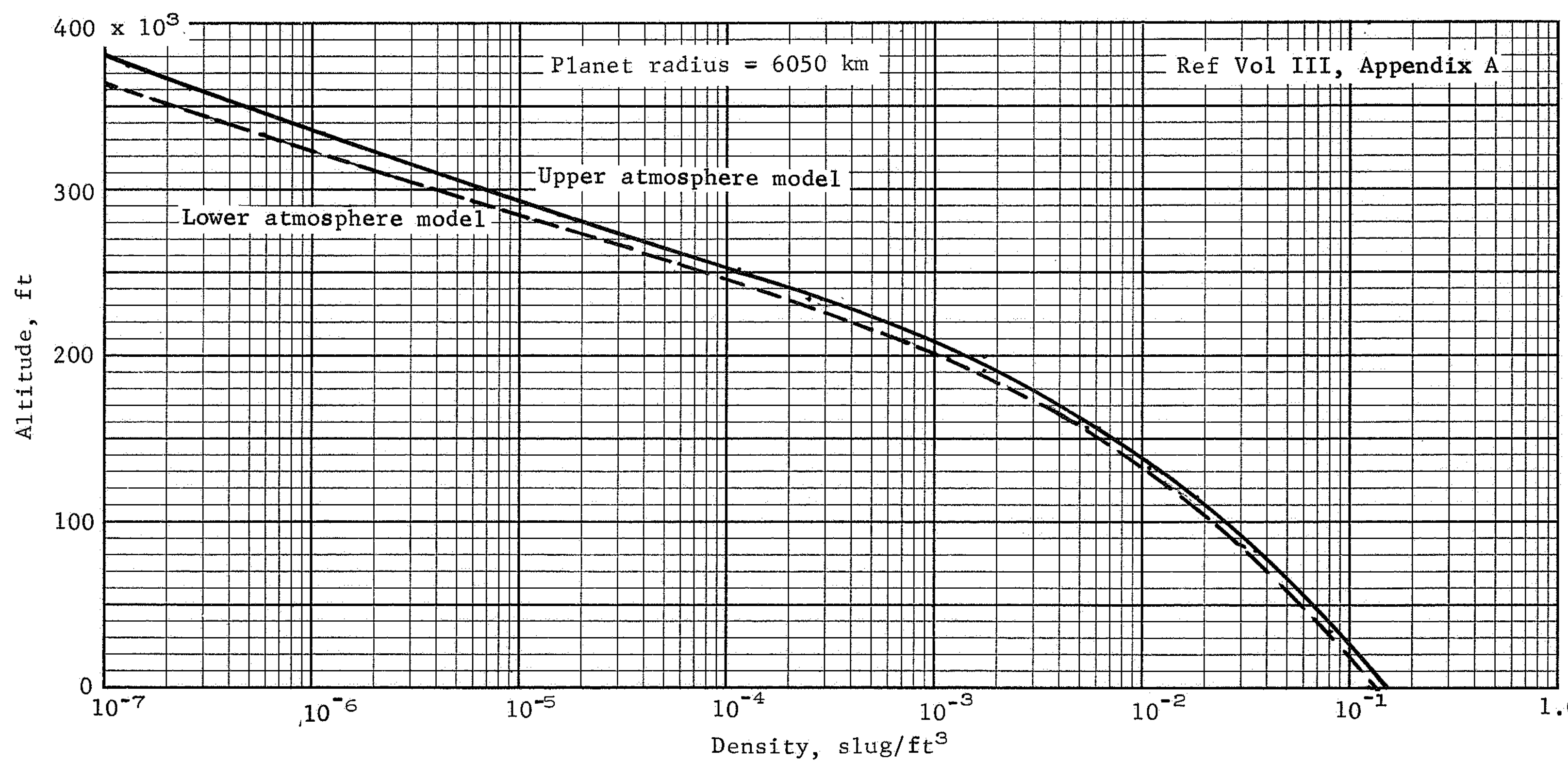

Figure 43.- Venus Atmosphere Models, Density vs Altitude

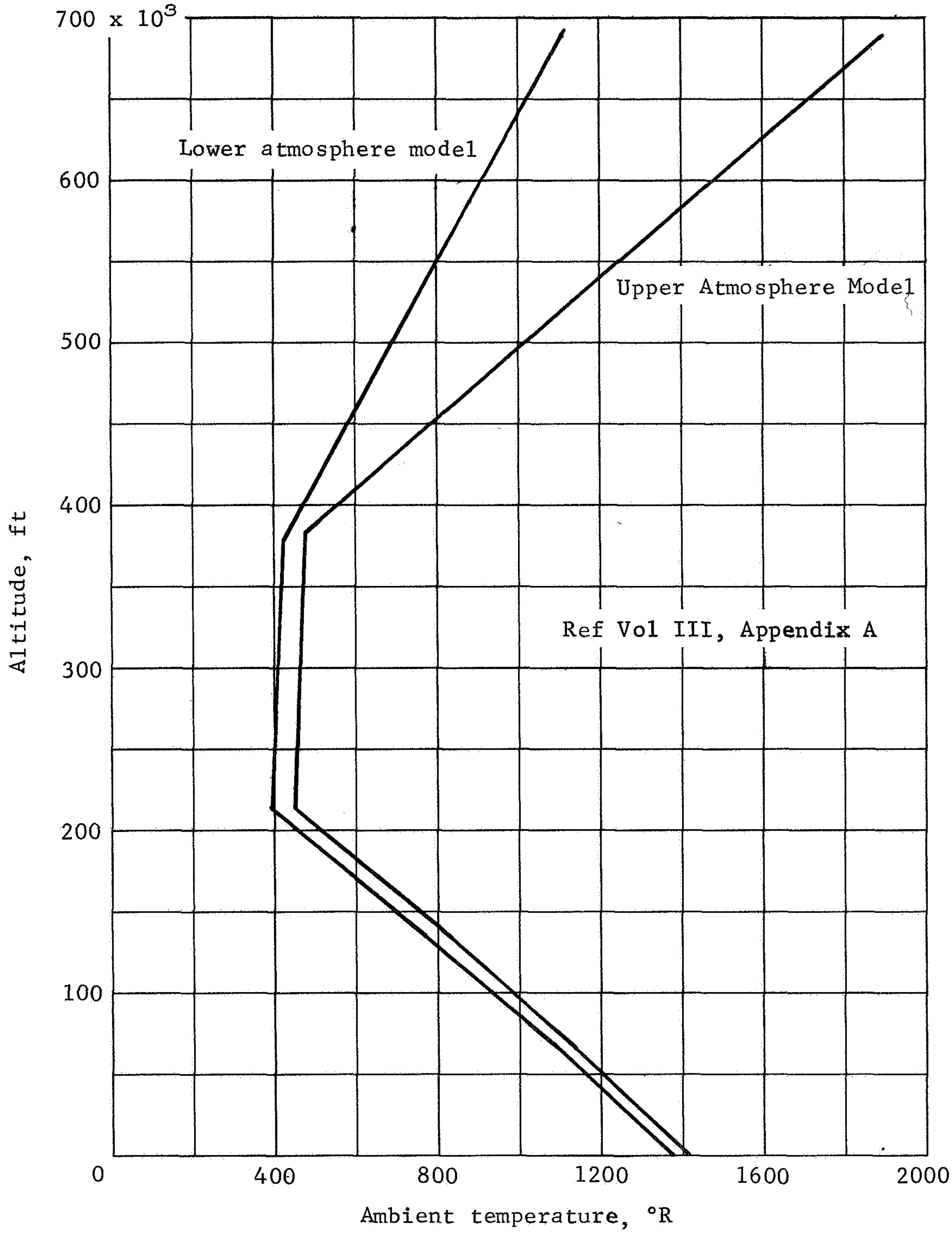

Figure 44.- **Venus Atmosphere Models,** Ambient Temperature vs Altitude

Entry trajectories were computed for the following tabulated parametric ranges during the course of the BVS study.

V_E, fps	B_E, slug/ft^2	$-\gamma_E$, deg	Atmosphere model
32 x 10^3	0.2, 0.3, 0.4	10, 20, 30, 40	Upper and lower
36	0.3, 0.4, 0.5	20, 30, 40, 50	Upper and lower
38	0.2, 0.3, 0.4, 0.5	20, 30, 40, 50	Upper and lower
44	0.3, 0.4, 0.5, 0.6	20, 30, 40	Upper and lower

Analysis of the above parametric data indicates that over the range studied, ballistic coefficient has a very minor effect on entry envrionment. For this reason, data in the following summary curves are not presented as a function of entry ballistic coefficient. One exception to the insensitivity to ballistic coefficient is dynamic pressure q experienced during entry. Peak dynamic pressure (not shown in plots) is related to max drag deceleration by the following expression:

$$q_{max} = (32.174\ g_{\oplus(peak)}\ B_E$$

Maximum dynamic pressure as a function of B_E can thus be calculated from the data of figure 47.

Time from entry altitude to aeroshell staging condition (Mach 0.5) as a function of entry velocity and initial entry flight path angle is shown for the upper and lower atmosphere models on figure 45. It is seen that entry time is a weak function of entry velocity and atmosphere model, but is quite sensitive to initial entry flight path angle. Entry time for a nominal entry condition is quite short, of the order of 60 sec.

The time at which the entry deceleration builds up to a level of 1.0 g is taken as the initiation point for a time sequencer controlling subsequent system events. The time between 1.0 g deceleration and staging is shown in figure 46.

Peak drag deceleration in earth gs as a function of entry velocity and initial entry flight path angle for the upper and lower atmosphere models is shown in figure 47. Peak drag acceleration is seen to be strongly affected by both entry velocity and entry flight path angle. Density scale height is nearly the same in both model atmospheres, so that peak g is relatively unaffected by atmosphere model. The lower atmosphere shows a slightly higher peak at all entry conditions studied.

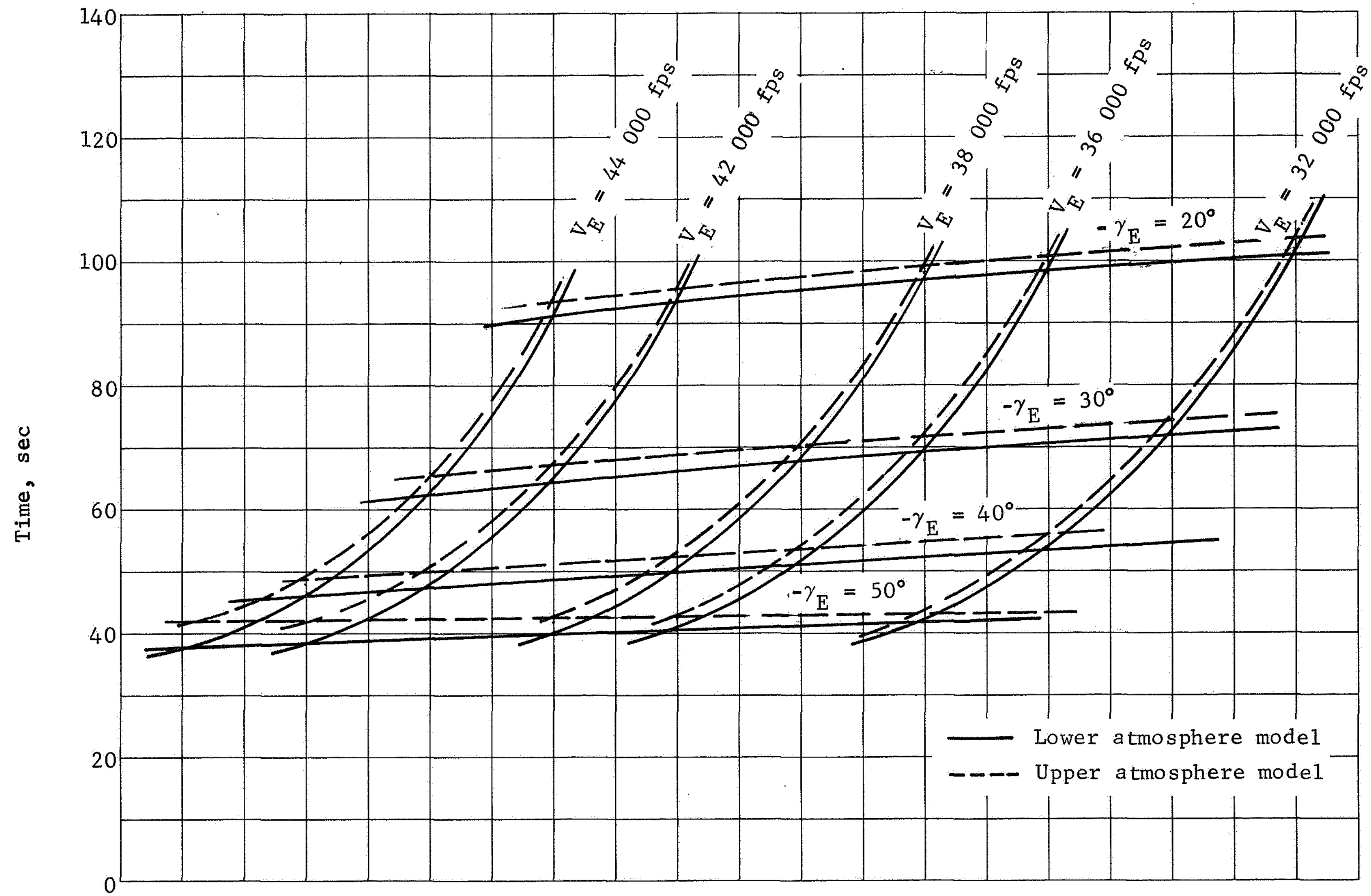

Figure 45.- Time between Entry and Staging

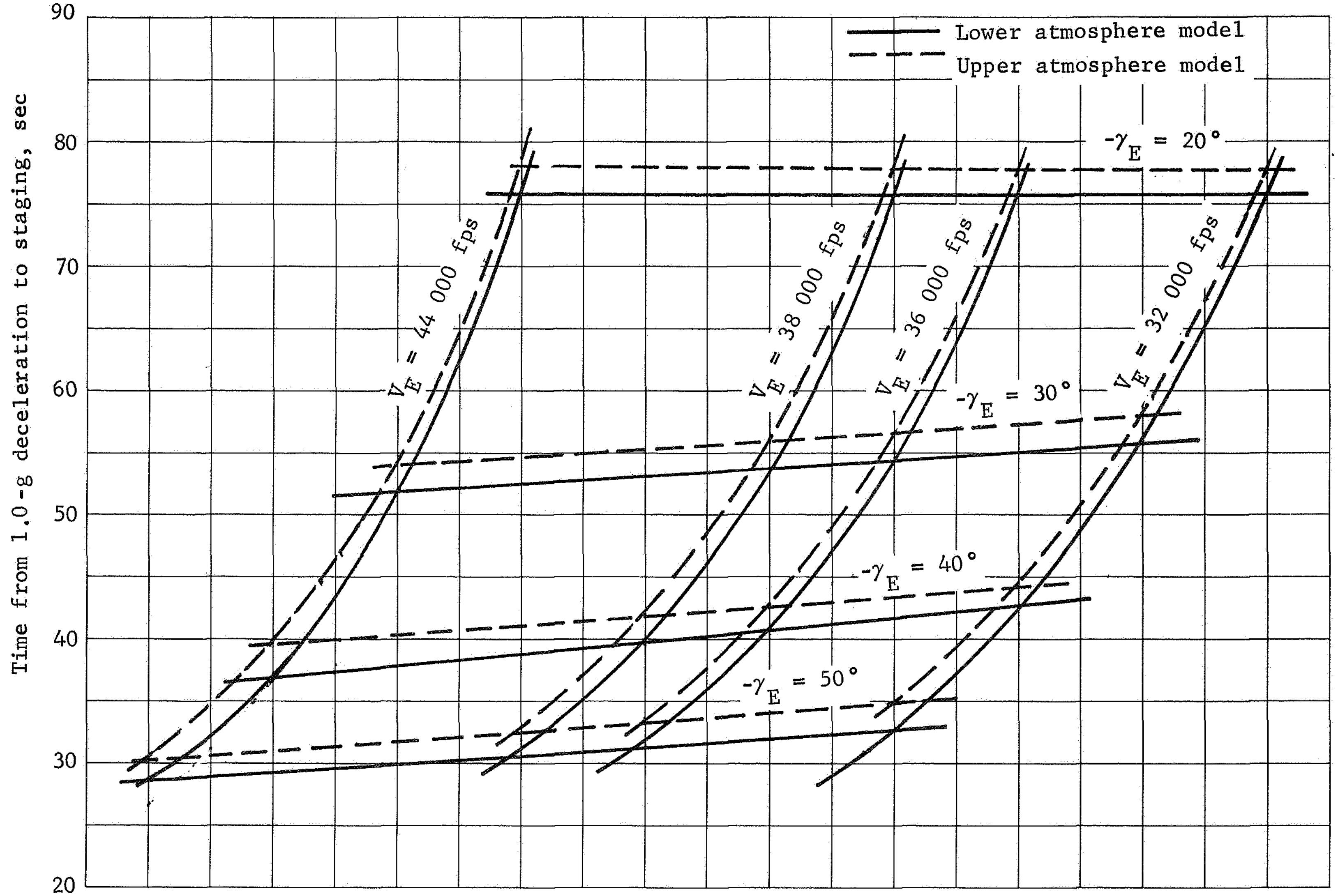

Figure 46.- Time between 1.0-g Deceleration and Staging

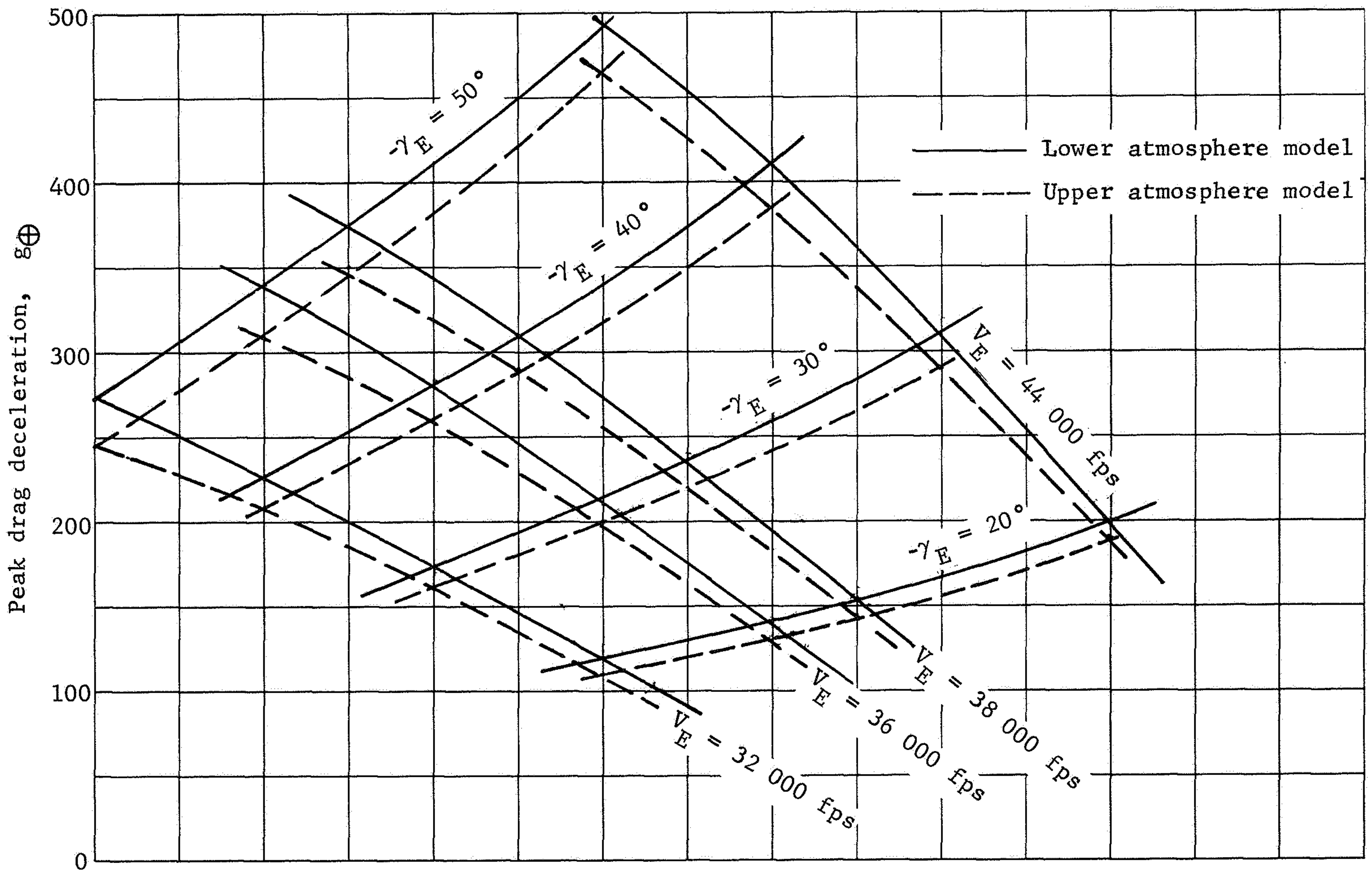

Figure 47.- Peak Entry Drag Deceleration

The altitude above the planet mean surface level at which aeroshell staging occurs is shown as a function of entry velocity and entry flight path angle for the atmosphere model in figure 48 and for the upper model in figure 49. The insensitivity of staging altitude with entry velocity is noted.

The central angle through which the entry vehicle moves during the entry portion of the mission profile is of importance in determination of balloon deployment location relative to the planet coordinate system and for evaluation of communication geometry. The down range angle from entry to aeroshell staging is shown in figure 50.

Thirty seconds after the aeroshell staging sequence begins, a subsonic probe is dropped. The descent time from the staging altitude to mean surface level is shown on figure 51(a). The nominal subsonic probe has a ballistic coefficient of 6.0 slug/ft^2, resulting in a drop time of 34.5 min in the upper atmosphere and 32.5 min in the lower atmosphere.

Drop sondes are jettisoned at the BVS nominal float altitude of 190 000 ft. These sondes have a ballistic coefficient at 5.0 slug/ft^2. Drop time from float altitude to mean surface level is shown on figure 51(b) as a function of sonde ballistic coefficient. A drop time of 33.5 min in the upper atmosphere model and 32.0 min in the lower atmosphere is shown.

Aerodynamic heating.- Spherically blunted cones are considered to be the most realistic configuration for these missions on the basis of previous planetary entry studies. The significant configuration variables are the radius of the spherical nose and the cone angle. Examination of the heating at the stagnation point and at the edge of the cone will allow adequate defination of optimum configurations and of their total heat loads.

Stagnation point convective heating estimates are based on the data of Marvin and Pope* which account for the effects of atmospheric composition. Convective heating distributions over the vehicle are obtained by use of the reference enthalpy technique. Major uncertainties associated with the convective distributions are the effects of flow transition and of vorticity interaction.

---

*Marvin, J. G. and Pope, R. B.: Laminar Convective Heating and ablation in the Mars Atmosphere. AIAA, vol. 5, no. 2, Feb. 1967.

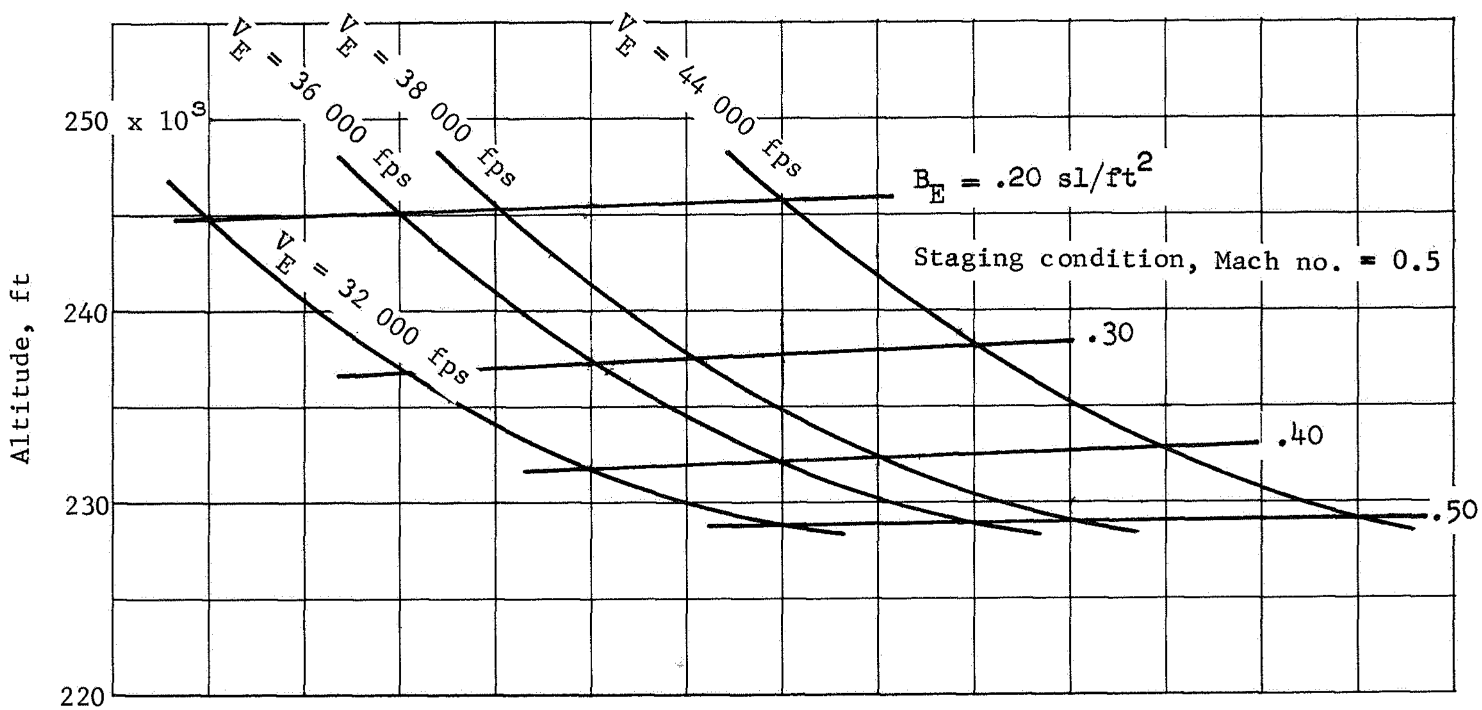

Figure 48.- Staging Altitude, Lower Atmosphere Model

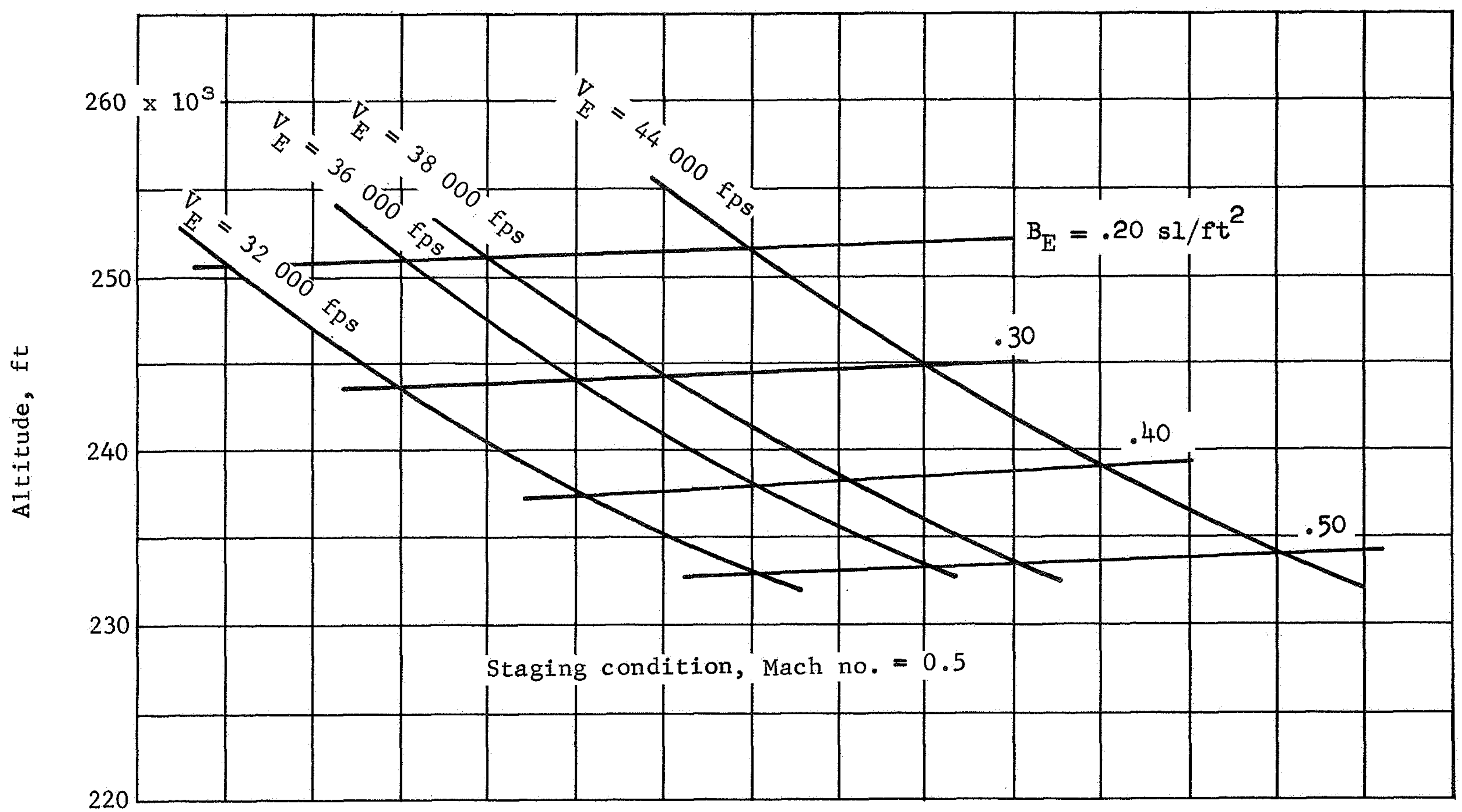

Figure 49.- Staging Altitude, Upper Atmosphere Model

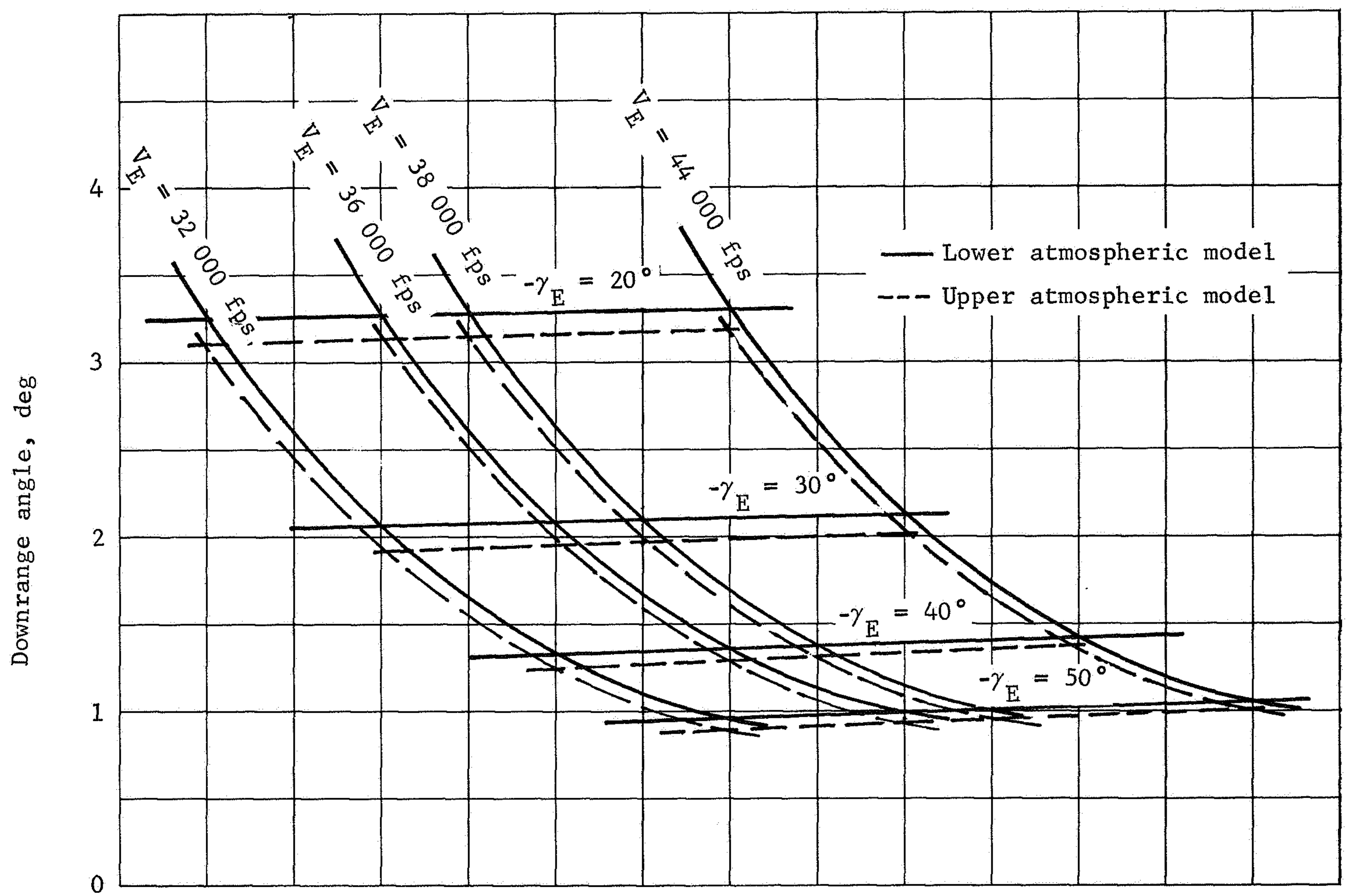

Figure 50.- Downrange Angle

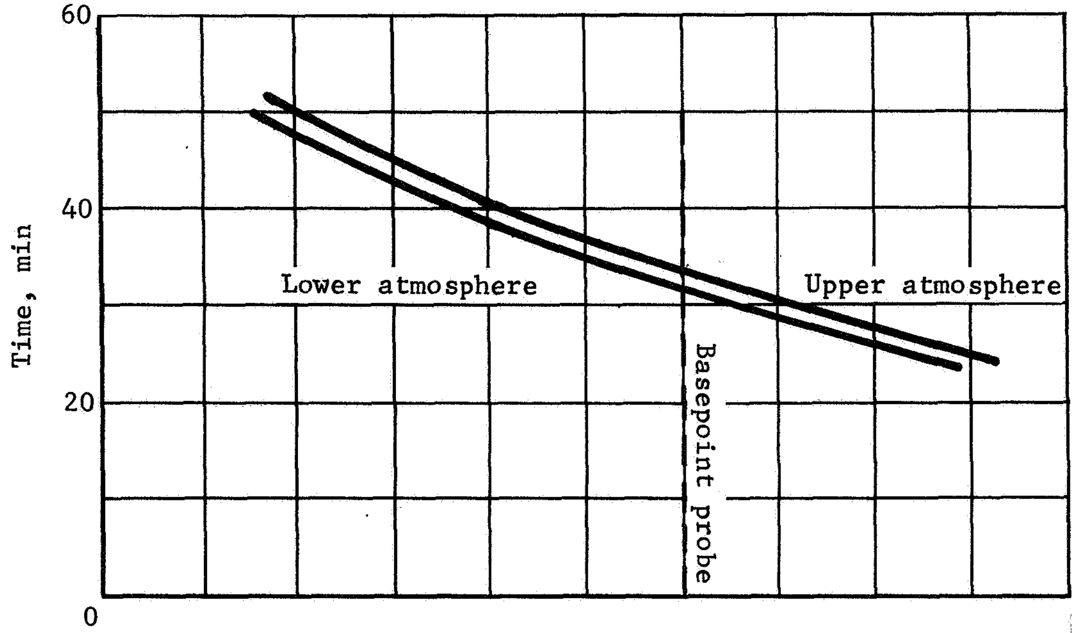

(a) Subsonic Probe, Staging Altitude to Surface

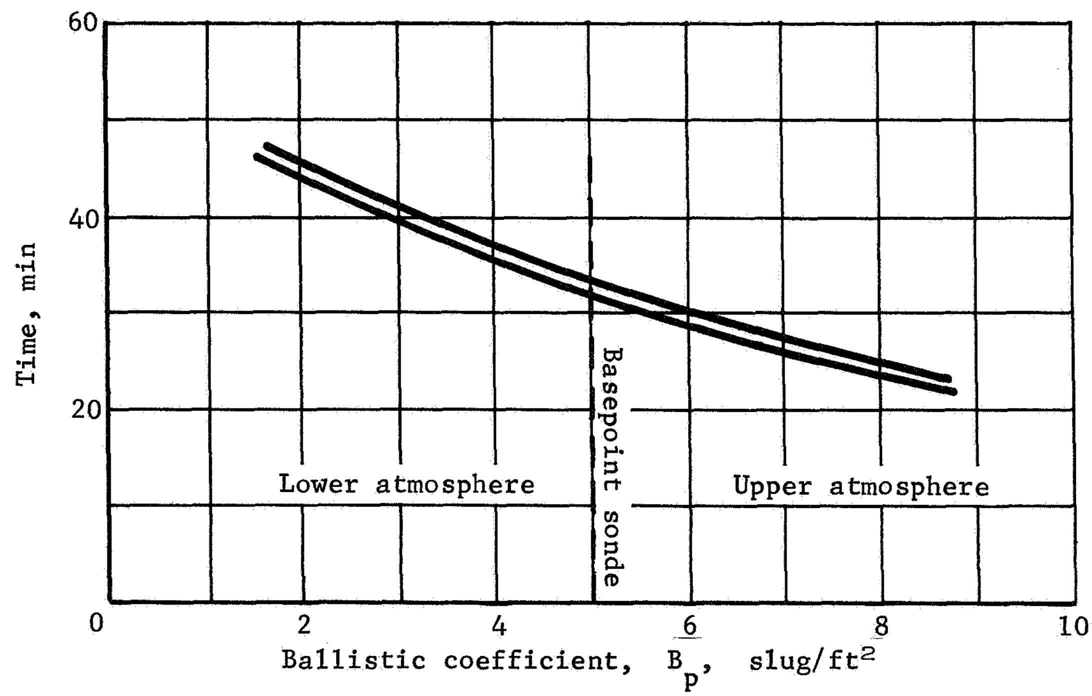

(b) Drop Sonde BVS Float Altitude, 58 km, to Surface

Figure 51.- Subsonic Probe and Drop Sonde Descent Times

Transition from laminar to turbulent flow (Hearne et al.*) was assumed to occur at a momentum thickness Reynolds number of 250. This criterion predicts transition at the cone edge slightly before the maximum convective heating time for most of the trajectories studied. Interaction of the turbulent boundary layer with the entropy layer can give rise to convective heating rates approaching sharp cone values on the cone surface. Calculations show that for a nominal configuration ($\theta_C = 55°$, $R_N = 1.0$, $R_B = 4.25$) the turbulent boundary layer thickness is much thicker than the entropy layer at the cone edge. Therefore, the turbulent boundary layer will be expected to engulf the entropy layer at the cone edge and extend into the high velocity cone flow. This phenomenon is a function of the nose radius and thus the convective heating at the cone edge is significantly affected by both nose bluntness and cone angle.

Radiative heating was computed as separate components of equilibrium and non-equilibrium heating for the spectral regime $0.125\ \mu < \lambda < 6.0\ \mu$ and of heating for the spectral regime $\lambda < 0.125\ \mu$ at the temperature associated with the equilibrium chemistry behind the shock wave. Primary radiators for the model atmosphere are CN (red and violet), CO(4+), and the continuum from radiative recombination of carbon and nitrogen. There is considerable uncertainty associated with the radiative heating estimates. The region of CO(4+) has not been experimentally verified; there is only a small amount of data on non-equilibrium radiation associated with the CN overshoot; and the far ultra-violet radiation ($\lambda < 0.125\ \mu$) is very dependent upon the temperature behind the shock -- a variable which is not accurately known for the gas compositions and flight velocities encountered in the Venus mission studies. The uncertainties in the shock-density relations can cause large variations in the radiation. For instance, an error of 10% in the temperature in the region of 10 000°K results in a factor of three change in the heat transfer. The lower CO_2 content atmosphere is critical for radiation heating.

Analysis of aerodynamic heating in the Venusian atmosphere is subject to uncertainties associated with the lack of experimental data for CO_2/N_2 mixtures. It is necessary to consider the uncertainties associated with current estimates of heating in this mission evaluation. The uncertainties are not the same for all the

---

*Hearne, L. F., Chine, J. H., and Woodruff, L. W.: Study of Aerothermodynamic Phenomena Associated with Reentry of Manned Spacecraft. Lockheed Missles and Space Co. (Contract NASA 9-3531), May 1966.

components of heating and different components of heating are predominant for different missions. Uncertainty factors were assigned to each of the identified components of heating to account for the lack of confidence in current prediction techniques. Both nominal aeroheating estimates and the uncertainties were used in the study. Nominal estimates are shown in this part of the report. The uncertainty factors used are shown as follows:

1) Convective heating, laminar and turbulent = 1.5;
2) Radiative heating, equilibrium = 1.5;
3) Radiative heating, U.V. equilibrium = 3.0;
4) Radiative heating, non-equilibrium = 3.0.

Much research is required to reduce the uncertainty associated with the prediction of the aerodynamic heating for the Venus missions.

The mission associated variables are entry velocity V_E, entry flight path angle γ_E and ballistic coefficient B_E. These parameters are tabulated below for the three missions considered here.

Mission	V_E, fps	γ_E, deg	B_E, slug/ft^2
Orbital	32 000	-30	0.33
Direct flyby	37 400	-30	0.375
V/M swingby	44 000	-35	0.58

Summary parametric heating data which cover this range of mission variables are shown in figures 52 thru 56. Maximum heating rates and total heat loads are plotted versus entry velocity which is the mission parameter with the strongest influence on aerodynamic heating. Data are presented for two flight path angles, γ_E = -30 and -40°. The configuration is fixed, the nose radius is 1.0 ft and the cone half angle is 55°. The radiation heating at the stagnation point is presented in figure 52 and the convective heating at the stagnation point is presented in figure 53. The most significant point shown by the data of figures 52 and 53 is the large increase in radiative heating with increased velocity, particularly in the higher velocity range. The effect of increasing ballistic coefficient on radiative heating is also magnified at the high entry velocities. Heating data for the cone edge (the cone surface at the max. diam) are given in figures 54 and 55, while the max, aerodynamic shear stress is shown in figure 56. These data for the cone edge show the same trends as the stagnation point data, namely increasing velocity and ballistic coefficient result in large increases in the radiative heating.

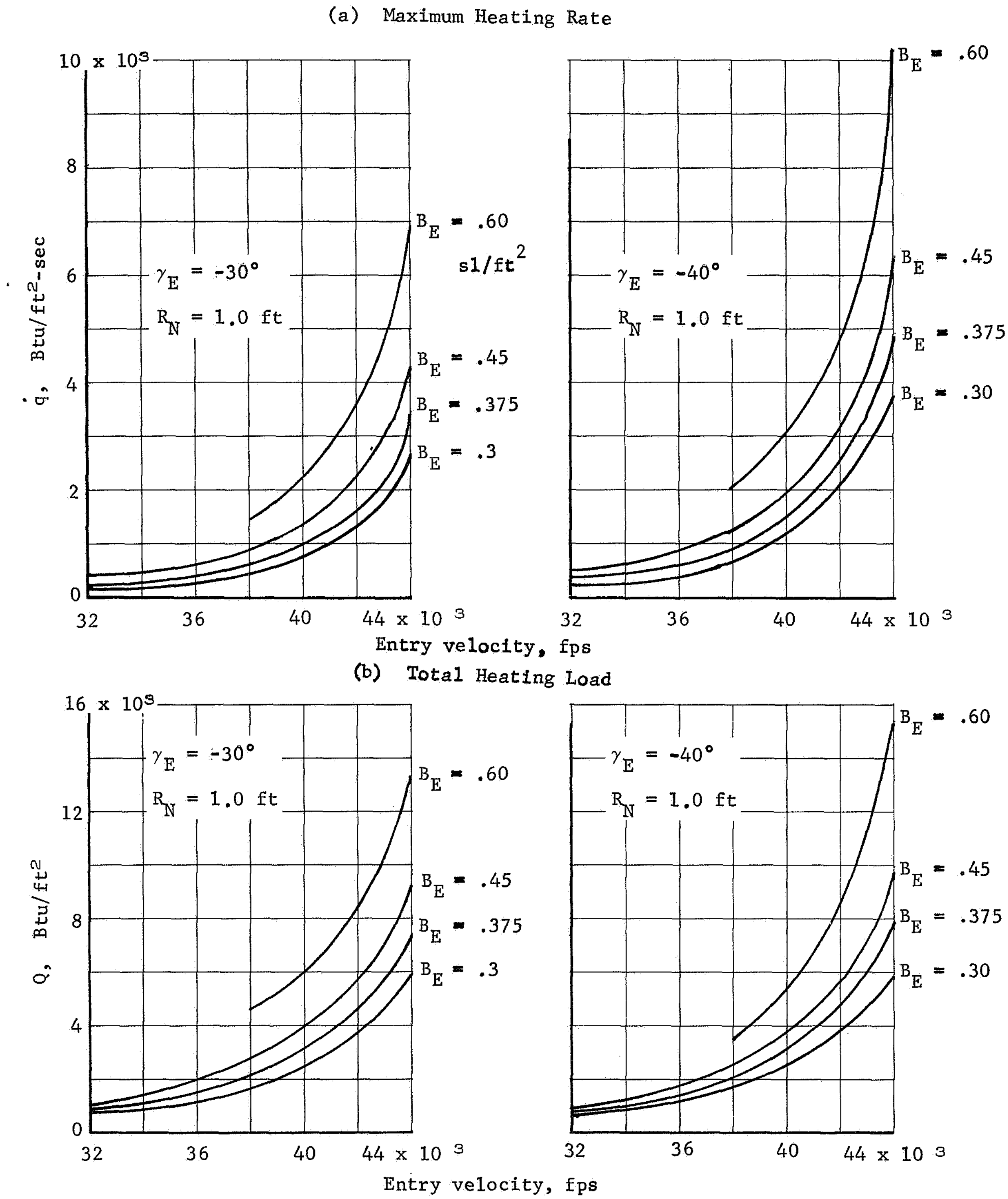

Figure 52.- Stagnation Point Radiation Heating

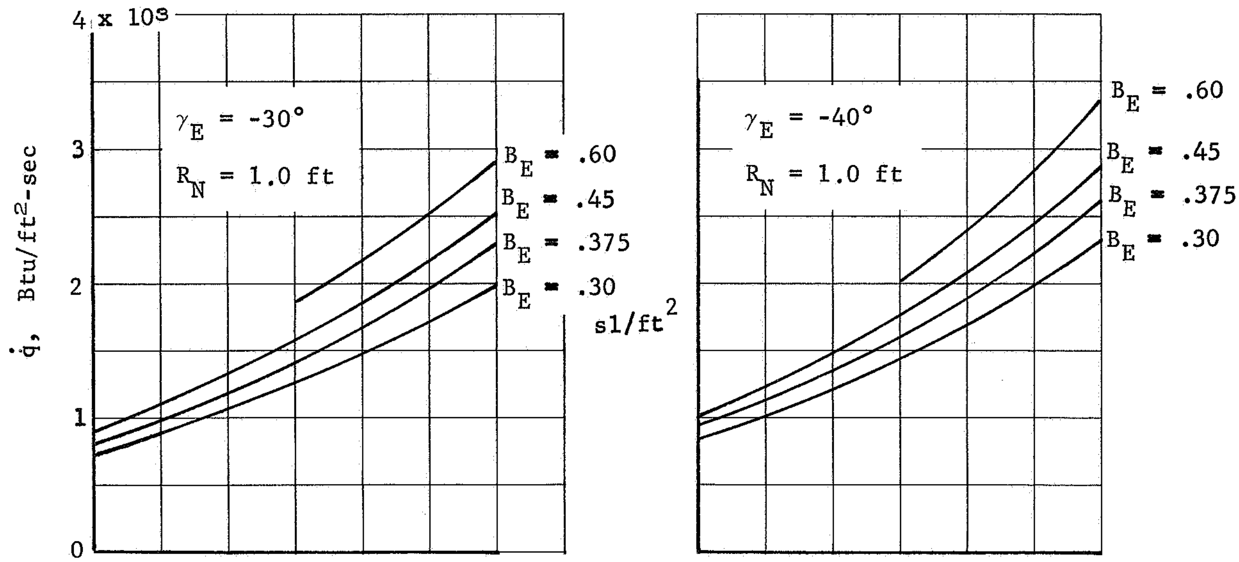

(a) Maximum Heating Rate

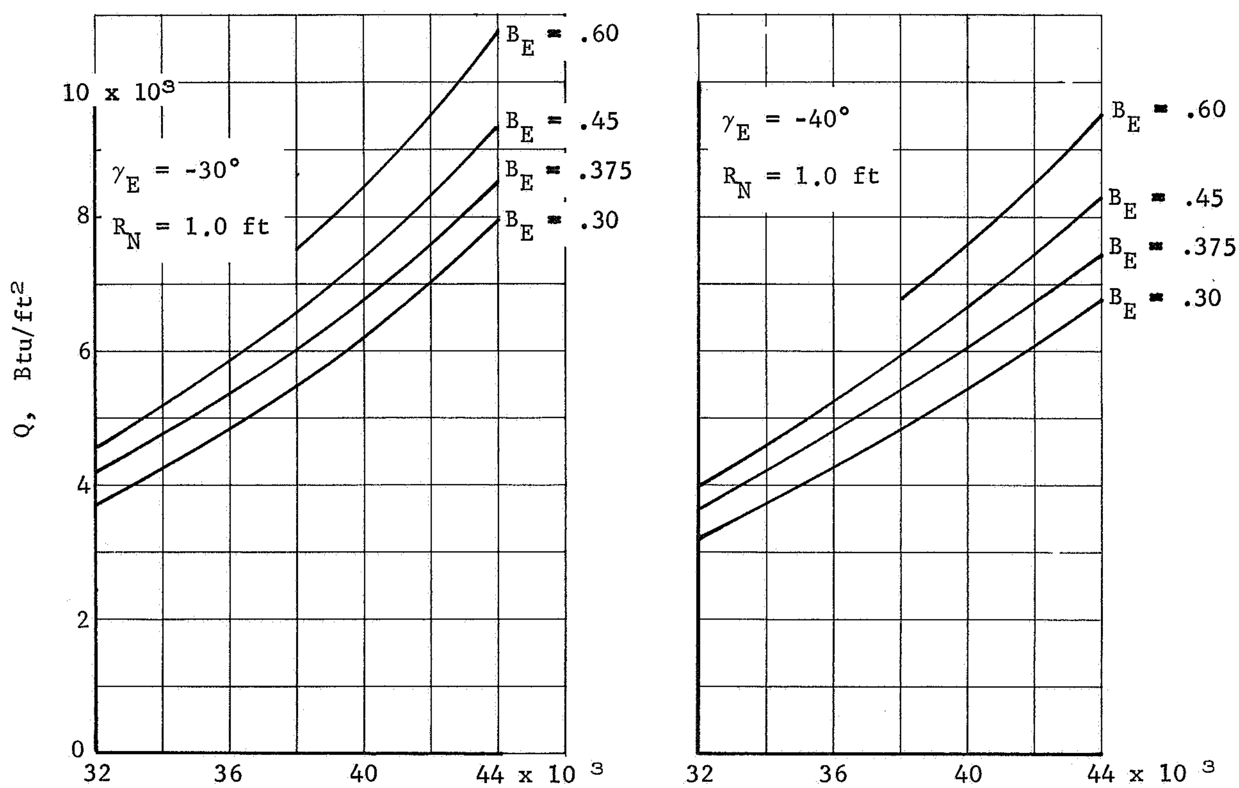

Entry velocity, fps

(b) Total Heating Load

Figure 53.- Stagnation Point Convection Heating

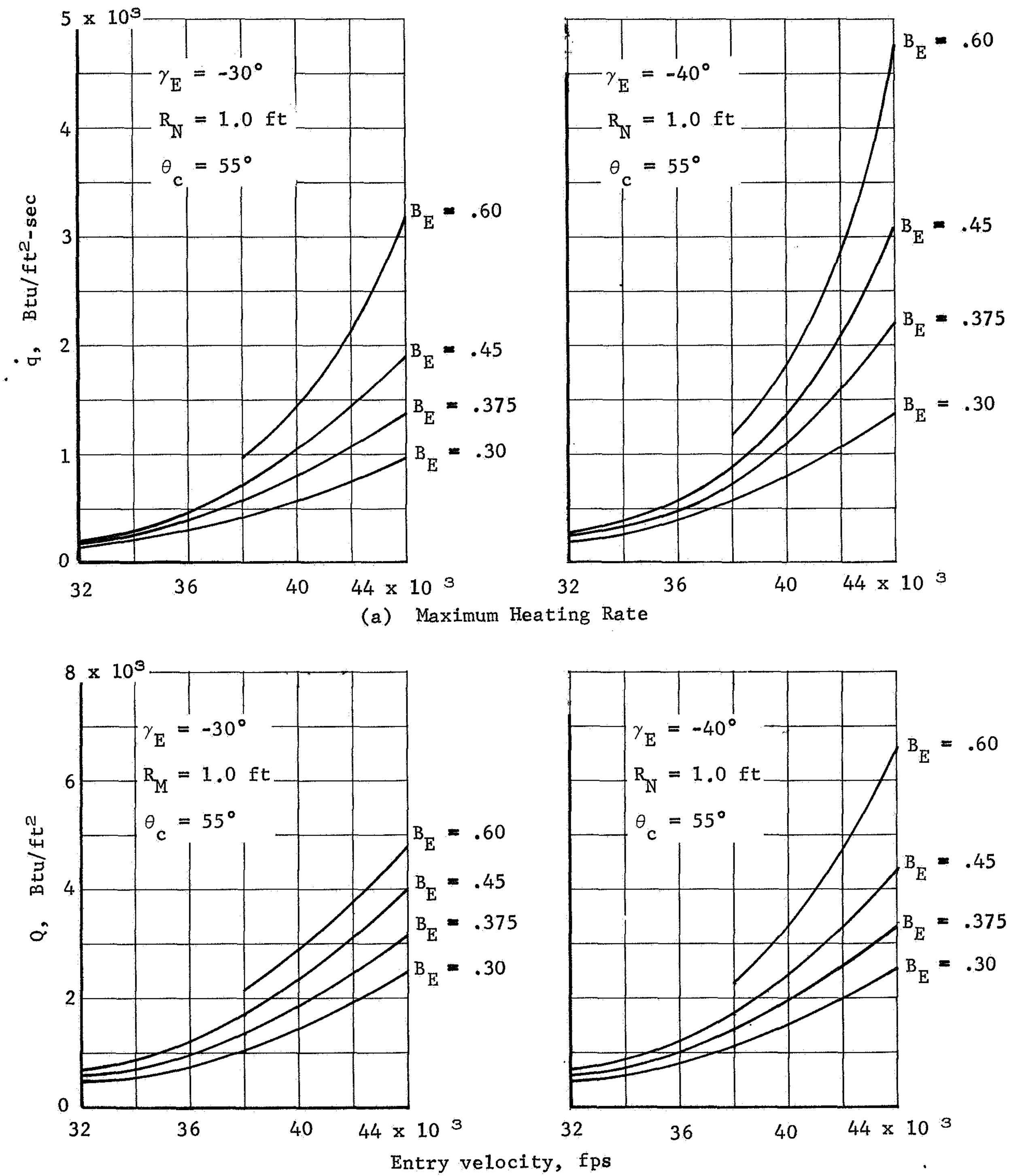

(a) Maximum Heating Rate

(b) Total Heating Load

Figure 54.- Cone Edge Radiation Heating

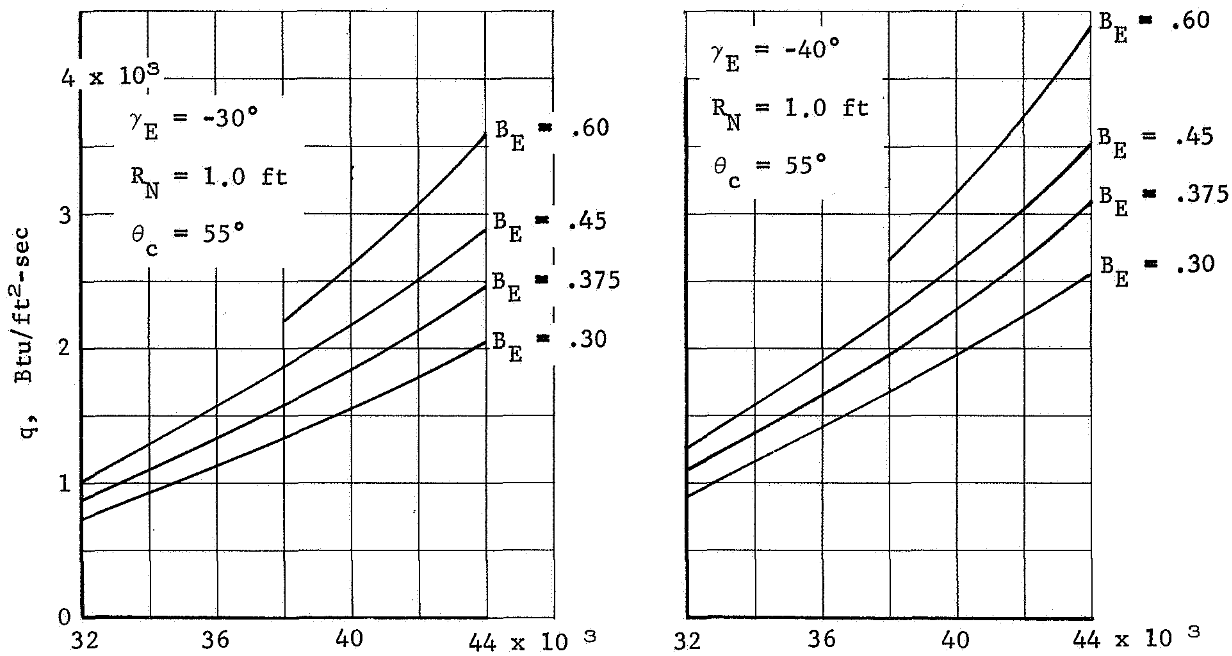

(a) Maximum Heating Rate

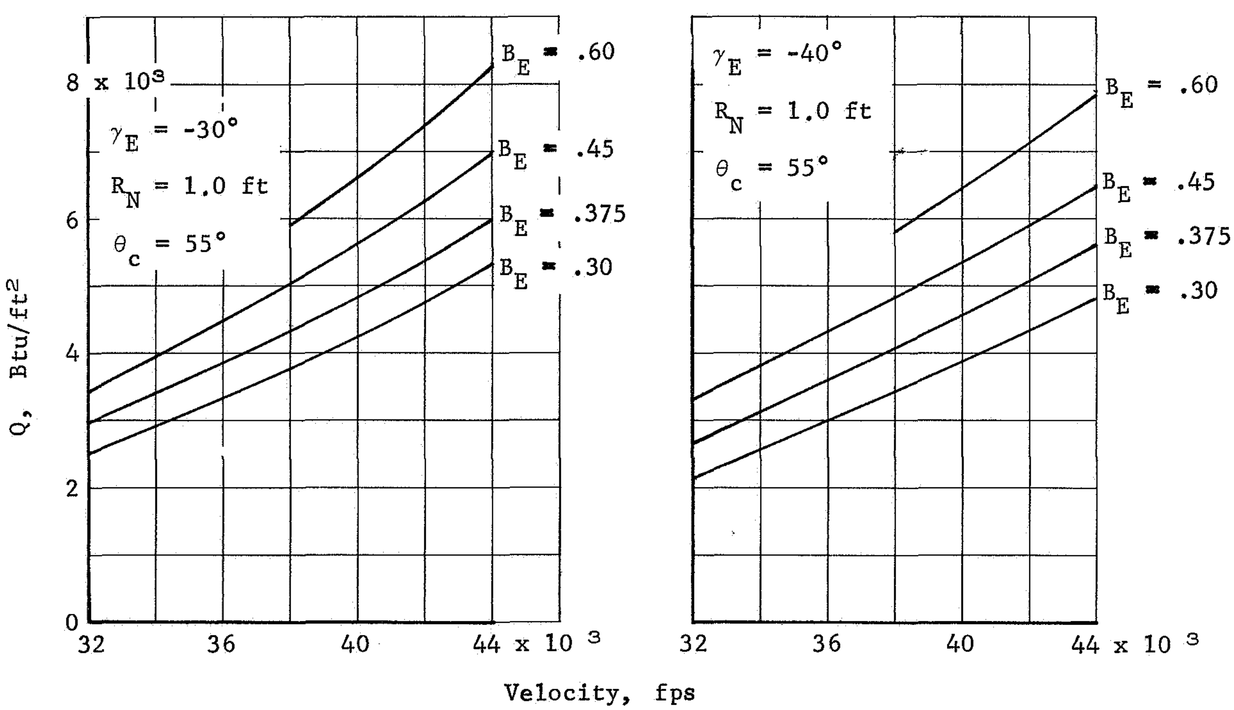

(b) Total Heating Load

Figure 55.- Cone Edge Convection Heating

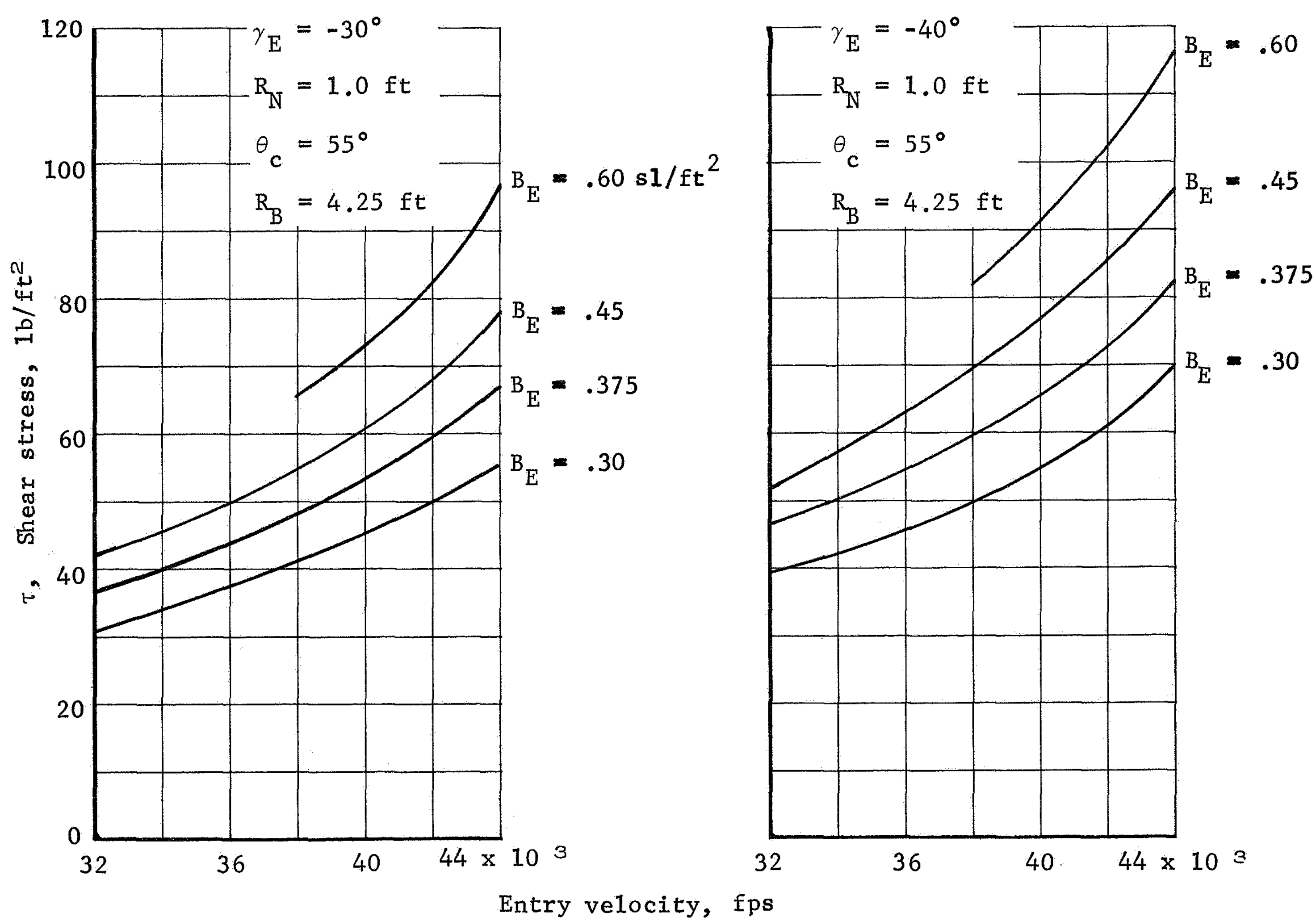

Figure 56.- Aerodynamic Shear Stress at Cone Edge

The effects of configuration variations on aerodynamic heating are shown in figure 57. This example is based on the direct entry flyby mission with an entry velocity of 38 000 fps, entry weight (W_E) of 885 lb and a vehicle diameter of 8.5 ft. Maximum heating rates, aerodynamic shear, and total heating loads are presented as functions of cone half angle. These data in figure 57 reflect the influence of cone half angle on drag coefficient and thus on ballistic coefficient. The heating parameters shown for the cone edge reflect both the direct effect of cone angle on the flow field and of the ballistic coefficient on the trajectory. The cone edge data show that convective heating and shear stress decrease with increasing cone angle, while radiative heating increases with increasing cone angle. Both sharp and blunt cone solutions are presented for the convective heating and shear stress The blunt cone solution results in significantly reduced heating and shear stress compared to the sharp cone solution. The difference between the sharp and blunt cone solutions is the vorticity interaction, i.e., the interaction of the boundary layer and the entropy layer. Analysis indicates that the heating on a cone with with a one-ft nose radius approaches that of the sharp cone. A three-ft nose radius is required to eliminate the vorticity interaction effect. The heating at the cone edge for intermediate nose radii is not well defined. The nose radius has no significant effect on the radiative heating at the cone edge. The significant point is the interaction between the effects of nose radius and cone angle with the result that these two geometric parameters cannot be optimized independently.

The entry configuration for the flyby direct entry mission has been selected primarily on the basis of maximizing confidence in the design rather than minimizing aeroshell structure and heat shield weight. For this mission a configuration with a one-ft nose radius, 55° half angle cone and a base radius of 8.5 ft will encounter heating rates (with all uncertainty factors applied) that are within the capability of materials test facilities (see Vol III Appendix B). However, this requires that the nose radius be not greater than one ft to keep the radiative heating within the test capability. This requires that the higher convective heating and shear associated with the sharp cone solution must be accepted on the cone surface. Thus a heat shield weight penalty is accepted in order to gain increased confidence in the design.

The same aeroshell configuration has been used for the orbital entry mission. All the heating rates and loads are low enough for this mission that a complete weight optimization could be performed within the test facility constraints. However, such an optimization is considered to be unnecessary at the present time due to the uncertainties in the heating estimates and the relatively small weight gain due to such optimization.

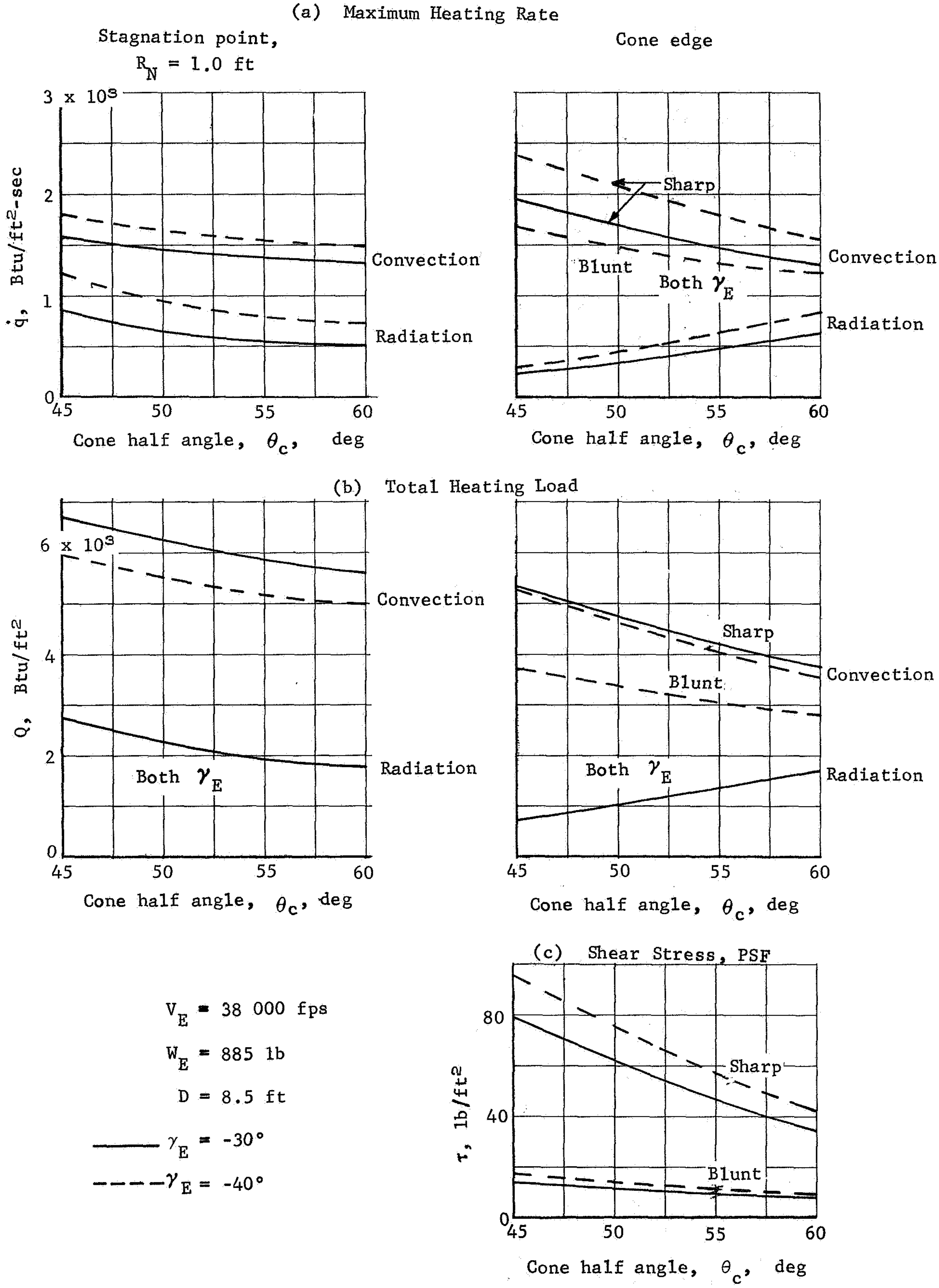

Figure 57.- Configuration Effects on Aerodynamic Heating

The heating rates for the Venus/Mercury swingby mission exceed the test facility constraints due to the increase in heating with velocity indicated by figure 52 thru 56. A detailed configuration optimization is not justified due to the even larger influence of the uncertainties in heating estimates for the mission. Therefore the same configuration is used for this mission as for the other missions. The largest weight influence is the relationship between aeroshell diameter and ballistic coefficient. Reducing the aeroshell to its minimum practical diameter of seven ft reduces the total heat shield weight although the ballistic coefficient and unit total heating load are increased.

Balloon Deployment and Sonde Trajectory

Balloon deployment on all of the BVS missions is initiated by a barometric pressure device set at 612.4 mb. This pressure corresponds to 190 288 ft (58 km) above the mean planet radius of 6050 km in the mean atmosphere, 191 624 ft in the upper atmosphere, and 188 643 ft in the lower atmosphere. The parachute descent trajectories before balloon deployment are shown in figure 58. Note that the heat shield is jettisoned 15 sec after main chute deployment (M = 0.5); the subsonic probe is dropped 30 sec after that. As seen below, trajectory conditions at balloon deployment in the upper and lower atmospheres are remarkably similar for the orbital mission:

Trajectory parameters	Upper	Lower
Altitude, ft	191 624	188 643
Velocity, fps	29.6	31.7
Flight path angle	90°	90°
Dynamic pressure, psf	.955	.955
Mach no.	.0319	.03515
Time from chute deploy, sec	1130.7	964.7

The balloon trajectories in upper, lower, and mean atmospheres are presented in figure 59. The balloon reaches an equilibrium float condition approximately 800 sec after beginning inflation. The float altitude varies from 58.22 to 57.68 km based on a common float density of 0.0659 lb/ft^3. The supertemperature in the balloon, the extent of venting, the atmosphere temperature, and the pressure influence the float altitude of the balloon.

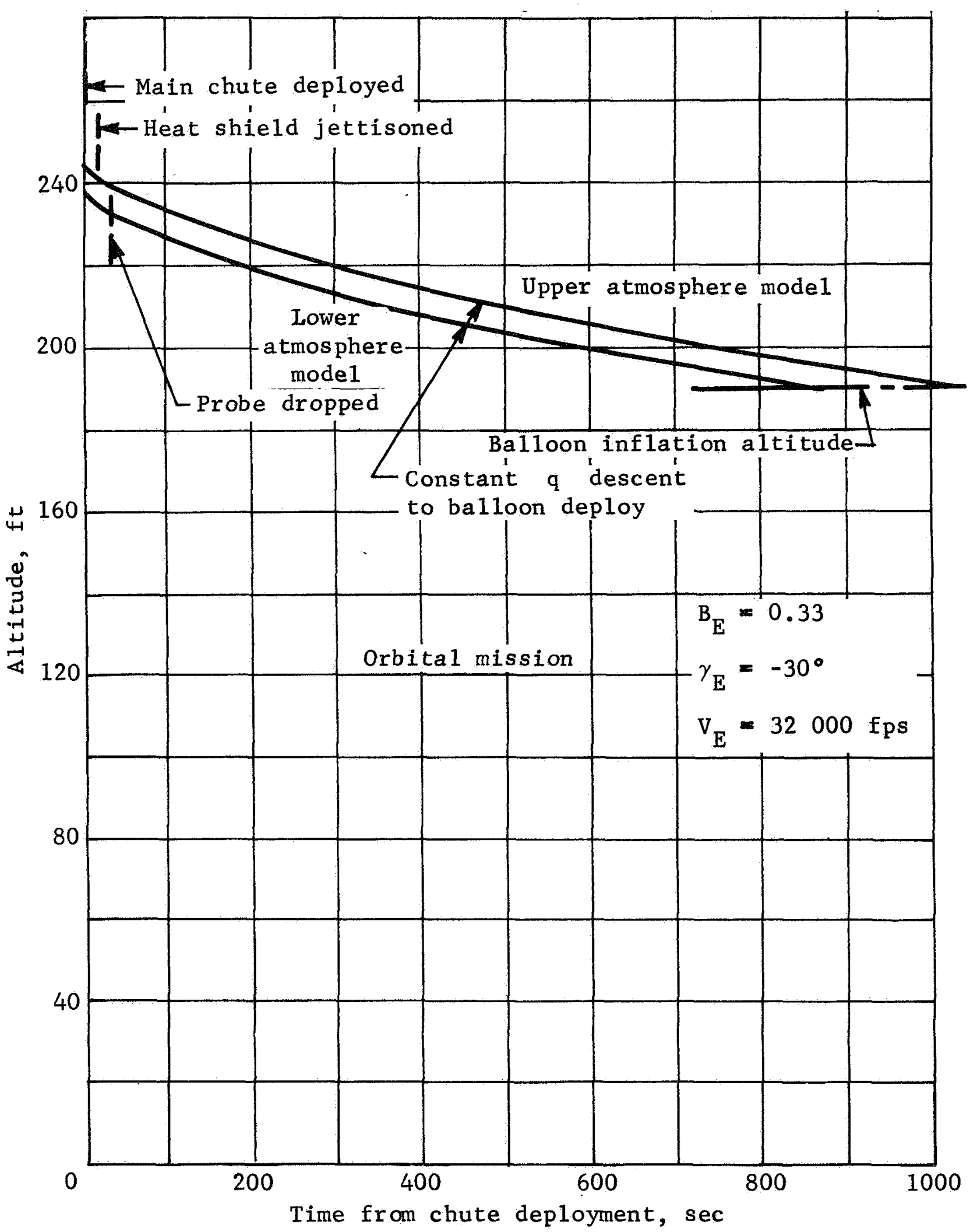

Figure 58.- Time from Chute Deployment to Balloon Inflation

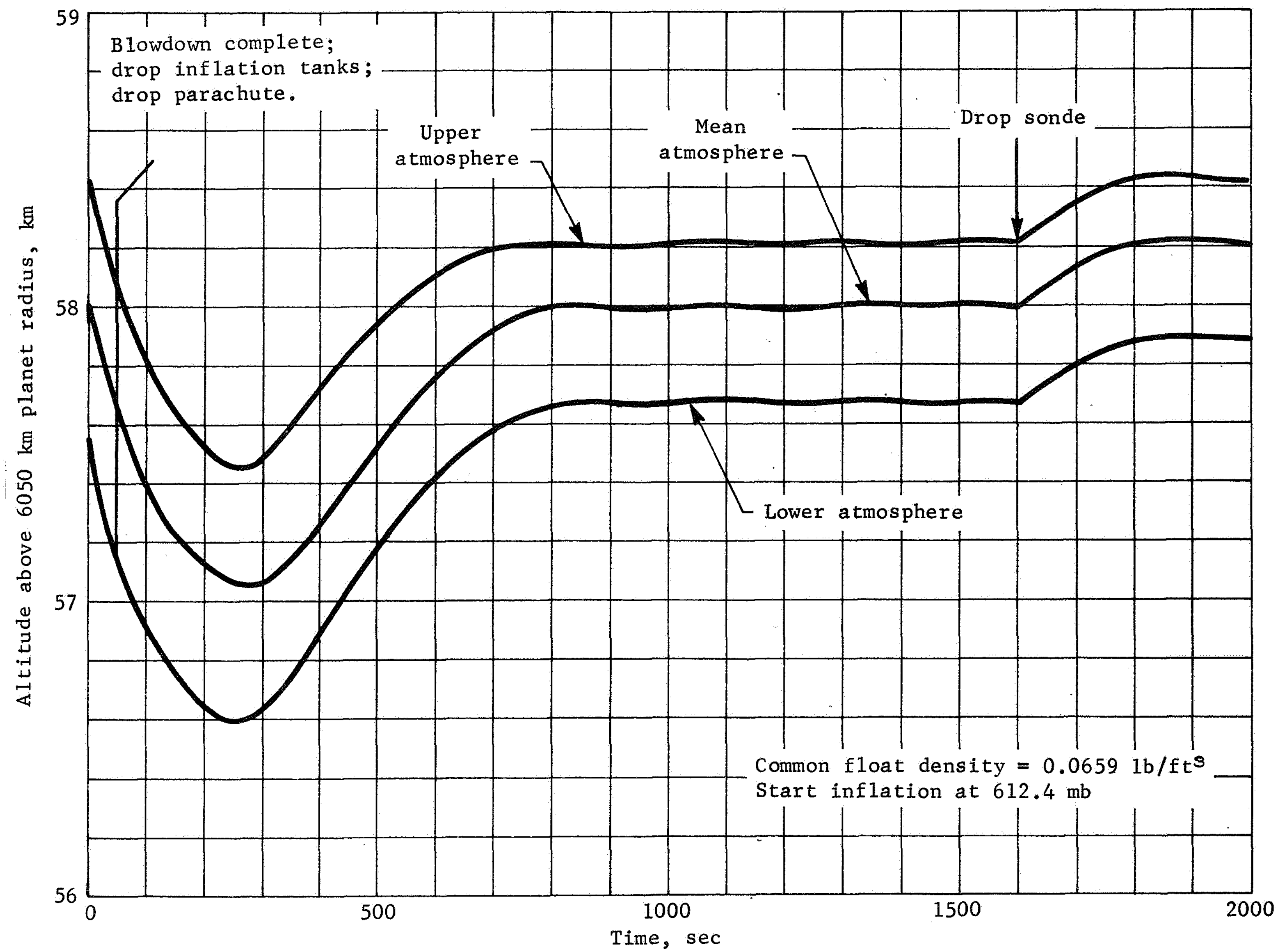

Figure 59.- Nominal Balloon Inflation Time History

At some time during the BVS mission, the system is capable of dropping 5 lb sondes on command. The effect of dropping a 5 lb sonde is shown in figure 59 at 1600 sec. The lighter gondola immediately seeks a new float altitude approximately 0.2 km higher than before the drop.

The drop sonde follows a descent time - history shown in figure 60, arriving at the planet surface in 2000 sec in the upper atmosphere.

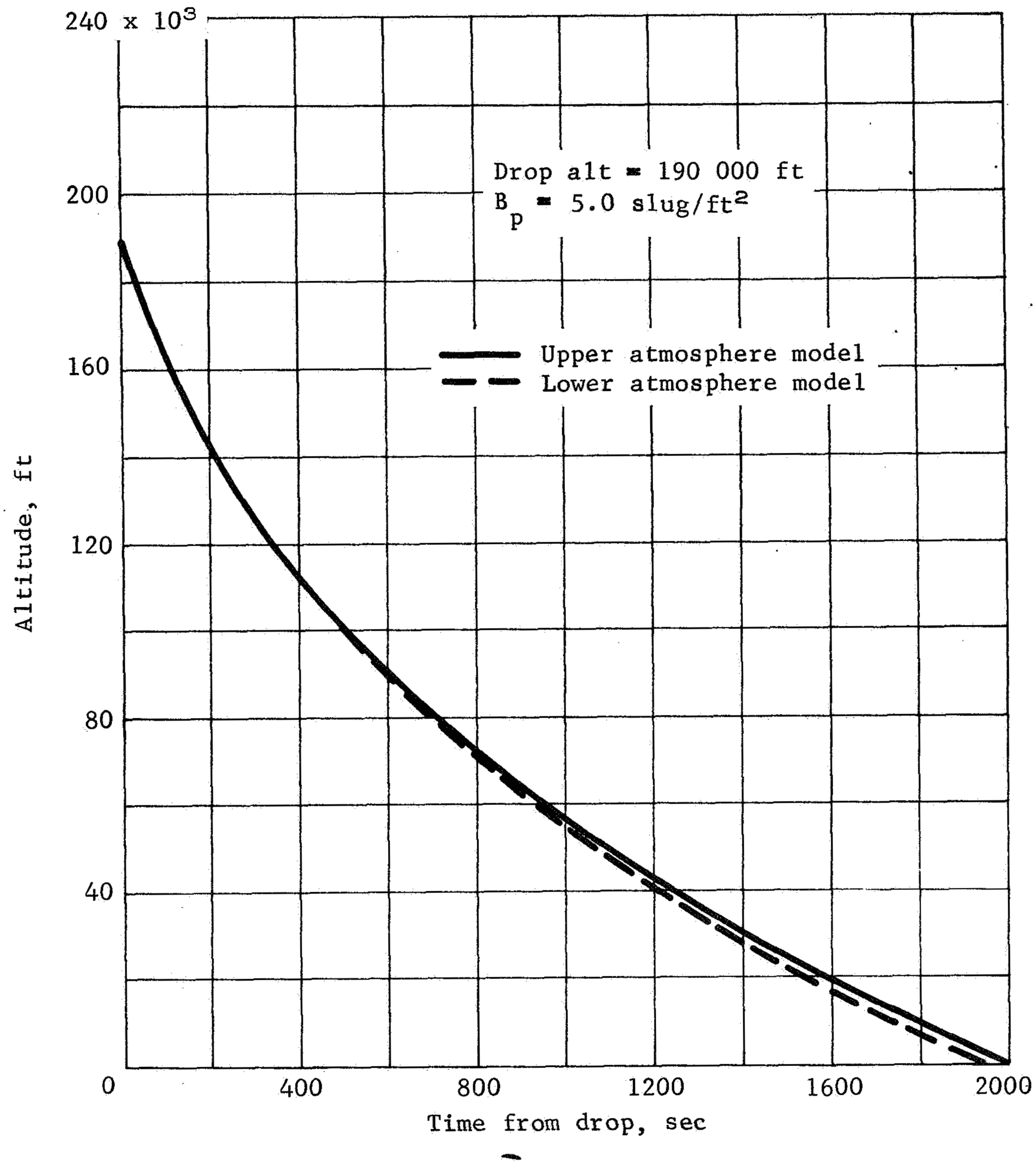

Figure 60.- Drop Sonde Descent Time History

MISSION PROFILE SUMMARIES

This section presents mission profile summaries for three reference BVS missions. These summaries define the important elements of the mission from launch through balloon inflation. The three reference missions, discussed in order, are (1) a 1972 flyby, (2) a 1973 orbital mission with entry from approach and entry from orbit, and (3) a 1973 Venus/Mercury swingby.

To develop an interplanetary mission profile, a number of diverse, and in some cases conflicting requirements, must be integrated into a workable and acceptable mission. Some of the factors that must be considered are launch opportunity, launch period, candidate launch vehicle performance, interplanetary transit time, earth-spacecraft communication geometry (distances and angles), planet approach geometry, mission science objectives at the planet, entry environment, and mission terminal phase conditions.

Because the BVS contract directed that only the 1972 and 1973 launch opportunities be considered, data in this report, considered only these two years. The required length of the launch period, defined as the number of consecutive days during which a launch window is available, depends on the abilities to launch the spacecraft on schedule and to recover from launch abort. Based on extensive launch experience, the launch period for both the SLV3C/C and Titan IIIC vehicle is 20 days.

The launch and planet arrival dates are selected primarily on the bases of launch energy requirements and planet approach velocity. The launch energy requirements must be within the capability of the candidate launch vehicles; furthermore, there must be constraints on the approach velocity because the entry velocity for the direct ejection is a function of the approach velocity. For a flyby mission, the maximum launch energy required is usually the governing factor, but for an orbital mission, the orbit insertion requirements bias the launch and arrival dates toward those on which the planet arrival energy is lowest. These launch vs arrival energy trade-offs are made from the C_3 and V_{HE} contours presented in figures 2 and 3.

Interplanetary transit time and communication geometry depend on the type of transfer trajectory. In a Type I trajectory, the spacecraft travels through a heliocentric angle $<180^{\circ}$. In a Type II trajectory, the heliocentric angle is $>180^{\circ}$. The launch and arrival dates and energy characteristics for both trajectories types are presented in figures 2 and 3.

In targeting for specific entry points on the planet, the fundamental consideration is the location of the hyperbolic excess velocity (V_{HE} vector) at arrival. The locus of natural periapsis is determined by the V_{HE} vector and by the periapsis altitude. The desired inclination angle for a flyby mission can be chosen during the final midcourse correction to give the most desirable of the available entry locations. The targeting angle β measured relative to periapsis is determined by two factors --the deflection propulsive impulse given the entry vehicle after separation from the spacecraft, and the distance from the planet when the impulse is applied. The major constraints on the targeting angle β are the entry flightpath angle and communication geometry. The available entry sites, the deflection propulsion required, the communications geometries and times, and the entry vehicle entry environment must be traded off within the subsystems characteristics and weight and size constraints.

The entry environment (aerodynamic heating, dynamic pressure and drag deceleration) is determined by entry velocity, flight path angle, vehicle ballistic coefficient at entry, and atmospheric model characteristics. Constraints are imposed on the maximum values of entry velocity and entry flight path angle, mainly to minimize aerodynamic heating. An entry velocity upper limit of 38 000 fps was imposed on the BVS system -- both for the 1972 flyby mission and for the entry from approach mode in the 1973 orbital mission. This limitation cannot be imposed on the Venus/Mercury swingby mission because of fundamental flight mechanics restrictions discussed in that section.

1972 Flyby Mission

The 1972 flyby mission is described in Tables 3 and 4 and in figures 61 thru 67. A Type I transfer trajectory was selected because it shortened the transit time to 120 days (as compared to 180 days for a Type II) and the earth-spacecraft communication distance at arrival. The launch and arrival dates are selected such that (1) the maximum departure energy C_3 is within the payload capability of the Titan III-C launch vehicle and (2) the entry velocity is less than 38,000 fps. The launch and arrival energy contours of figure 2 were used to select the launch dates; the primary consideration was to minimize C_3 and, therefore, maximize the launch vehicle payload. Figure 4 relates V_{HE} and the entry velocity.

Targeting constraints for this mission dictate that the entry site (1) be on the sunlite side of the planet, (2) at least 20° from the terminator (to allow sufficient drift time in the sunlight to complete the mission), and (3) be less than 60° from the subearth point (for direct earth-link communication considerations). Targeting data are in Table 3.

Figures 61 thru 64 show targeting information related to the mission arrival date. The entry point for the first day of the launch period, April 1, 1972, is shown in figure 61. The right ascension is measured from the ascending mode of the Venus orbital plane on the ecliptic. The loci of possible entry location for γ_E of -30 and -40° are shown. The entry point is an angle φ_L back from the V_{HE} as discussed previously under direct mode targeting. The ground trace of the approach trajectory is shown for an inclination of about 15° and is 22° west of the morning terminator. Due to the retrograde motion of Venus about its axis, the morning terminator is east of the subsolar point. The entry point is about 40° from the subearth point, and thus allows for a direct communication link. A similar targeting plot (figure 62) is shown for the last day of the launch period, April 21, 1972. The inclination of the reference approach trajectory is 48°. The declination needed to keep the entry point 22° west of the morning terminator is 34°. The entry point is 50° from the subearth point. This is still adequate for a direct link.

The time history of the Earth-to-spacecraft communication distance is shown in figure 63 for the first, middle, and last day of the launch period. The flight times vary between 102 and 122 days. The arrival date is constant, August 1, 1972, and thus the distance at arrival, 0.51 AU, is independent of launch date. The sun-to-spacecraft distance is also shown as a function of time. As is typical of Type I trajectories the arrival occurs before perihelion. The closest approach to the sun is 0.715 AU. The variation of the cone and clock angles of the Earth (as viewed from the spacecraft) is shown in figure 64 for the cruise phase. These angles are important in the mounting of antennas on the spacecraft.

The 8.5-ft diameter entry vehicle has a hypersonic ballistic coefficient of 0.38 slug/ft^2. The nominal entry angle of -30° is within heat shield design criteria limitations and also meets communications geometry and leadtime requirements. The heating rates and heat loads shown in Table 3 were used to design the heat shield for the direct entry mission. The time history of the drag deceleration during entry and the time history from entry to balloon inflation are shown on figures 65 thru 67.

TABLE 3.- 1972 FLYBY MISSION PROFILE, TYPE I TRANSFER TRAJECTORY

Launch period, days		20
Launch dates	April 1 thru April 21, 1972	
Arrival date		August 1, 1972
Departure energy, (max. during period) C_3, km^2/sec^2		20.0
Venus arrival energy, V_{HE}, km/sec . .		5.0
Payload in transfer trajectory (TIIIC after midcourse correction), lb .		2360
Periapsis, km		2000
Targeting		
Radius at deflection, km		1 000 000
ΔV deflection, m/sec		50
Coast time (deflection to entry), hr .		52.8
Nominal latitude, deg		13°-30'
Angle from terminator, deg		22
Angle from sub-earth point, deg . . .		42
Angle from sub-solar point, deg . . .		68.5
Entry environment $(h_E = 200$ km$)$		
Ballistic coefficient, $slug/ft^2$ . . .		0.380
Velocity, fps		37 400
Flight path angle, deg		-30°
Angle of attack, deg		-2.0
Peak drag deceleration, g (see figure 65 for time history).		250.0
Altitude for staging from aeroshell, ft	[a]245 000	[b]237 000

[a]Upper atmosphere

[b]Lower atmosphere

TABLE 3.- 1972 FLYBY MISSION PROFILE, TYPE I TRANSFER TRAJECTORY - Concluded

Time history (see figures 66 and 67) .		
Downrange angle, deg[c]	[a] 2.0	[b] 2.06
Heating environment		
$\dot{q}$ convective, Btu/ft^2-sec	[d] 1405	[e] 1600
$\dot{q}$ radiative, Btu/ft^2-sec	[d] 620	[e] 525
Q_T convective, Btu/ft^2	[d] 5390	[e] 4000
Q_T radiative, Btu/ft^2	[d] 2430	[e] 1185

[a] Upper atmosphere

[b] Lower atmosphere

[c] Based on 55° half-angle cone, 8.5 ft diam, with 1 ft nose rad.

[d] Stagnation point

[e] Cone edge

TABLE 4.- 1972 FLYBY MISSION SEQUENCE

Event		Time
1.	Liftoff; begin vertical rise	0
2.	Start roll in azimuth	7 sec
3.	Start pitchover	10 sec
4.	Start angle of attack attitude control	20 sec
5.	Begin zero-lift flight	30 sec
6.	Terminate zero-lift flight	80 sec
7.	Stage I ignition	111 sec
8.	Sold rocket motor burnout and jettison	122 sec
9.	Initiate Stage I shutdown	254 sec
10.	Jettison Stage I, Stage II ignition	255 sec
11.	Jettison payload fairing	280 sec
12.	Initiate Stage II tailoff	457 sec
13.	Jettison Stage II	468 sec
14.	Start Transtage 1st main propulsion burn	470 sec
15.	Shutdown 1st main transtage burn; initiate orbit orientation; coast	476 sec
17.	Shutdown 2nd main burn and orient for payload release	1745 sec (29.1 min)
18.	Separate spacecraft	30 min
19.	Deploy solar panels	53 min
20.	Turn on attitude control	57 min
21.	Sun acquired	60 min (1 hr)
22.	Start magnetometer calibration	4 hr
23.	Begin Canopus acquisition	16.6 hr
24.	Canopus acquired	17 hr
25.	Begin midcourse (M/C) correction	2 to 10 days
26.	End M/C correction	M/C + 1 hr 45 min
27.	Sun acquired	M/C + 2.10 hr
28.	Canopus acquired	M/C + 3.10 hr
29.	Second correction maneuver if required	10 days

TABLE 4.- 1972 FLYBY MISSION SEQUENCE - Concluded

30.	Switch to low bit rate transmission	36 days
31.	Begin Venus encounter sequence	120 days
32.	Venus encountered	121 days
33.	Initiate capsule system and turn on aeroshell sequencer	S (Capsule separation) -5 min
34.	Fire capsule separation pyro	S (Capsule separation) = 0.0
35.	Spinup entry capsule	S + 1 sec
36.	Fire deflection propulsion	S + 20 min
37.	Power down capsule for cruise	S + 22 min
38.	Power up capsule for entry	S + 52 hr 48 min
39.	Turn on truss sequence, aeroshell science, and accelerometer	S + 52 hr 49 min
40.	Sense 1 g, increasing	E (Entry time) = 0.0
41.	Fire afterbody chute deployment pyro	E + 56 sec
42.	Fire BVS chute deployment pyro	E + 57 sec
43.	Stage aeroshell from BVS; initiate bus sequencer	E + 1 min 26 sec
44.	Fire balloon inflation pyro; BVS deployment	E + 15 min 5 sec
45.	Fire inflation termination pyro; science warmup initiation; BVS flotation	E + 16 min
46.	Initiate science experiments	E + 19 min 30 sec
47.	Transmit stored data	E + 8 hr and every 8 hr from then until mission termination

Launch: April 1, 1972
Arrive: August 1, 1972
V_{HE} = 4.95 km/sec

C_3 = 16.25 km^2/sec^2

γ_L = 15°
22° from term.

$i_{♀op}$ = 50°

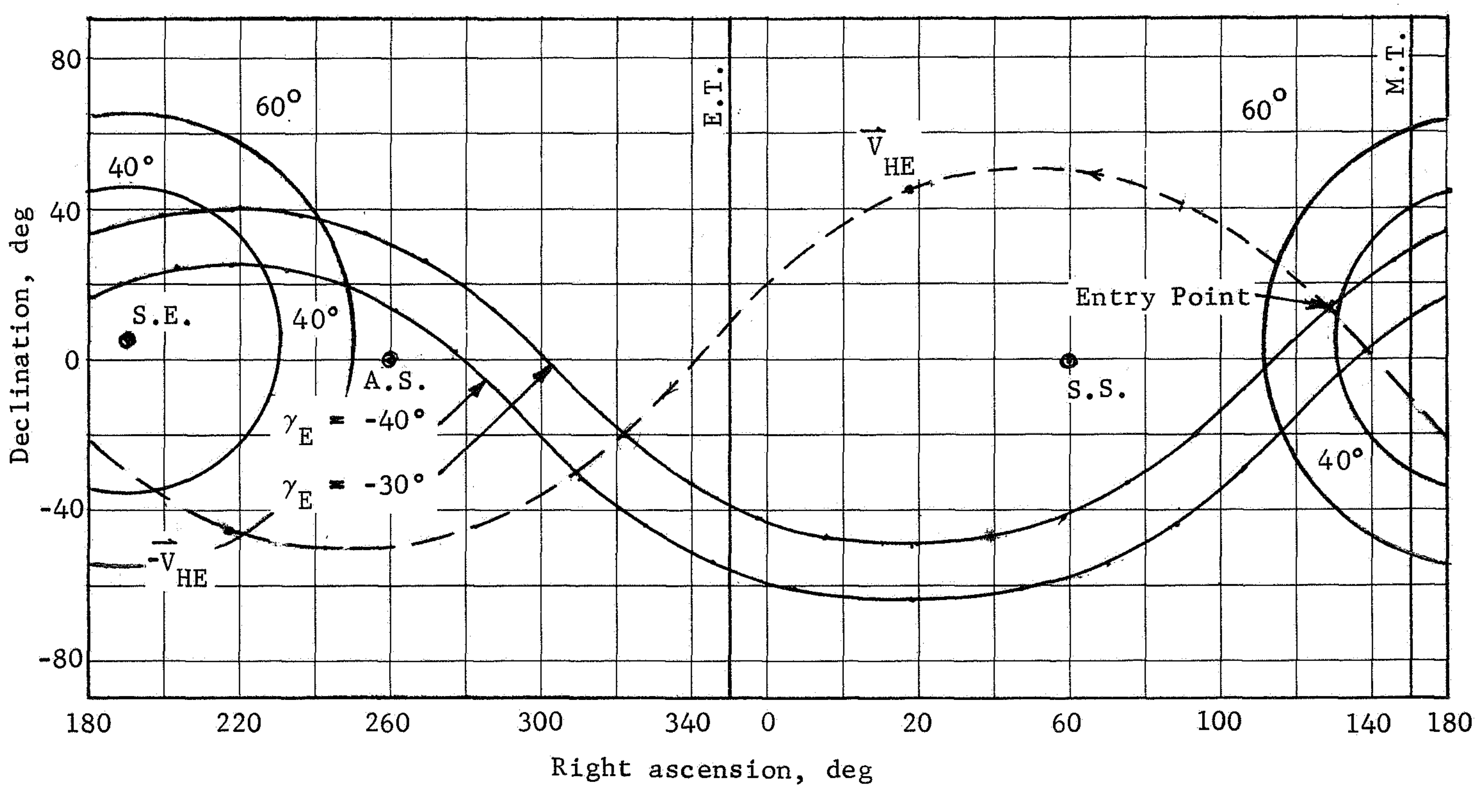

Figure 61.- 1972 Flyby Mission, Targeting Summary, First Day

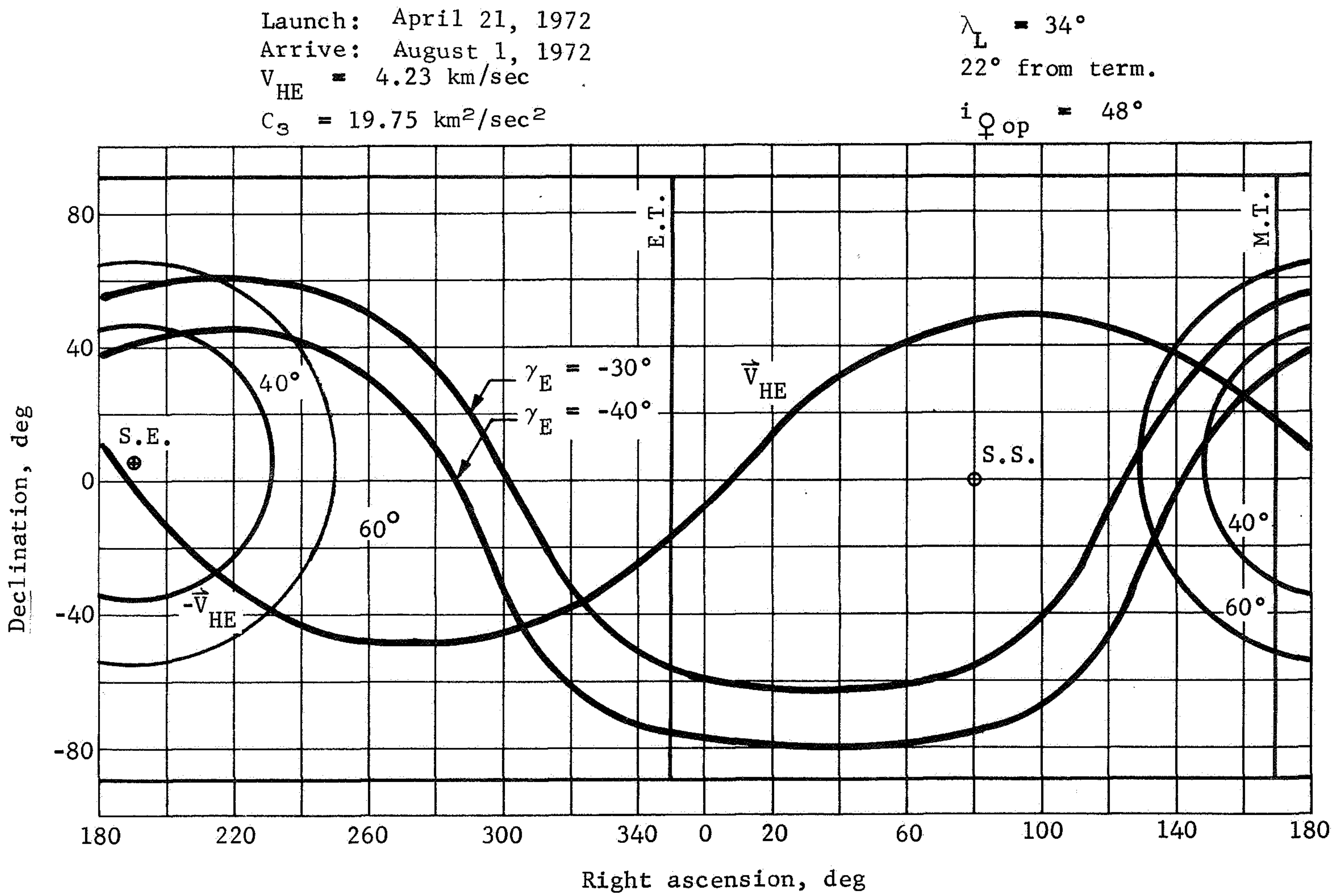

Figure 62.- Flyby Mission, Targeting Summary, Last Day

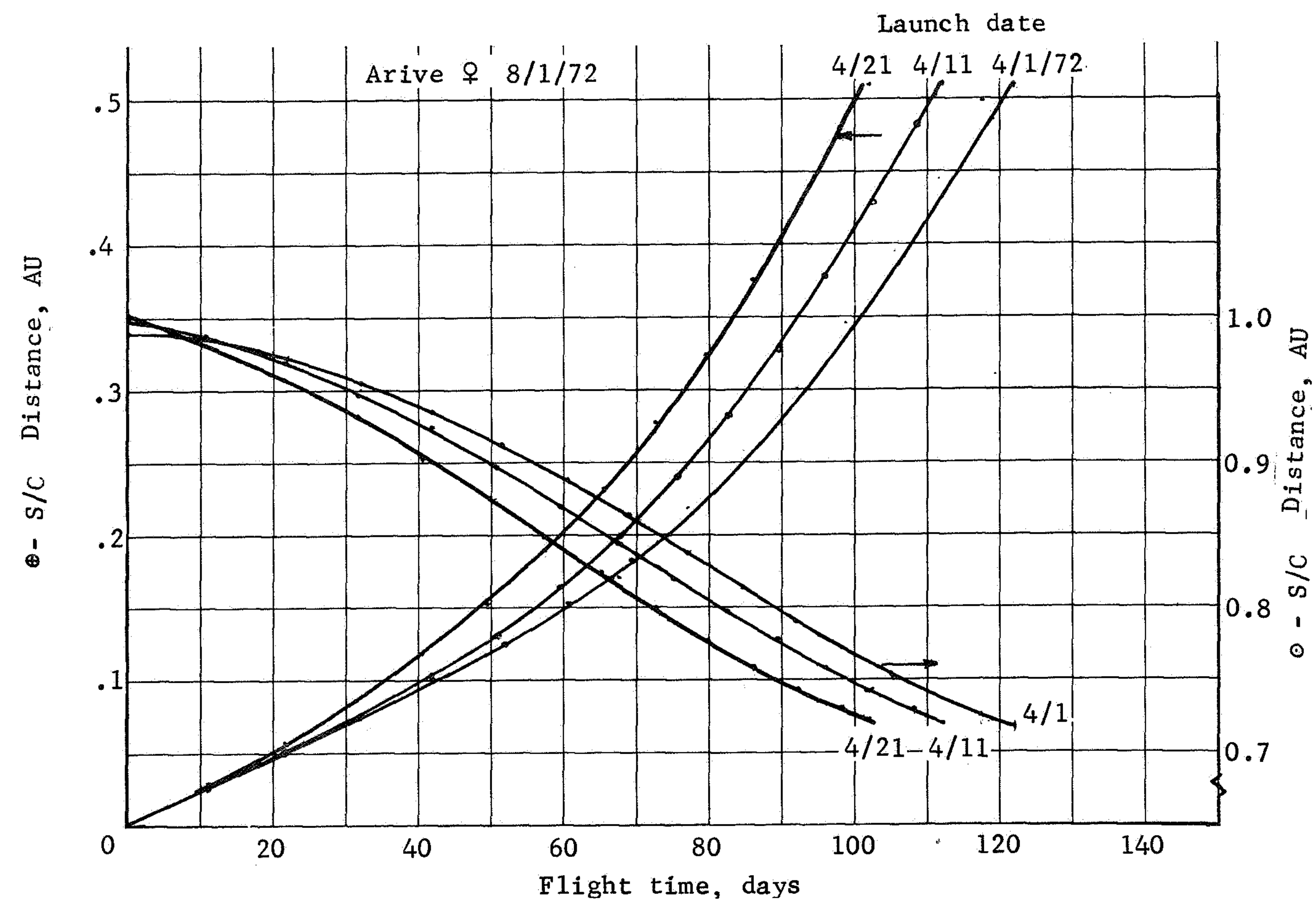

Figure 63.- ⊕ - S/C and ⊙ - S/C Time History, 1972 Flyby

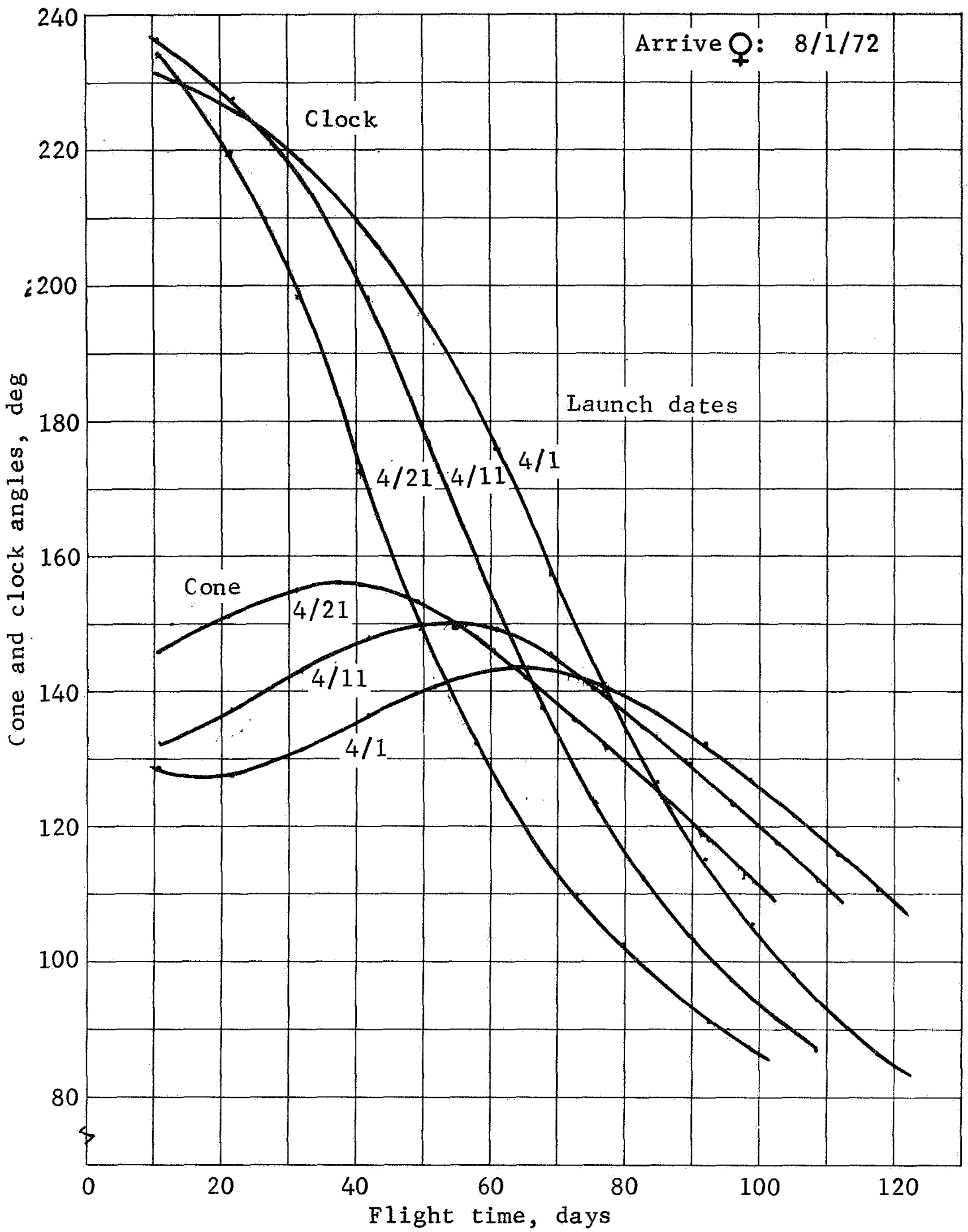

Figure 64.- Cone-Clock Angle Time History, 1972 Flyby

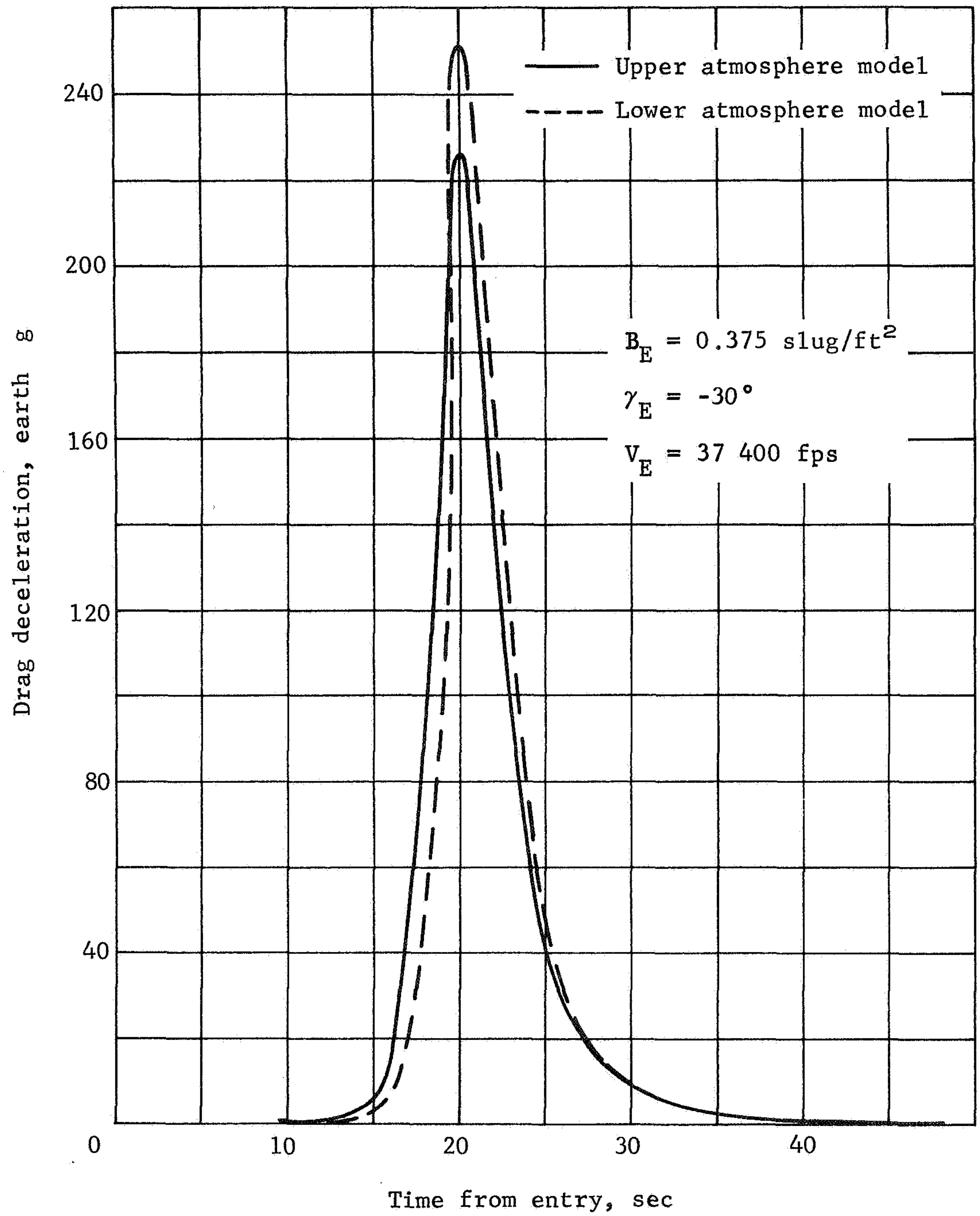

Figure 65.- Drag Deceleration Time History, 1972 Flyby

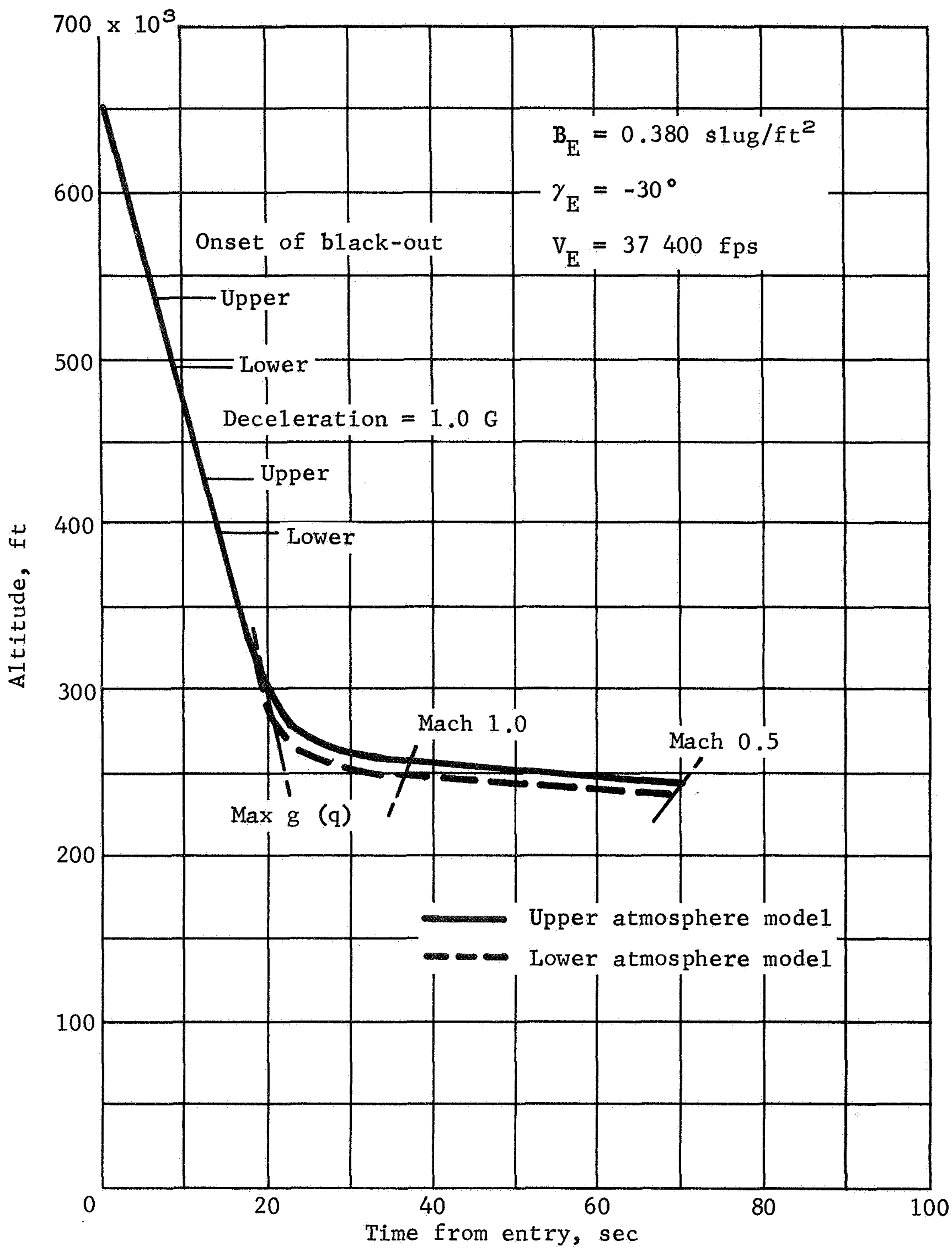

Figure 66.- Entry Time History, 1972 Flyby

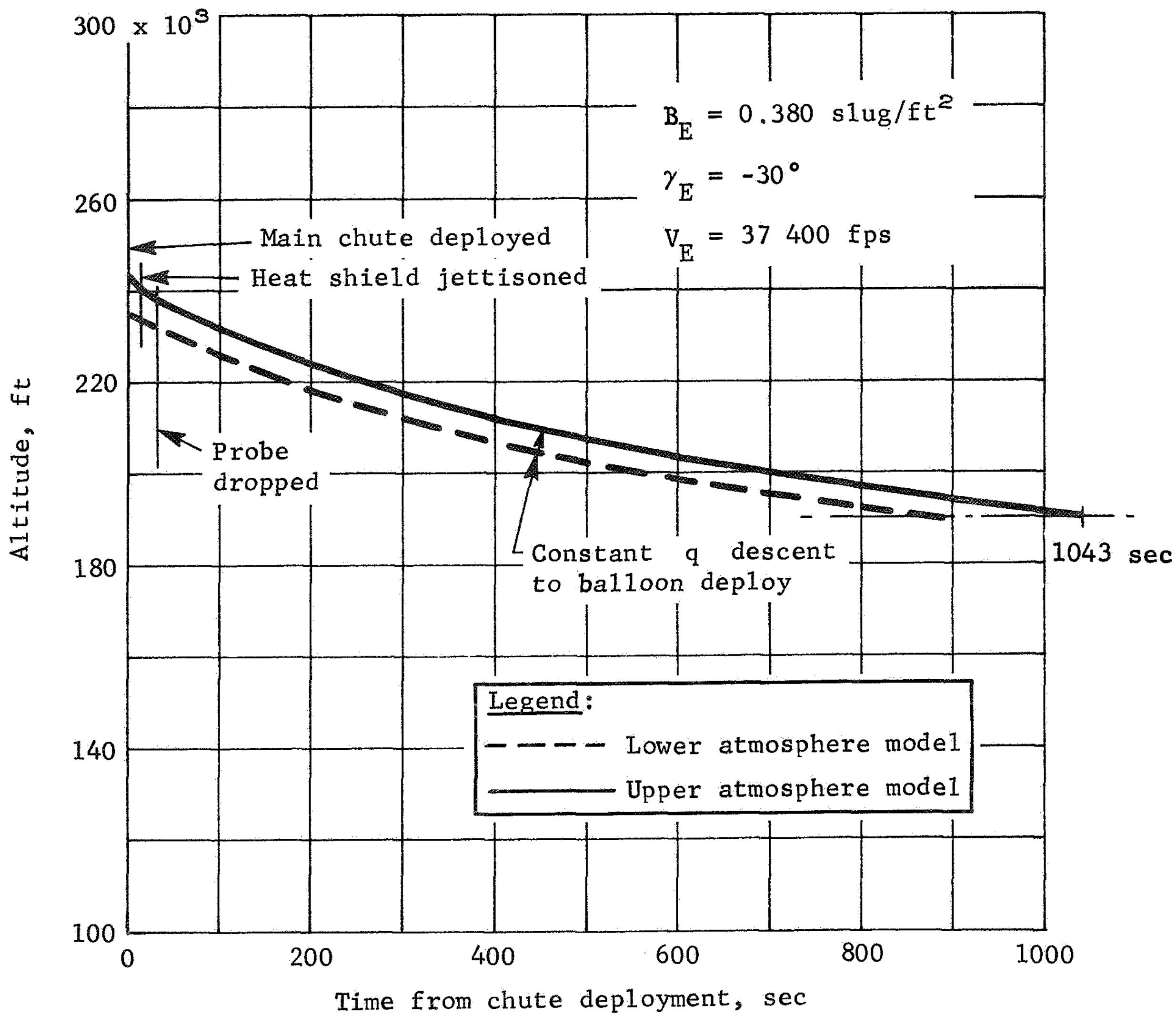

Figure 67.- Descent Trajectory on Chute, 1972 Flyby

1973 Orbiter Mission

The orbiter mission for 1973 is described in tables 5 thru 7 and figures 68 thru 77. Two entry modes, entry from approach and entry from orbit, are shown. A Type II Earth-Venus transfer trajectory was chosen because it permits a heavier payload. The launch and arrival contour plots from figure 3, were used to select the launch and arrival dates shown in tables 5 and 6. The launch and arrival dates minimize the arrival V_{HE} over the launch period to reduce the ΔV required for orbital insertion. For the entry from approach mode, the entry velocity is less than the 38 000 fps criteria limit.

Targeting constraints for the 1973 orbital mission specify entry on the sunlit side of the planet a minimum of 20° from the terminator. Communication is via a relay system that uses the orbiter for the Venus-Earth link. An additional constraint is that the orbiting vehicle must have an orbit lifetime of at least 50 yr. This requirement stems from planetary contamination criteria and the fact that the orbiter is not sterilized. Solar gravitational perturbations on the orbiting spacecraft lower the orbit periapsis for all orbit inclinations except those between 132.7 and 143.2° and those between 35.6 and 60° to such an extent that the lifetime is less than 50 yr. For a light side entry, only inclination angles between 132.7 and 143.2° produce satisfactory orbits. These highly eccentric orbits result from adhering to the orbit insertion propulsion requirements. Orbit selection criteria are discussed in detail in a previous section.

The entry point for the first day of the launch period, November 1, 1973, is shown in figure 68. The nominal γ_E is -30°, and the entry location paramter, β, is 65°, as described in orbit mode targeting. The location of orbiter periapsis shown corresponds to orbit insertion at periapsis of the approach trajectory and, thus, to the minimum orbit insertion ΔV. The reference entry point is about 15° west of the subsolar point and has a declination of 8°. The specific orbiter inclination was chosen to satisfy the orbit lifetime criteria of 50 yr. The reference entry point for the last day of the launch period, November 21, 1973, is shown in figure 69. The declination of the entry point is 18°.

The Earth-to-spacecraft communication distance is shown in figure 70, and is a maximum, 0.79 AU, at arrival on the first launch day. The spacecraft passes through perihelion before arrival at Venus. The perihelion is 0.71 AU.

The time history of the Earth cone and clock angles is given in figure 71.

The entry velocity (entry from orbit) of 32 000 fps (table 5) results from a deorbit maneuver that occurs near apoapsis. The flight path angle at entry, and communication geometry and times are satisfactory for this deorbit maneuver.

The entry velocity (entry from approach) is 36 400 fps. The heating rates and heat loads associated with this higher entry velocity require a heavier heat shield. The difference in entry ballistic coefficients for the two entry modes (0.33 and 0.35 $slugs/ft^2$ respectively, shown in tables 5 and 6) result from this heat shield weight difference.

TABLE 5.- 1973 ORBITER MISSION PROFILE, ENTRY FROM ORBIT

Launch period, days	20
Launch dates	Nov. 1 thru Nov. 21, 1973
Arrival dates	April 13 thru April 19, 1974
Departure energy (max. during period), C_3, km^2/sec^2	8.36
Venus arrival energy (max. during period), V_{HE}, km/sec	4.32
Payload in transfer orbit (TIIIC after M/C correction), lb	3700
Orbit characteristics	
Periapsis altitude, km	2000
Apoapsis altitude, km	66 450
Eccentricity	.80
Period, hr	25
Ejection from orbit	
ΔV deflection, m/sec	250
Coast time, (deflection to entry), hr	10
β, deg	65
λ, deg	-55
Nominal entry latitude, deg	9° N
Angle from subsolar point, deg	15
Entry environment	
Ballistic coefficient, $slug/ft^2$	.33
Velocity, fps	32 000
Flight path angle, deg	-30
Angle of attack, deg	-5
Peak drag deceleration, g (see figure 72 for time history)	172

TABLE 5.- 1973 ORBITER MISSION PROFILE, ENTRY FROM ORBIT - Concluded

Altitude for staging from aeroshell, ft	[a]243 000	[b]239 000
Time history (see figures 73 and 74)		
Downrange angle, deg	[a]1.98	[b]2.04
Heating environment		
$\dot{q}$ convective, Btu/ft^2-sec	[c]760	[d]805
$\dot{q}$ radiation, Btu/ft^2-sec	[c]215	[d]160
Q_T convective, Btu/ft^2	[c]3900	[d]3625
Q_T radiative, Btu/ft^2	[c]820	[d]540

[a]Upper atmosphere

[b]Lower atmosphere

[c]Stagnation point

[d]Cone edge

TABLE 6.- 1973 ORBITER MISSION PROFILE, ENTRY FROM APPROACH[a]

Ejection from approach		
Radius at ejection, km		1 000 000
ΔV deflection, m/sec		50
Coast time (deflection to entry), hrs		60
Nominal entry latitude, deg		30° N
Angle from subsolar point, deg		37
β, deg		42.5
Entry environment (h_E = 200 km)		
Ballistic coefficient, slug/ft^2		.35
Velocity, fps		36 400
Flight path angle, deg		-30
Angle of attack, deg		-20
Peak drag deceleration, $g_\oplus$ (see fig. 75 for time history)		220
Attitude for staging from aeroshell	[b]245 000	[c]235 000
Time history (see figures 76 and 77)		
Downrange angle, deg	[b]2.0	[c]2.05
Heating environment		
$\dot{q}$ convective, Btu/ft^2-sec	[d]1190	[e]1280
$\dot{q}$ radiative, Btu/ft^2-sec	[d]440	[e]340
Q_T convective, Btu/ft^2	[d]5380	[e]3880
Q_T radiative, Btu/ft^2	[d]1850	[e]940

[a]Same constraints on inclination angle as entry from orbit

[b]Upper atmosphere

[c]Lower atmosphere

[d]Stagnation point

[e]Cone edge

TABLE 7.- 1973 ORBITER MISSION SEQUENCE

Event		Time
1.	Liftoff; begin vertical rise	0
2.	Start roll in azimuth	7 sec
3.	Start pitchover	10 sec
4.	Start angle of attack attitude control	20 sec
5.	Begin zero-lift flight	30 sec
6.	Terminate zero-lift flight	80 sec
7.	Stage I ignition	111 sec
8.	Sold rocket motor burnout and jettison	122 sec
9.	Initiate Stage I shutdown	254 sec
10.	Jettison Stage I, Stage II ignition	255 sec
11.	Jettison payload fairing	280 sec
12.	Initiate Stage II tailoff	457 sec
13.	Jettison Stage II	468 sec
14.	Start transtage 1st main propulsion burn	470 sec
15.	Shutdown 1st main transtage burn; initiate orbit orientation; coast	476 sec
16.	Start 2nd transtage burn	1336 sec
17.	Shutdown 2nd main burn and orient for payload release	1745 sec (29.1 min)
18.	Separate spacecraft	30 min
19.	Deploy solar panels	53 min
20.	Turn on attitude control	57 min
21.	Sun acquired	60 min (1 hr)
22.	Start magnetometer calibration	4 hr
23.	Begin Canopus acquisition	16.6
24.	Canopus acquired	17 hr
25.	Begin midcourse (M/C) correction	2 to 10 days
26.	End M/C correction	M/C + 1 hr 45 min
27.	Sun acquired	M/C + 2.10 hr
28.	Canopus acquired	M/C + 3.10 hr

TABLE 7.- 1973 ORBITER MISSION SEQUENCE - Concluded

29.	Second corrective maneuver, if required	10 days
30.	Switch to low bit rate transmission	36 days
31.	Begin Venus encounter sequence	163 days
32.	Venus encountered	164 days
33.	Orient for orbit insertion (OI)	OI - 2.0 hr
34.	Orbit insertion	OI = 0.0
35.	Determine orbit ephemeris; initiate oribtal science experiments	Nominal orbit period, 25 hrs
36.	Update capsule separation (s) orientation data	S - 3.0 hr
37.	Re-orient spacecraft for capsule separation	S - 1.0 hr
38.	Capsule separation	S + 0.0
39.	Spin up capsule	S + 1.0 sec
40.	Initiate retro propulsion	S + 20 min
41.	Shut down retro propulsion	S + 24 min 17 sec
42.	Separate propulsion module	S + 24 min 30 sec
43.	Power down capsule; coast	S + 24 min 32 sec
44.	Power up for entry; turn on aeroshell science	S + 10 hr 19 min 37 sec
45.	Partial de-spin	S + 10 hr 19 min 40 sec
46.	Sense 1 g, increasing	E (Entry time) = 0.0
47.	Fire afterbody chute deployment pyro	E + 58 sec
48.	Fire BVS chute deployment	E + 1 min 10 sec
49.	Stage aeroshell from BVS; initiate bus sequencer	E + 1 min 26 sec
50.	Fire balloon inflation pyro; BVS deployment	E + 15 min 5 sec
51.	Fire inflation termination pyro; science warmup; BVS flotation	E + 16 min
52.	Initiate science experiments	E + 19 min 30 sec
53.	Transmit stored data	E + 25 hr every 25 hr from then until mission termination

Launch: November 1, 1973

Arrive: April 13, 1974

V_{HE} = 4.32 km/sec

C_3 = 7.68 km/sec^2

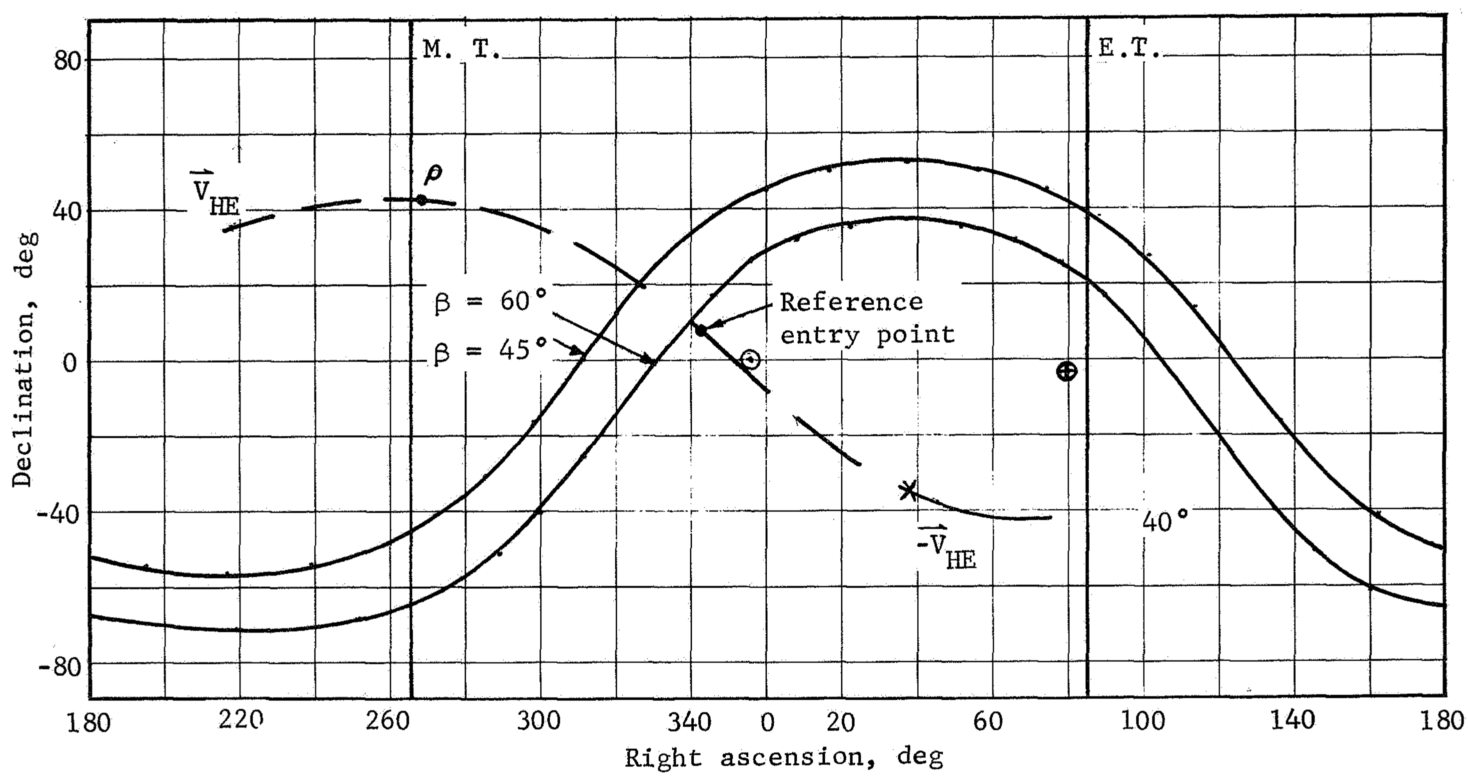

Figure 68.- 1973 Orbiter Mission, Targeting Summary, First Day

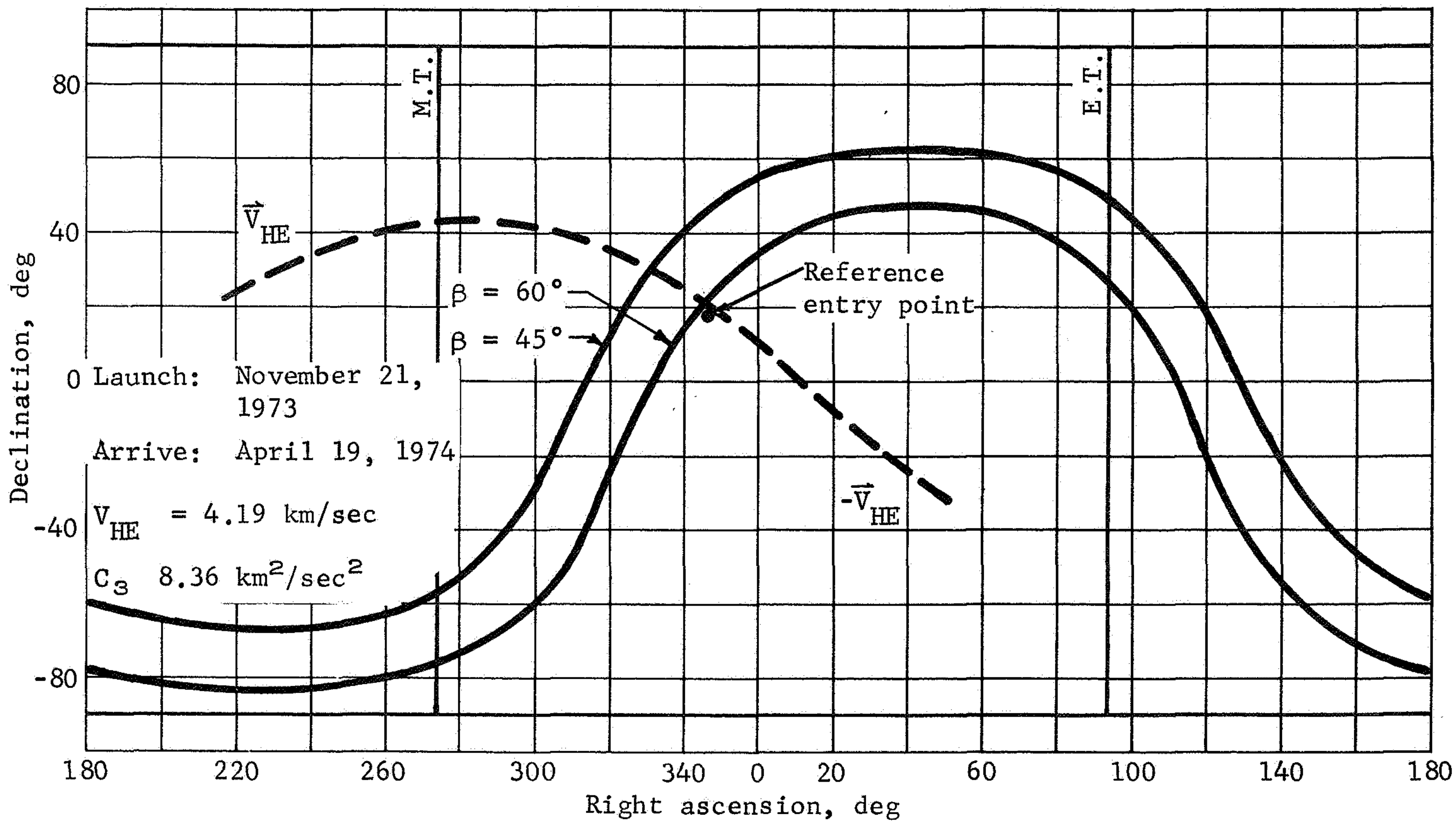

Figure 69.- 1973 Orbiter Mission, Targeting Summary, Last Day

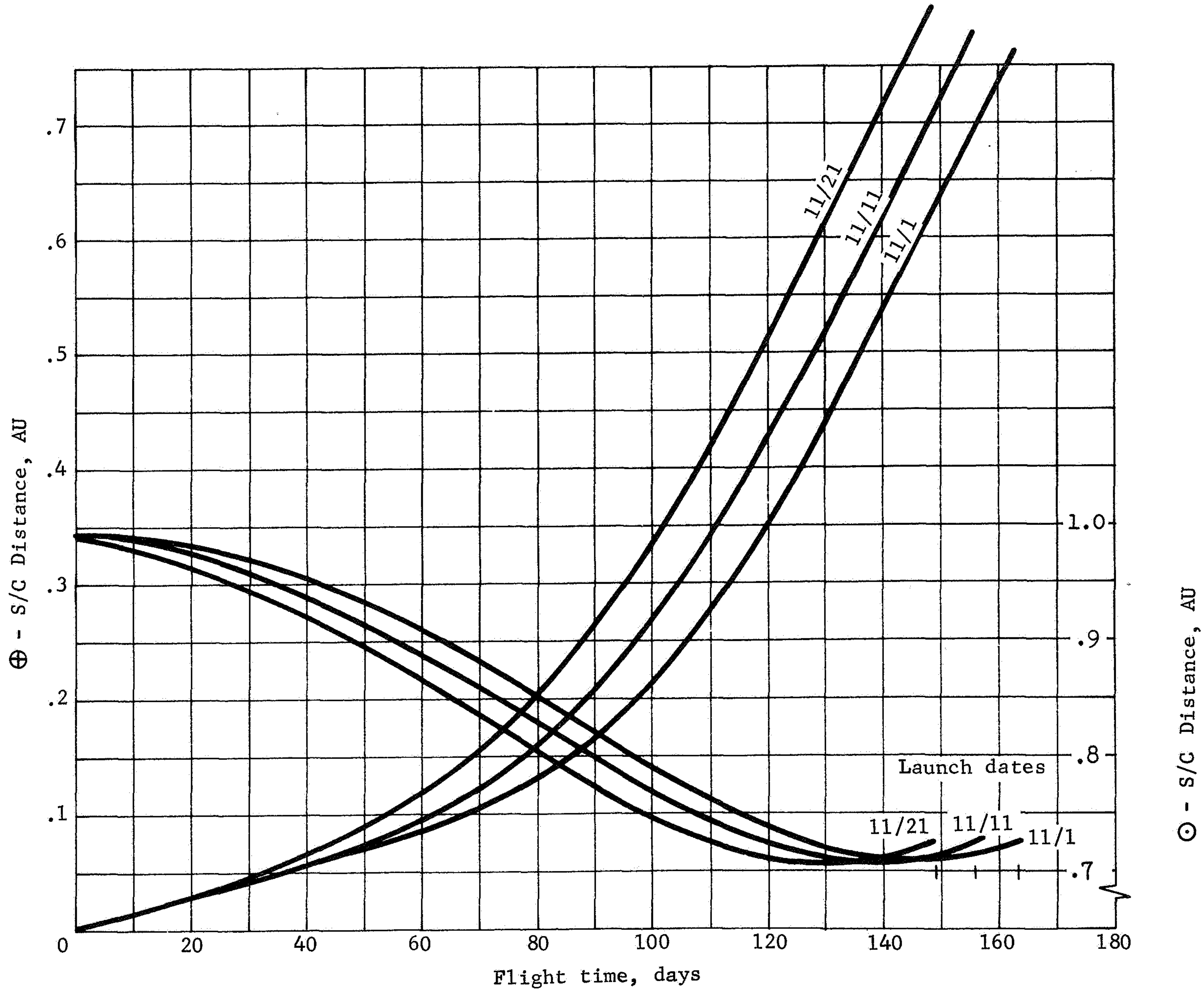

Figure 70.- ⊕ - S/C and ⊙ - S/C Time History, 1973 Orbiter

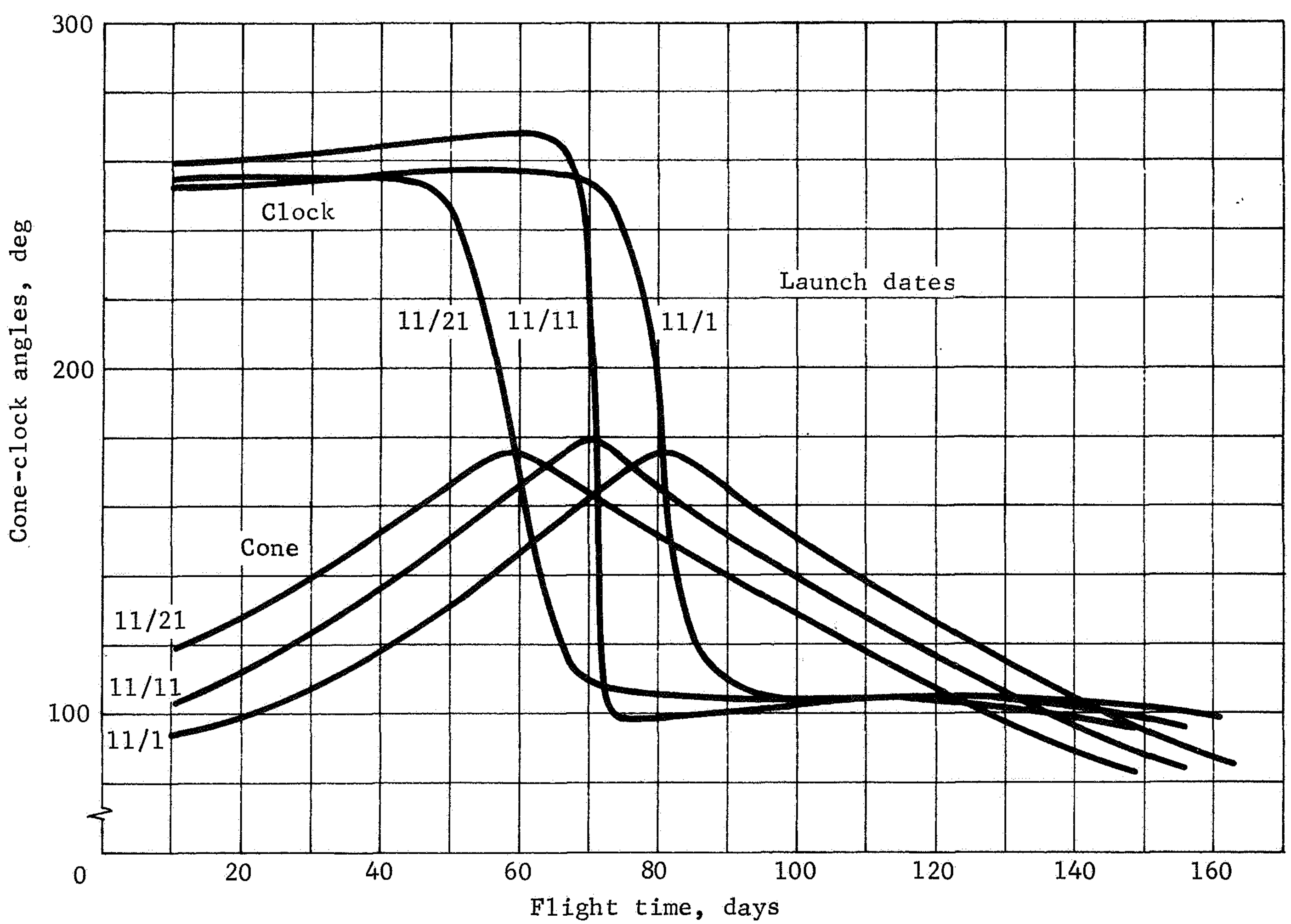

Figure 71.- Cone-Clock Angle Time History, 1973 Orbiter

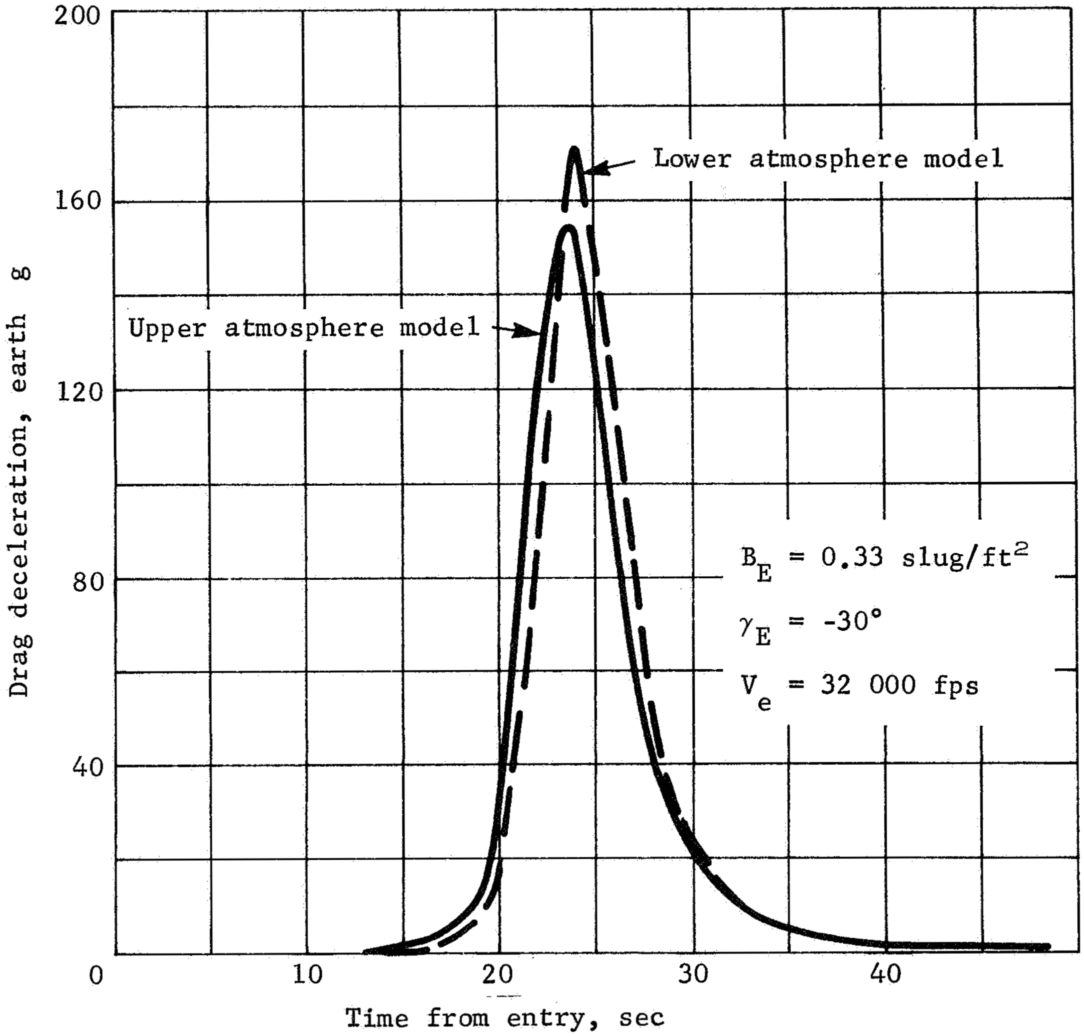

Figure 72.- Drag Deceleration Time History, 1973 Orbiter, Entry from Orbit

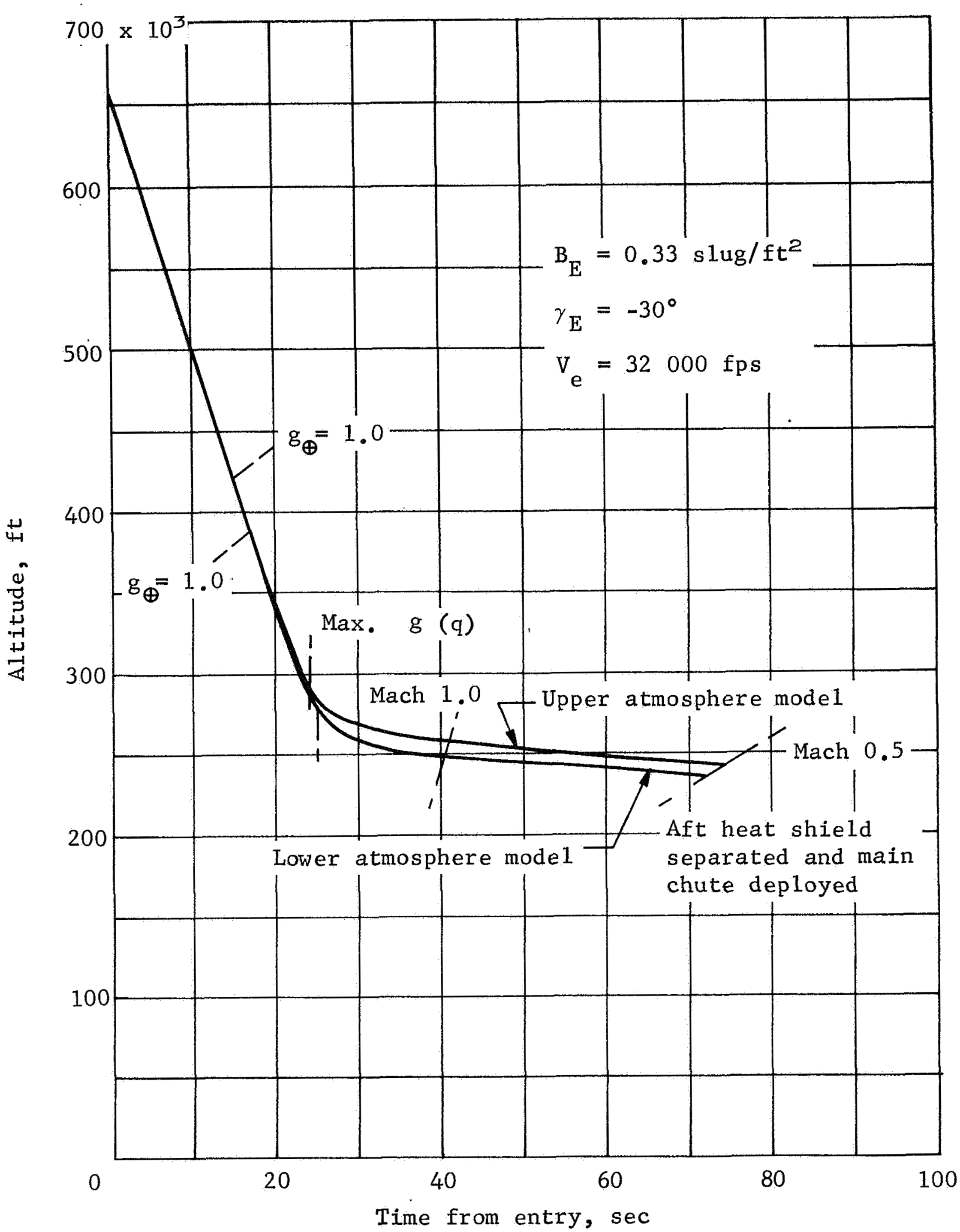

Figure 73.- Entry Time History, 1973 Orbiter, Entry from Orbit

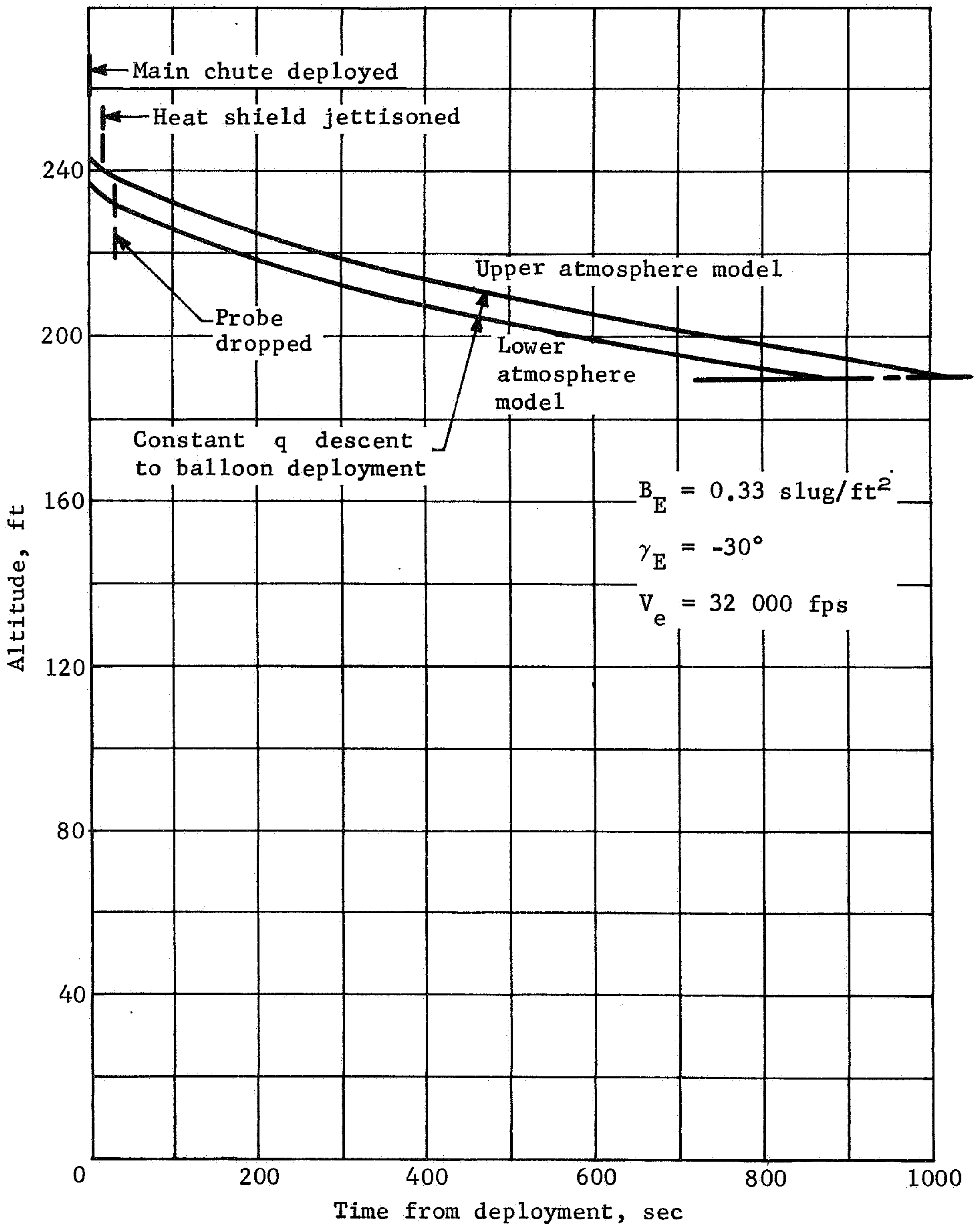

Figure 74.- Descent Trajectory on Chute, 1973 Orbiter

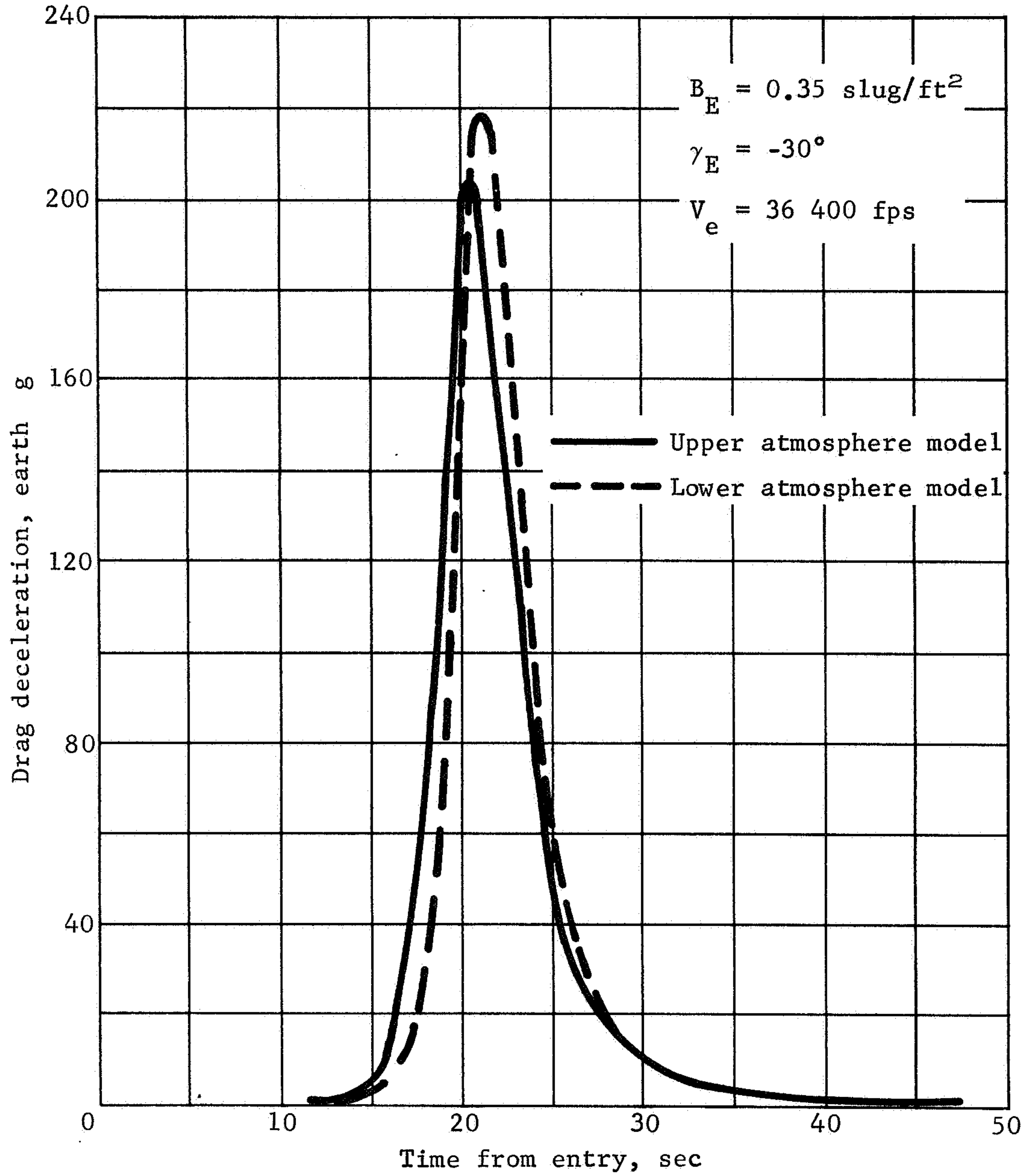

Figure 75.- Drag Deceleration Time History, 1973 Orbiter, Entry from Approach

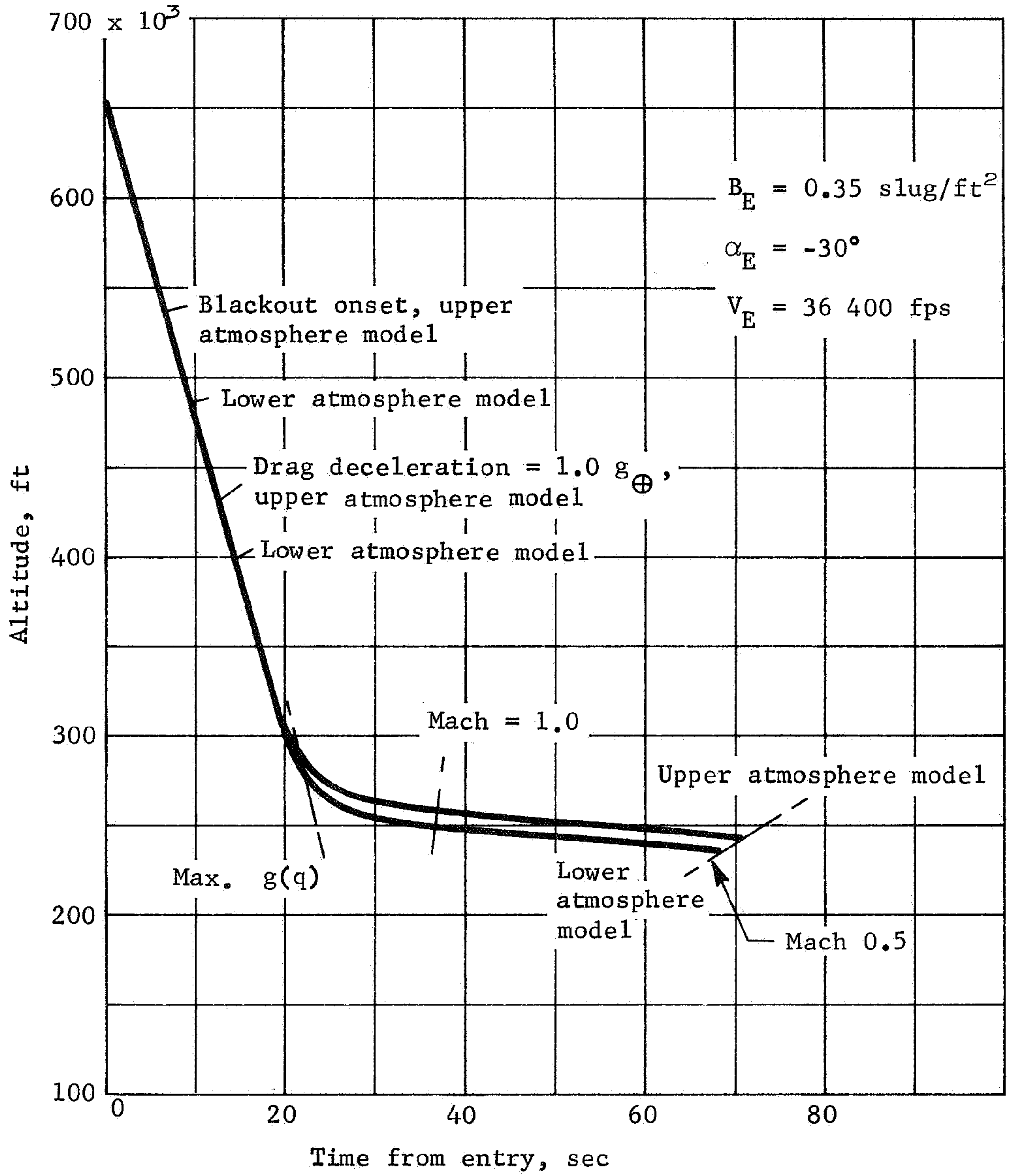

Figure 76.- Entry Time History, 1973 Orbiter, Entry from Approach

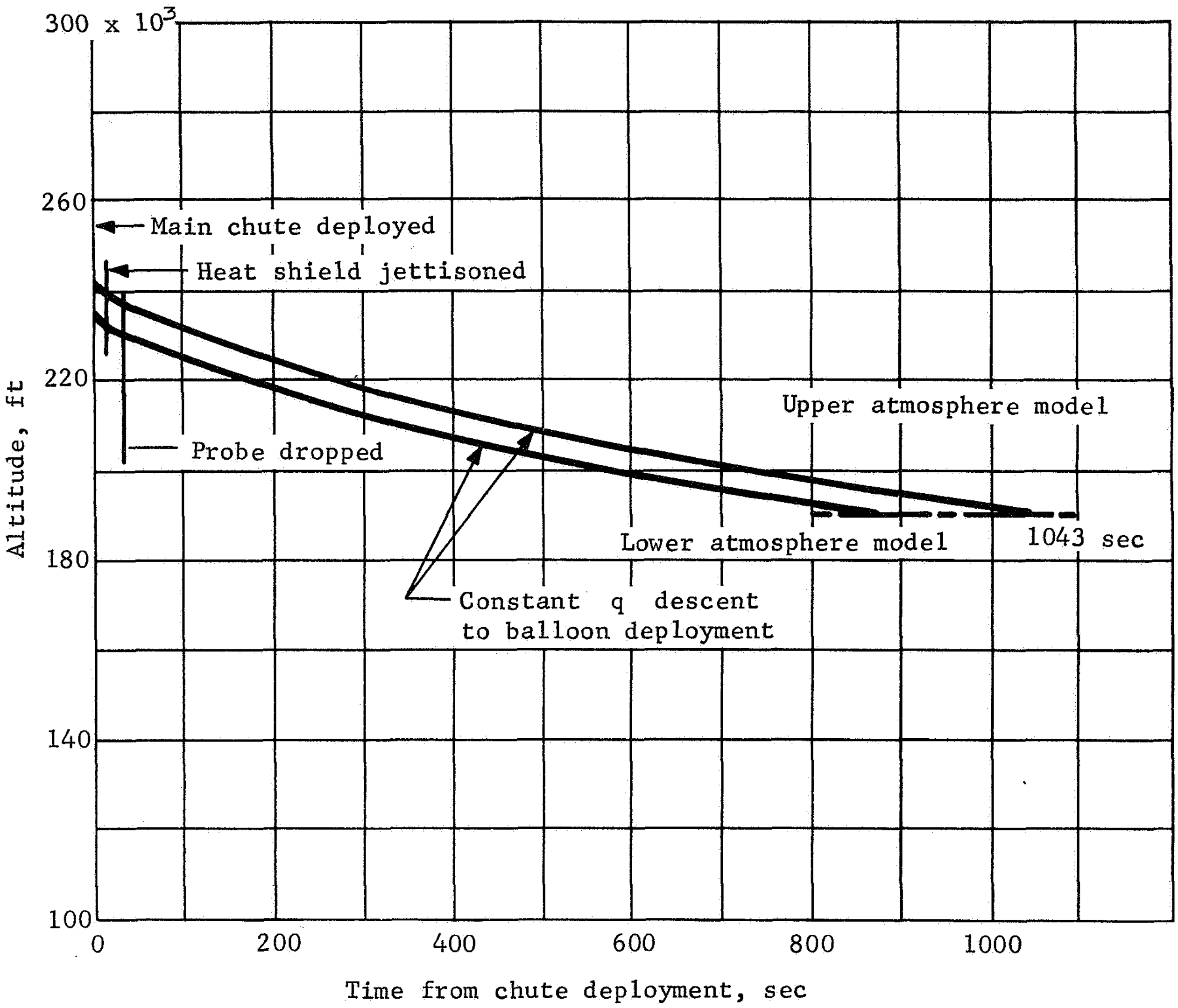

Figure 77.- Descent Trajectory on Chute, 1973 Orbiter, Entry from Approach

1973 Venus/Mercury Swingby Mission

The 1973 Venus/Mercury swingby mission, described in tables 8 and 9 and in figures 78 through 81, is complex. The mission considers only the ballistic transfer trajectory mode, in which the entire turn maneuver at Venus is accomplished by gravity. In 1973, only a Type I ballistic swingby mission is possible. Furthermore, because of the large rates-of-change in departure and arrival energies at the required arrival date, the launch period is reduced from 20 to 14 days. The C_3 during the launch period is within the capability of the TIIIC launch vehicle. Finally, the V_{HE} of 8.5 km/sec at arrival results in an entry velocity of 43 500 fps thus violating the entry velocity criteria which complicates the design of the heat shield.

Venus periapsis altitudes between 5505 and 5575 km (depending on launch date) are required to properly deflect the spacecraft for the Mercury portion of the mission.

A basic targeting criterion of the BVS study, that the entry point be on the sunlit side of the planet, is also violated by the Venus/Mercury swingby mission, since only dark side entry points are possible. During entry the spacecraft cannot be used as a relay communication link. Direct Earth communication requires that the spacecraft be deflected out-of-plane to enter within 60° of the subearth point, and to keep the deflection propulsion requirements tolerable, the deflection point is relatively far out (2 000 000 km) and the coast time (68 hr) is relatively long.

The swingby trajectory ground trace for the first launch day of the reference launch period, October 25, 1973, is shown in figure 78. The locus of possible entry points for a given entry flight path angle, γ_E, is a circle about the approach direction as described under direct mode targeting. Loci of entry for γ_E of -30, -35, and -40° are shown. The shallower the γ_E, the further the entry point is from the approach directon. Loci 30 and 40° from the subearth point are shown. To minimize the distance between the entry point and the subearth point, an out-of plane ejection maneuver is made to place the BVS/entry vehicle on a trajectory that passes over the subearth point and enters about 30° east of the morning terminator, in darkness, with a declination of -40°. The out-of-plane ejection angle required is 145°. The required ΔV_{EJ} is 93 m/sec for an ejection distance of 2 million km.

The high entry velocity associated with the Venus/Mercury swingby mission results in heat rates, heat loads, and aerodynamic shear loads that complicate heat shield design. To keep the heat shield weight within mission capability, the entry vehicle diameter was reduced from 8.5 to 7.0 ft, thus making the entry ballistic coefficient 0.58 slug/ft^2.

TABLE 8.- 1973 VENUS/MERCURY SWINGBY MISSION PROFILE

Launch period, days	14
Launch date	Oct. 25 thru Nov. 7, 1973
Arrival date	Feb. 5, 1974
Departure energy (max. during period), C_3, km^2/sec^2	19.0
Venus arrival energy (max. during period), V_{HE}, km/sec	8.5
Payload in transfer trajectory (after midcourse correction), lb	2460
Periapsis, km	5505 to 5575
Targeting (Venus entry vehicle)	
Radius at deflection, km	2 000 000
ΔV deflection, m/sec	93
Coast time, deflection to entry, hr	68
Nominal entry latitude	41
Angle from terminator, deg	[a]30
Angle from sub-earth point, deg	41
Angle from subsolar point, deg	120
Entry environment	
Ballistic coefficient, $slug/ft^2$	0.58
Velocity, fps	43 500
Flight path angle, deg	-35
Angle of attack, deg	5
Peak drag deceleration, $g_\oplus$ (see figure 79 for time history)	360

[a]Dark side

TABLE 8.- 1973 VENUS/MERCURY SWINGBY MISSION PROFILE - Concluded

Altitude for staging aeroshell	[b]235 000	[c]228 000
Time history (see figures 80 and 81) . .		
Downrange angle, deg[d]	[b]1.6	[c]1.73
Heating environment		
$\dot{q}$ convective, Btu/ft^2-sec	[e]3000	[f]3750
$\dot{q}$ radiative, Btu/ft^2-sec	[e]7800	[f]3700
Q_T convective, Btu/ft^2	[e]10 200	[f]7800
Q_T radiative, Btu/ft^2	[e]13 200	[f]5800

[a]Dark side

[b]Upper atmosphere

[c]Lower atmosphere

[d]Based on 55° half cone angle, 7 ft in diam with 1 ft nose rad.

[e]Stagnation point

[f]Cone edge

TABLE 9.- 1973 VENUS/MERCURY SWINGBY MISSION SEQUENCE

Event		Time
1.	Liftoff; begin vertical rise	0
2.	Start roll in azimuth	7 sec
3.	Start pitchover	10 sec
4.	Start angle of attack attitude control	20 sec
5.	Begin zero-lift flight	30 sec
6.	Terminate zero-lift flight	80 sec
7.	Stage I ignition	111 sec
8.	Sold rocket motor bunrout and jettison	122 sec
9.	Initiate Stage I shutdown	254 sec
10.	Jettison Stage I, Stage II ignition	255 sec
11.	Jettison payload fairing	280 sec
12.	Initiage Stage II tailoff	457 sec
13.	Jettison Stage II	468 sec
14.	Start transtage 1st main propulsion burn	470 sec
15.	Shutdown 1st main transtage burn; initiate orbit orientation; coast	476 sec
16.	Start 2nd transtage burn	1336 sec
17.	Shutdown 2nd main burn and orient for payload release	1745 sec (29.1 min)
18.	Separate spacecraft	30 min
19.	Turn on attitude control	57 min
21.	Sun acquired	60 min (1 hr)
22.	Start magnetometer calibration	4 hr
23.	Begin Canopus acquisition	16.6 hr
24.	Canopus acquired	17 hr
25.	Begin midcourse (M/C) correction	2 to 10 days
26.	End M/C correction	M/C + 1 hr 45 min
27.	Sun acquired	M/C + 2.10 hr
28.	Canopus acquired	M/C + 3.10 hr
29.	Second correction maneuver, if required	10 days

TABLE 9.- 1973 VENUS/MERCURY SWINGBY MISSION SEQUENCE - Concluded

30.	Switch to low bit rate transmission	36 days
31.	Begin Venus encounter sequence	100 days
32.	Venus encountered	101 days
33.	Initiate capsule system and turn on aeroshell sequencer	S (Capsule separation) -5 min
34.	Fire capsule separation pyro	S = 0.0
35.	Spinup entry capsule	S + 1 sec
36.	Fire deflection propulsion	S + 20 min
37.	Power down capsule for cruise	S + 22 min
38.	Power up capsule for entry	S + 68 hr
39.	Turn on truss sequence, aeroshell science, and accelerometer	S + 68 hr 1 min
	(total transit time-104 days)	
40.	Sense 1 g, increasing	E (Entry time) = 0.0
41.	Fire afterbody chute deployment pyro	E + 45 sec
42.	Fire BVS chute deployment	E + 46 sec
43.	Stage aeroshell from BVS; initiate bus sequencer	E + 1 min 1 sec
44.	Fire balloon inflation pyro; BVS deployment	E + 15 min 15 sec
45.	Fire inflation termination pyro; science warmup; BVS flotation	E + 16 min
46.	Initiate science experiments	E + 19 min 30 sec
47.	Transmit stored data	E + 8 hr and every 8 hr from then until mission termination

Launch: October 25, 1973

Arrive: February 5, 1974

V_{HE} = 8.0 km/sec

C_3 = 19 km^2/sec^2

Reference system

Venus orbital plane
ACS. node of orbital plane on ecliptic = 0°

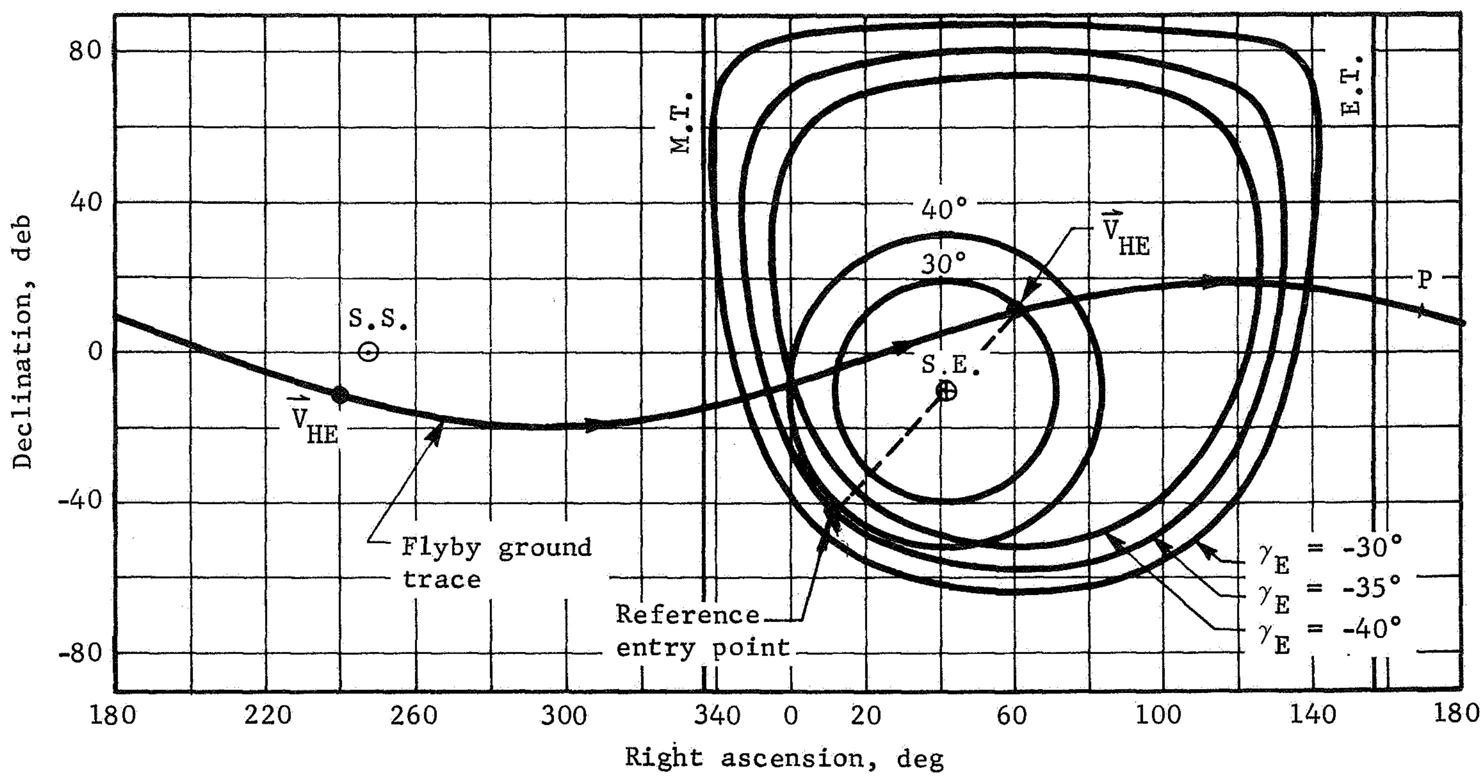

Figure 78.- 1973 Venus/Mercury Swingby Mission, Targeting Summary

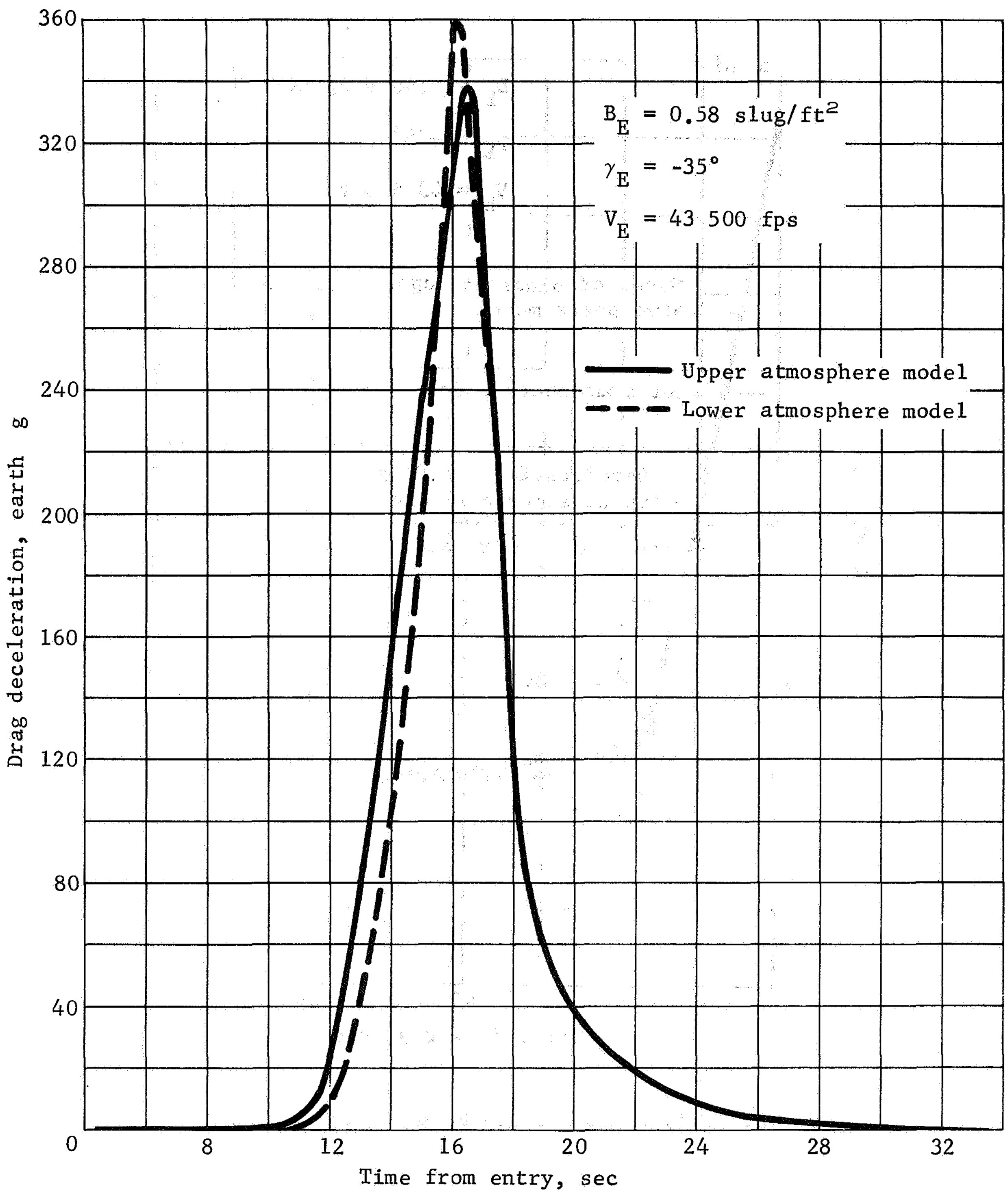

Figure 79.- 1973 Venus/Mercury Swingby, Drag Deceleration Time History

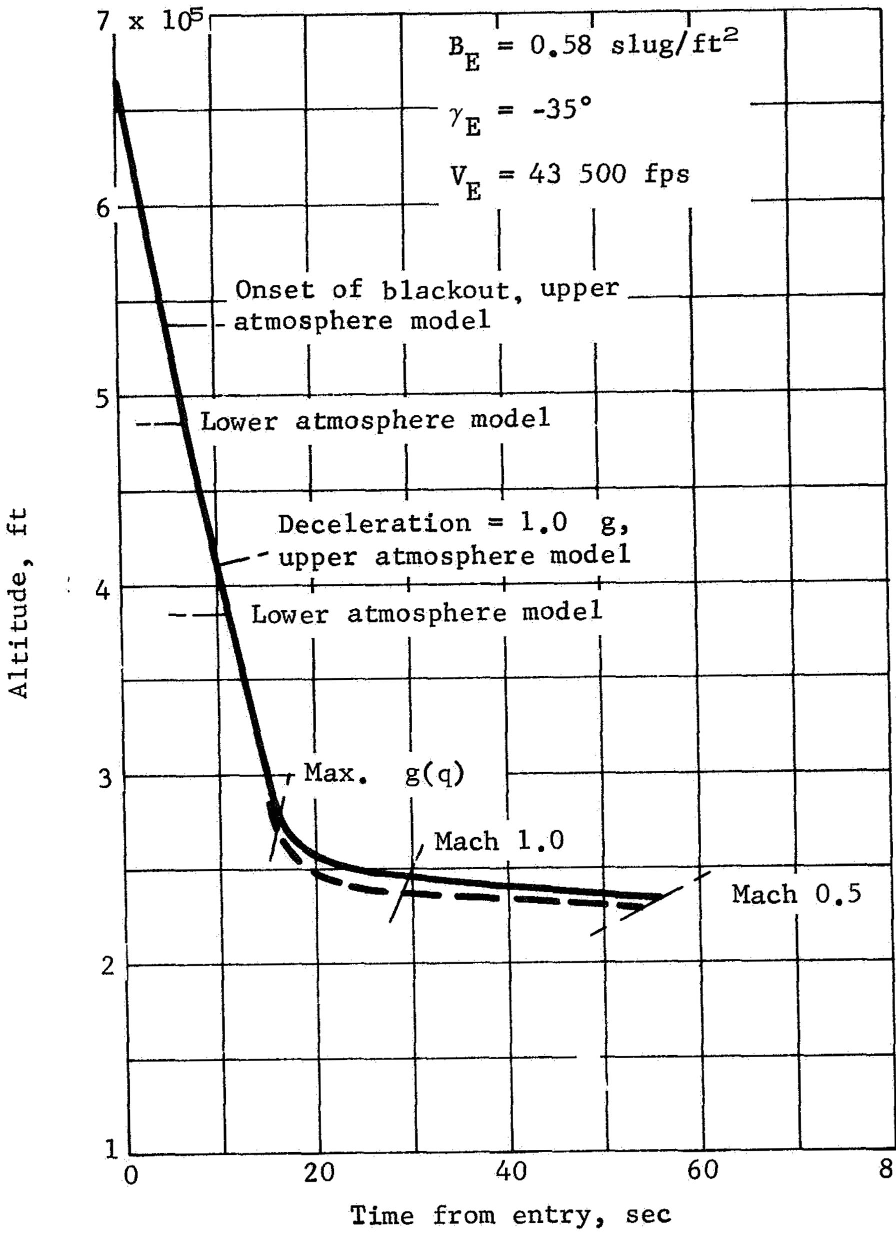

Figure 80.- 1973 Venus/Mercury Swingby, Entry Time History

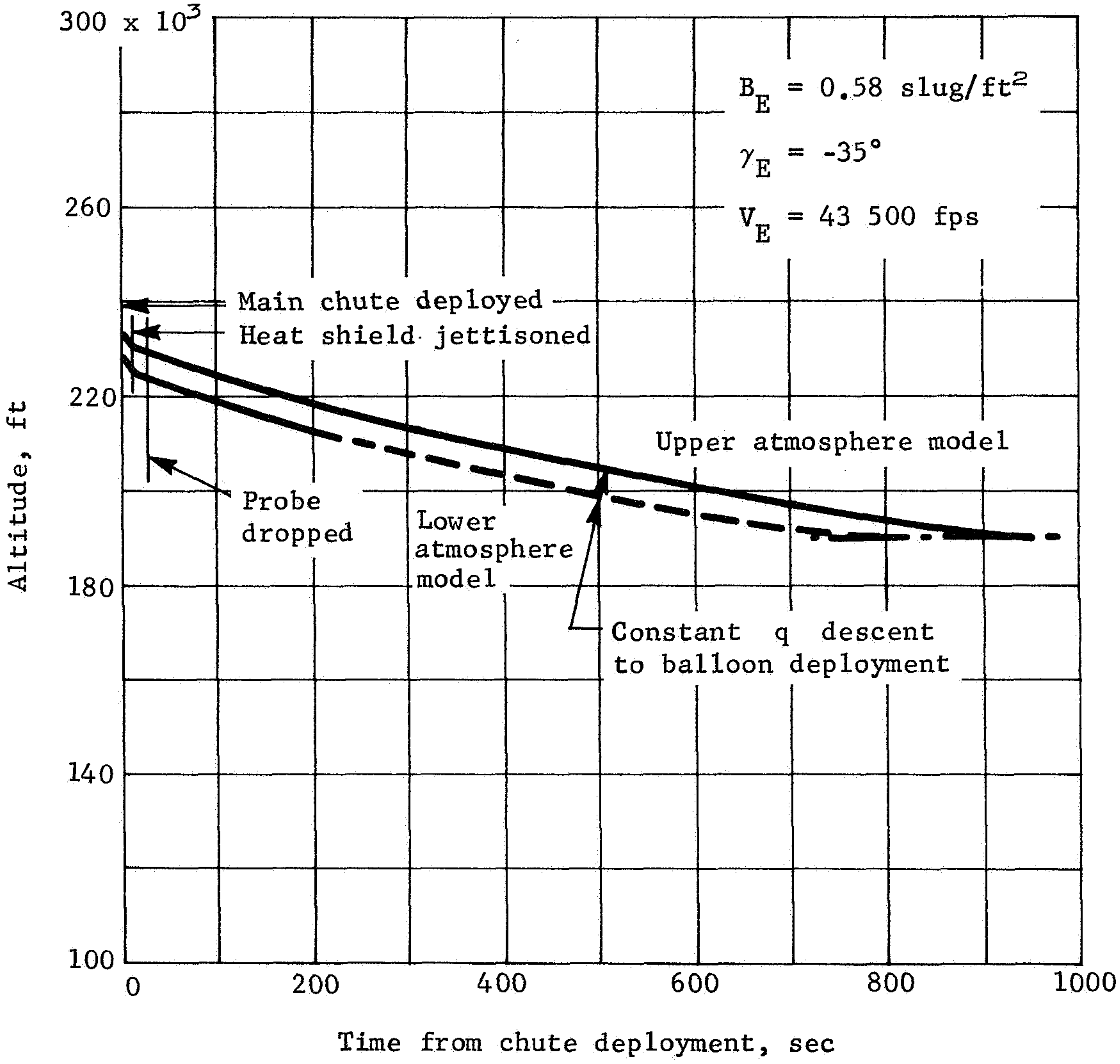

Figure 81.- 1973 Venus/Mercury Swingby, Descent Trajectory on Chute

CONCLUSIONS

Adequate launch periods and daily launch windows exist for both the 1972 and 1973 BVS launch opportunities. Both the SLV3C/C and Titan IIIC candidate launch vehicles have adequate payload capability for the 1972 flyby mission and for the 1973 entry from approach mode. For the 1973 entry from orbit mode, however, only the Titan IIIC has adequate launch performance capability with the specified orbiting spacecraft. For the 1973 Venus/Mercury swingby, the launch period is reduced from 20 to 14 days.

Satisfactory targeting capability exists for the 1972 flyby and 1973 orbital missions for sunlight entry in areas of scientific interest; however, for the 1973 Venus/Mercury swingby mission, targeting is restricted to dark-side entry.

For the flyby and orbital missions, communication geometry is satisfactory from launch through balloon flotation. The primary communication mode is direct-to-Earth for the 1972 flyby mission and relay-link-via-the-orbiting-spacecraft for the 1973 orbiter mission. For the Venus/Mercury mission, an out-of-plane deflection maneuver is required to position the BVS for the required direct Earth communication link.

Martin Marietta Corporation
Denver, Colorado, January 8, 1969